PULSED NEUTRON EXPERIMENTS IN GRAPHITE

Thesis by

Harold Finley McFarlane

In Partial Fulfillment of the Requirements

for the Degree of

Doctor of Philosophy

California Institute of Technology

Pasadena, California

1971

(Submitted May 27, 1971)

ACKNOWLEDGMENTS

I wish to express my sincere appreciation to my thesis advisor, Professor Noel Corngold, for his guidance during the final stages of this research. His many suggestions and his enthusiasm for the research were essential for the successful completion of this thesis. In addition, I express my considerable gratitude to Dr. Jerome Shapiro who introduced me to the problem of pulsed neutron research, tutored me in the experimental techniques, and spent many long hours in helping with the data collection.

I gratefully acknowledge financial support provided by the Atomic Energy Commision in the form of a Special Fellowship in Nuclear Science and Engineering for 1967-1970. Financial support was also provided by the California Institute of Technology through a Graduate Teaching Assistantship during 1969-1971. To the administrators of these sources of support, I express my thanks.

ABSTRACT

Detailed pulsed neutron measurements have been performed in graphite assemblies ranging in size from 30.48 cm x 38.10 cm x 38.10 cm to 91.44 cm x 66.67 cm x 66.67 cm. Results of the measurement have been compared to a modeled theoretical computation.

In the first set of experiments, we measured the effective decay constant of the neutron population in ten graphite stacks as a function of time after the source burst. We found the decay to be non-exponential in the six smallest assemblies, while in three larger assemblies the decay was exponential over a significant portion of the total measuring interval. The decay in the largest stack was exponential over the entire ten millisecond measuring interval. The non-exponential decay mode occurred when the effective decay constant exceeded 1600 sec^{-1}.

In a second set of experiments, we measured the spatial dependence of the neutron population in four graphite stacks as a function of time after the source pulse. By doing an harmonic analysis of the spatial shape of the neutron distribution, we were able to compute the effective decay constants of the first two spatial modes. In addition, we were able to compute the time dependent effective wave number of neutron distribution in the stacks.

Finally, we used a Laplace transform technique and a simple modeled scattering kernel to solve a diffusion equation for

the time and energy dependence of the neutron distribution in the graphite stacks. Comparison of these theoretical results with the results of the first set of experiments indicated that more exact theoretical analysis would be required to adequately describe the experiments.

The implications of our experimental results for the theory of pulsed neutron experiments in polycrystalline media are discussed in the last chapter.

TABLE OF CONTENTS

Table of Contents (Cont'd)

I. INTRODUCTION

A. Pulsed Neutron Experiments

Pulsed neutron experiments are a broad class of experiments in applied neutron physics which consist of three basic elements: (1) a strong neutron source of finite duration and regular repetition rate, (2) a medium with which the neutrons can interact, and (3) collection of data related to the neutron field and its interaction with the medium. One must describe the energy, spatial, and time distribution of the source, the nature of the medium, and the type of information (data) the experiment is designed to acquire in order to classify a pulsed neutron experiment. Pulsed neutron sources are usually of the high energy type (> 1 MEV) produced by reactions in an accelerator or of the thermal (< 1 EV) type produced by a chopped beam of neutrons from a reactor. Materials are classified according to their fission, scattering, and absorption properties. Data acquisition may be classified as to whether spatial and/or energy distributions are measured in addition to the time response of the neutron population.

We shall be concerned with pulsed neutron experiments performed on such neutron moderators as water, beryllium, beryllium oxide, and in particular, graphite. When a burst of high energy neutrons collides with a neutron moderating material, the energy is degraded from several MEV to a few EV in a time which is short relative to the measuring times of most experiments on

these materials. Upon reaching this energy range, the population experiences a process known as thermalization, in which the neutrons exchange energy with the moderator atoms as the average energy of the neutron population approaches that of the moderator atoms. Measurement of the time constant τ with which the average neutron energy approaches an asymptotic value after the pulse injection is a common type of pulsed neutron experiment designed to study the thermalization process.

The thermalized neutron population attenuates by parasitic absorption and, in a finite system, by escape through the system boundaries. The decrease in neutron population can be described as an exponential decay $\sim e^{-\lambda t}$ during at least a portion of the measuring times for many moderator systems. The most common type of pulsed neutron experiment is to measure the asymptotic decay constant λ associated with neutron populations in various sizes of a single moderator. Rather than to classify a particular system by its geometry and dimensions, it is convenient to specify a single parameter, the geometric buckling B^2, whose prescription (see equation I-13) is defined for such regular geometries as slabs, spheres, and right-circular cylinders. The decay constant λ increases monotonically with B^2. Because the dispersion curve $\lambda(B^2)$ can be related to important quantities in reactor physics calculations, as we shall demonstrate in section B, considerable research effort has been put into pulsed neutron experiments since von Dardel[1, 2, 3] published his original papers more than seventeen

years ago.

Two other types of pulsed neutron experiments are considerably less common. One is the measurement of the decay of the neutron field as a function of position in the moderator. The other is measurement of the neutron energy distribution as a function of time after the pulse. These two types of experiments are more rich in information, and correspondingly more difficult to perform, than the other two types. As one might expect, the existing data are roughly inversely proportional to the difficulty of the experiment.

B. Theory of Pulsed Neutron Experiments

The theoretical framework for the analysis of the pulsed neutron experiments is the Boltzmann equation for neutrons, [4]

$$\left[\frac{\partial}{\partial t} + \underline{v}\cdot\nabla + v\,\Sigma_T(v)\right] n(\underline{r}, \underline{v}, t) = \int v' \Sigma_s(\underline{v}' \rightarrow \underline{v})\, n(\underline{r}, v', t)\, d^3v' + S(\underline{r}, \underline{v}, t) \tag{I-1}$$

which describes the neutron population in the moderator at times after the source burst. The neutron distribution function $n(\underline{r}, \underline{v}, t)$ is the probable neutron density in d^3r around $\underline{r}$, with velocity d^3v about $\underline{v}$, at time t. The total macroscopic neutron cross section of the moderator is represented by $\Sigma_T(v)$. $S(\underline{r}, \underline{v}, t)$ is the neutron source distribution function, usually set equal to zero for $t > 0$. The quantity $\Sigma_s(\underline{v}' \rightarrow \underline{v})$ is the differential scattering cross section for neutrons scattering from d^3v' about $\underline{v}'$ to d^3v about $\underline{v}$. The

appropriate boundary condition for the pulsed source problem is that neutrons escaping the physical boundaries of the moderator do not return. If $\underline{e}_R$ is a unit normal vector pointing out of the moderator at $\underline{R}$ on the surface, then

$$n(\underline{R}, \underline{v}, t) = 0 \quad \text{if} \quad \underline{v} \cdot \underline{e}_R < 0 \quad . \tag{I-2}$$

Obtaining the differential scattering cross section from the general theory of scattering of particles is almost as difficult as solving equation I-1 for $n(\underline{r}, \underline{v}, t)$. Although presentation of the complete formalism for construction of the scattering kernel (differential scattering cross section) would principally serve to distract us from the real problem, a few words on the general properties of scattering kernels and on the form of $\Sigma_s(\underline{v}' \rightarrow \underline{v})$ for polycrystalline materials are in order. To facilitate the discussion, we introduce the neutron energy E and a unit vector $\underline{\Omega}$ such that $\underline{v} = v\underline{\Omega}$.

The principle of detailed balance, borrowed from the theory of statistical mechanics, holds for the scattering kernel. A neutron gas, in thermal equilibrium with a surrounding, non-absorbing, infinite, homogeneous medium at uniform temperature T, assumes an energy distribution proportional to a Maxwellian energy distribution M(E) given by

$$M(E) = \frac{E}{T^2} e^{-E/T} \quad . \tag{I-3}$$

The principle of detailed balance may then be stated as[4]

$$M(E')\Sigma_s(E' \rightarrow E, \underline{\Omega}' \rightarrow \underline{\Omega}) = M(E)\Sigma_s(E \rightarrow E', \underline{\Omega} \rightarrow \underline{\Omega}'). \qquad (I\text{-}4)$$

To construct a scattering kernel, one considers a system of atoms, whose nuclei have very short range (point) nuclear potentials, scattering neutron waves of various energies. In the thermal energy range the chemical binding between scattering centers, which is the same order of magnitude as the neutron energy, is responsible for space-time correlation between the scattering particles. This correlation results in coherent scattering in which the scattered neutron waves interfere. There is also an incoherent contribution to the scattering cross section. The nature of the chemical binding determines the allowable energy exchange processes while the nuclear potential determines the amplitude of the scattering cross section. The scattering kernel is usually decomposed into an elastic $\delta(E'-E)$ term and an inelastic term[5]. Each term is composed of a coherent and an incoherent part. In practice, one assumes that the scattering depends only on the angle between $\underline{\Omega}'$ and $\underline{\Omega}$, although the assumption is not valid for graphite which is composed of highly anisotropic crystallites. If one defines $\mu_o = \underline{\Omega}' \cdot \underline{\Omega}$, the total macroscopic differential scattering cross section may be written as $\Sigma_s(E' \rightarrow E, \mu_o)$.

Because of the regular ordering of the nuclei in crystals, the coherent, elastic scattering term has a relatively significant

amplitude for neutrons with wave lengths not exceeding twice the maximum spacing between adjacent planes (corresponding to energies above the Bragg energy). One must appeal to the language and the results of solid state physics in order to compute the necessary cross sections for polycrystalline moderators such as graphite. Williams[4] gives the results for the coherent, elastic differential cross section averaged over all crystal orientations as

$$\Sigma_{e\ell,\,coh}(E'\to E,\mu_o)=\Sigma_{coh}\frac{\pi}{4EV_o}\sum_{k\neq o}^{k<\sqrt{8E}}\frac{z(k)}{k}e^{-2W_D(k)}\delta(1-\frac{k^2}{4E}-\mu_o)(E-E') \qquad (I\text{-}5)$$

where k is the amplitude of a reciprocal lattice vector, $W_D(k)$ is the DeBye - Waller factor, $Z(k)$ is a reciprocal lattice weighting factor, V_o is the volume of a unit cell in the lattice, and the units are such that $\hbar$ and the neutron mass are set equal to one. The elastic, incoherent cross section remains finite below the Bragg energy E_B and has the simpler form

$$\Sigma_{e\ell,\,inc}(E'\to E,\mu_o)=\frac{\Sigma inc}{4\pi}e^{-2W_D}\delta(E-E') \qquad (I\text{-}6)$$

where the scattering has been assumed to be isotropic.

The inelastic scattering term is generated by treating the scatterers as a system of quantized, harmonic, lattice vibrations (phonons). Since multiple phonon exchanges are possible,

the inelastic scattering term is quite complicated and is usually handled in some approximate fashion. One technique is to expand the term in a power series in which the n^{th} term represents the contribution from n-phonon exchange processes. The other common technique, used for heavy crystals, is to expand the inelastic kernel in powers of 1/A, where A is the nucleus to neutron mass ratio. If the inelastic term is assumed to be totally incoherent, the mass expansion yields to order 1/A, [4]

$$\Sigma_{in}(E' \rightarrow E, \mu_o) = \frac{\Sigma_b}{4\pi} \left(\frac{E}{E'} \right)^{\frac{1}{2}} \frac{\kappa^2}{2A} \int_{-\infty}^{+\infty} \frac{f(\omega)\delta(E-E'-\omega)}{\omega(e^{\omega/T}-1)} d\omega \qquad (I-7)$$

where Σ_b is the bound atom scattering cross section, κ is the magnitude of the neutron momentum transfer, and $f(\omega)$ is the phonon frequency distribution.

The complicated structure of the scattering integral has been partially responsible for the failure of equation I-1 to yield an exact solution. The gradient term $\underline{v} \cdot \nabla n(\underline{r}, \underline{v}, t)$ together with the exact boundary condition I-2 also makes the solution difficult. Consequently, approximate equations have been used to obtain the neutron distribution function. The approximations fall into two logical categories: (1) the energy dependence is neglected and the monoenergetic Boltzmann equation is studied for the exact spatial dependence, or (2) the spatial dependence is approximated and the thermalization process is studied.

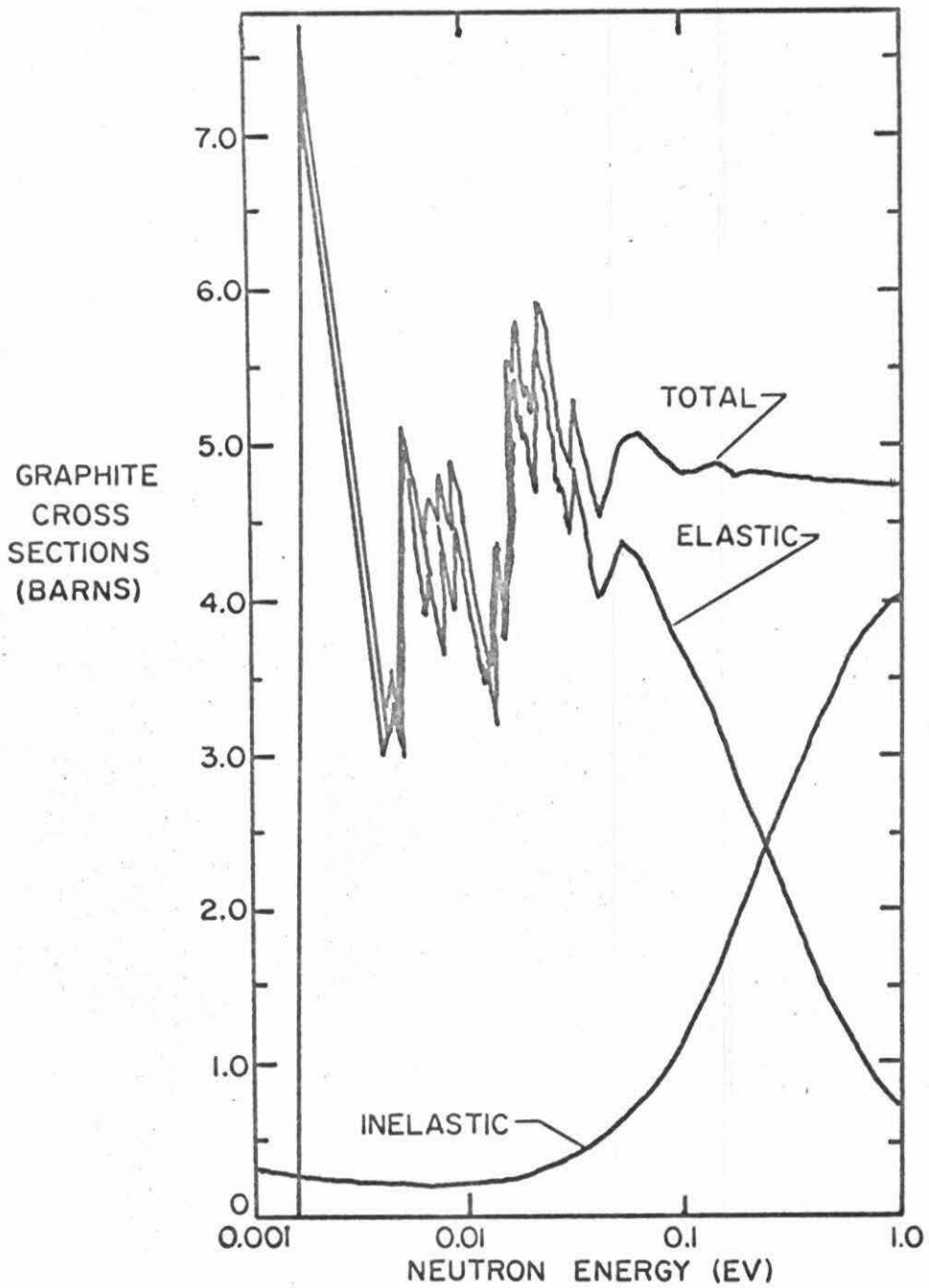

Figure I-1. Theoretical values of the microscopic cross sections of graphite in the thermal energy range.[59]

Since pulsed neutron experiments are designed principally to study the thermalization process, one would not expect the monoenergetic Boltzmann (transport) equation,

$$\left[\frac{\partial}{\partial t} + v_o \Omega \cdot \nabla + v_o \Sigma_T\right] n(\underline{r}, \underline{\Omega}, t) = v_o \int \Sigma_s(\Omega' \rightarrow \underline{\Omega})\, n(\underline{r}', \underline{\Omega}', t)\, d\Omega' + S(\underline{r}, \underline{\Omega}, t) \quad \text{(I-8)}$$

to yield much information about the time dependence of transient neutron populations. Information from the solution to I-8 can be helpful in modeling the spatial dependence for the energy dependent problem. For this purpose, the steady state (constant source) solution is often adequate. Solutions for the spatial distributions are usually decomposed into two parts, an asymptotic solution which holds for most of the interior region of the moderator, and a transient solution which is most evident near the surface. The asymptotic solution can be extrapolated to zero at some point outside the moderator. The distance between the surface of the moderator and the point where the asymptotic solution extrapolates to zero is called the extrapolation length Z_o. The concept of the extrapolated endpoint comes from the famous Milne problem,[6] the steady state, half-space version of equation I-8. Computations of Z_o for finite geometries, such as that of Erdmann and Shapiro[7] slabs of water, indicate that Z_o is a weak function of system size. One-speed transport theory indicates that Z_o increases as the system dimensions shrink. However, there is a competing effect due to distortion of the neutron energy distribution,[8] so that the exact

behavior of $Z_o(B^2)$ is not monotonic.

For the analysis of pulsed neutron experiments, it is usually more instructive to relax the conditions for detailed knowledge of the spatial distribution and to emphasize the energy - time behavior of the neutron field. The energy dependent diffusion equation,[4]

$$\left[\frac{\partial}{\partial t} - vD(E)\nabla^2 + v\Sigma_a(E) + v\Sigma_s(E)\right] n(\underline{r}, E, t) =$$

$$\int_o^\infty dE' v' \Sigma_s(E' \rightarrow E) n(\underline{r}, E', t) + S(\underline{r}, E, t) \qquad \text{(I-9)}$$

is a reasonable representation in many physical situations and is the usual basis for analysis of the raw data from the experiments. $D(E)$ is the diffusion coefficient[9] for neutrons of energy E. $\Sigma_a(E)$ and $\Sigma_s(E)$ are the total absorption and scattering cross sections, respectively. The usual boundary condition requires that the neutron density vanish at some extrapolated boundary of the system. For a slab of width 2a, this condition is

$$n(\pm(a + Z_o),\ E,\ t) = 0 \ . \qquad \text{(I-10)}$$

The spatial distribution is easily obtained using this boundary condition. If we use spatial eigenfunctions which are solutions to the Helmholtz equation,

$$\nabla^2 X_k(\underline{r}) + B_k^2 X_k(\underline{r}) = 0 \ . \qquad \text{(I-11)}$$

the solution for $n(\underline{r},E,t)$ is then

$$n(\underline{r}, E, t) = \sum_k n(B_k^2, E, t)\, X_k(\underline{r}) \qquad \text{(I-12)}$$

The lowest eigenvalue B_1^2 of the Helmholtz equation defines the buckling for the system. For the slab case

$$B_k^2 = \left[\frac{k\pi}{2(a+Z_o)} \right]^2 . \qquad \text{(I-13)}$$

If we define the scattering operator $\hat{O}$ such that

$$\hat{O}\, f(E) = \int_o^\infty dE'\, v'\, \Sigma_s(E' \to E)\, f(E') - v\, \Sigma_s(E) f(E) \qquad \text{(I-14)}$$

then we may write the equation for the energy-time distribution of the fundamental spatial mode as

$$\left[\frac{\partial}{\partial t} + v D(E) B^2 + V \Sigma_a(E) \right] n(B^2, E, t) = \hat{O}\, n(B^2, E, t) + S(B^2, E, T). \qquad \text{(I-15)}$$

The form of the equation suggests that after sufficient waiting time, energy-time separability is a reasonable assumption. Hence, we try the ansatz

$$n(B^2, E, t) = n(B^2, E) e^{-\lambda t} \qquad \text{(I-16)}$$

in the homogeneous equation, leaving us with

$$\left[-\lambda + v D(E) B^2 + v \Sigma_a(E) \right] n(B^2, E) = \hat{O}\, n(B^2, E) . \qquad \text{(I-17)}$$

It seems natural to identify the eigenvalue λ with the experimentally determined decay constant for a moderator of buckling B^2.

We can obtain a perturbation solution to equation I-17 by expanding $n(B^2, E)$ and λ in powers of B^2:

$$n(B^2, E) = \phi_o(E) + \phi_1(E)B^2 + \phi_2(E)B^4 + \ldots$$

and (I-18)

$$\lambda = \lambda_a + D_o B^2 - CB^4 + FB^6 + \ldots .$$

The functions $\phi_j(E)$ are eigenfunctions of the scattering operator for the infinite medium ($B^2 = 0$) case. If the absorption cross section varies as $1/v$, as is often the case, the first term $\phi_o(E)$ will be the Maxwellian distribution.[4] The names of the coefficients in the expansion of λ are chosen for historical reasons.

Substituting the expansions into I-17 and equating equal powers of B^2 yields the following set of equations:

$$[- \lambda_a + v\Sigma_a] \phi_o(E) = \hat{O}\phi_o(E) \quad \text{(I-19)}$$

$$[-D_o + vD(E)] \phi_o(E) = \hat{O}\phi_1(E) \quad \text{(I-20)}$$

$$[-D_o + vD(E)] \phi_1(E) - C\phi_o(E) = \hat{O}\phi_2(E) . \quad \text{(I-21)}$$

We can integrate these equations over energy and obtain the values for λ_a, D_o, and C. The ansatz I-16 explicitly assumes an asymptotic energy distribution so that

$$\int_0^\infty \hat{O}\,\phi(E)\,dE = 0 \quad . \tag{I-22}$$

With the assumption of 1/v absorption, we have

$$\lambda_a = v_o \Sigma_{ao}, \tag{I-23}$$

$$D_o = \frac{\int_0^\infty dE\, vD(E)\, M(E)}{\int_0^\infty dE\, M(E)} \tag{I-24}$$

and

$$C = \frac{\int_0^\infty [vD(E) - D_o]\ \phi_1(E)\,dE}{\int_0^\infty dE\, M(E)} \quad . \tag{I-25}$$

It is the relation of the experimental dispersion curve $\lambda(B^2)$ to the diffusion parameters λ_a, D_o, and C that has spurred much of the pulsed neutron research.

Although the above model is quite useful, it is difficult to make much headway with a general, complicated scattering kernel. However, a similar model, the multi-group diffusion equations,

$$\left[\frac{\partial}{\partial t} - v_i D_i \nabla^2 + v_i \Sigma_i\right] n_i(\underline{r}, t) = \sum_j v_j \Sigma_{j \to i} n_j(\underline{r}, t)\ ,\ t > 0, \quad i, j = 1, 2, \ldots N \tag{I-26}$$

can be solved even for very complicated scattering kernels, provided each energy group satisfies the same boundary condition. The time dependent spatial distribution for the $i^{\underline{th}}$ group is

$n_i(\underline{r}, t)$, $\Sigma_{j \to i}$ is the averaged differential cross section for the scattering from the $j^{\underline{th}}$ group to the $i^{\underline{th}}$ group, Σ_i is the average total cross section for the $i^{\underline{th}}$ group, and D_i is the average diffusion coefficient for the $i^{\underline{th}}$ group. If E_{i-1} and E_i are the energy boundaries for the $i^{\underline{th}}$ group, then the average quantity f_i is defined as

$$f_i = \frac{\int_{E_{i-1}}^{E_i} W(E) f(E) dE}{\int_{E_{i-1}}^{E_i} W(E)\, dE} \qquad \text{(I-27)}$$

where W(E) is some weighting function, often taken to be the Maxwellian energy distribution.

There are always N eigenvalues for each spatial harmonic, hence the solution can be written as

$$n_i(\underline{r}, t) = \sum_{k=1}^{\infty} \sum_{j=1}^{N} A_{ikj} e^{-\lambda_{kj} t} X_k(\underline{r}) , \quad i = 1, 2, \ldots N . \qquad \text{(I-28)}$$

The lowest eigenvalue λ_{11} can be identified with the experimental decay constant λ.

Based on the analysis of the last two models, one might suspect that the experimental decay constants can be identified with the eigenvalues of the Boltzmann equation. Hence, it is worthwhile to re-examine equation I-1, considering the eigenvalue spectrum rather than trying to solve for the neutron distribution function.

Kuščer[10] has reviewed the techniques for obtaining the eigenvalue spectrum. If we define the linear Boltzmann operator $\hat{A}$,

$$\hat{A}f(\underline{r}, \underline{v}) = \underline{v} \cdot \nabla f(\underline{r}, \underline{v}) + v \Sigma_T (v) f(\underline{r}, \underline{v}) - \int d^3v' \Sigma_s (\underline{v}' \rightarrow \underline{v}) f(\underline{r}, v') \tag{I-29}$$

we may write the Boltzmann equation in the suggestive form

$$\left[\frac{\partial}{\partial t} + \hat{A} \right] n(\underline{r}, \underline{v}, t) = S(\underline{r}, \underline{v}) \delta(t) \quad . \tag{I-30}$$

One technique is to make the ansatz

$$n(\underline{r}, \underline{v}, t) = n(\underline{r}, \underline{v}) e^{-\lambda t}, \qquad t > 0 \tag{I-31}$$

then look for the eigenvalues of the homogeneous equation

$$\hat{A}\, n(\underline{r}, \underline{v}) = \lambda\, n(\underline{r}, \underline{v}) \tag{I-32}$$

where A is a linear operator defined on a Hilbert space, using the spectral theory of operators and functional analysis. An alternate and perhaps more straightforward approach is to Laplace transform I-30 and then examine the analyticity of the transformed distribution function.

This type of analysis has been successful for various system geometries and for various scattering kernels. Very general results have been found by Albertoni and Montagnini[11] for the case of a finite, homogeneous, convex body of arbitrary shape surrounded by a vacuum and the isotropic, free gas scattering kernel. There results for the eigenvalue spectrum are that the

half-plane $\mathrm{Re}\,\lambda > [v\,\Sigma_s(v)]_{min}$ is filled with a continuous spectrum and that there exists at most a finite number of real, discrete eigenvalues on the line $0 < R_e\,\lambda < [v\,\Sigma_s(v)]_{min}$. Furthermore, for sufficiently small bodies, the number of discrete eigenvalues reduces to zero. Borysiewicz and Mika[12] have extended these results to the case of a non-square integrable scattering kernel (the elastic scattering contribution for polycrystals) and shown that the essential features of the eigenvalue spectrum do not change.

The disappearance of the discrete eigenvalues for sufficiently small systems has some important implications for pulsed neutron experiments which are designed to measure a discrete decay constant. The situation is particularly serious for the polycrystalline materials which have a very sharp drop in the scattering cross section below the Bragg energy. Although the work of Borysiewicz and Mika[12] pretty well describes the state of the art of eigenvalue analysis for the Boltzmann operator it is worthwhile to consider some approximate theories which can give more quantitative results for what one can expect experimentally.

One particularly useful approximation is to represent the spatial distribution by the asymptotic reactor theory[13] ansatz, $e^{i\underline{B}\cdot\underline{r}}$, where the square of the magnitude of the wave vector $\underline{B}$ can be identified with the buckling of the system. This infinite medium representation of the problem is equivalent to considering a single spatial mode in the finite case. Shapiro and

Corngold[14], considering the infinite medium ($B^2 = 0$) case, using the heavy crystal approximation and the Einstein and the Debye representations for the phonon frequency distribution, found that for reasonable values of the Einstein frequency or the Debye temperature, no more than one discrete eigenvalue exists. Hence, the approach to equilibrium time constant τ, which is identified as the reciprocal of the second discrete eigenvalue, is not well defined for graphite. Conn and Corngold[15] combined asymptotic reactor theory with the isotropic part of the full scattering kernel to obtain a complicated eigenvalue spectrum for polycrystals. Figure 2, in which $\left[v \Sigma_s(v) \right]_{min}$ is represented as λ_*, shows the eigenvalue spectra found by Albertoni and Montagnini[11] and by Conn and Corngold.[15].

Despite the complicated nature of the theoretical eigenvalue spectra, experimentalists have reported decay constants for polycrystalline systems with B^2 well in excess of B_*^2, where B_*^2 is the value of the buckling such that $\lambda(B_*^2) = \lambda_*$. (The value of λ_* is not well known for graphite, as we shall see in the next chapter.) In light of this disparity, Corngold and Durgun attacked the problem using diffusion theory and a simple modeled kernel which approximated a polycrystal kernel. They found that the detector response for the fundamental spatial mode could be represented as

$$D_r(t) = A_o e^{-\lambda_o t} + \int_{\lambda_*}^{\infty} A(\lambda) e^{-\lambda t} d\lambda \qquad \text{(I-33)}$$

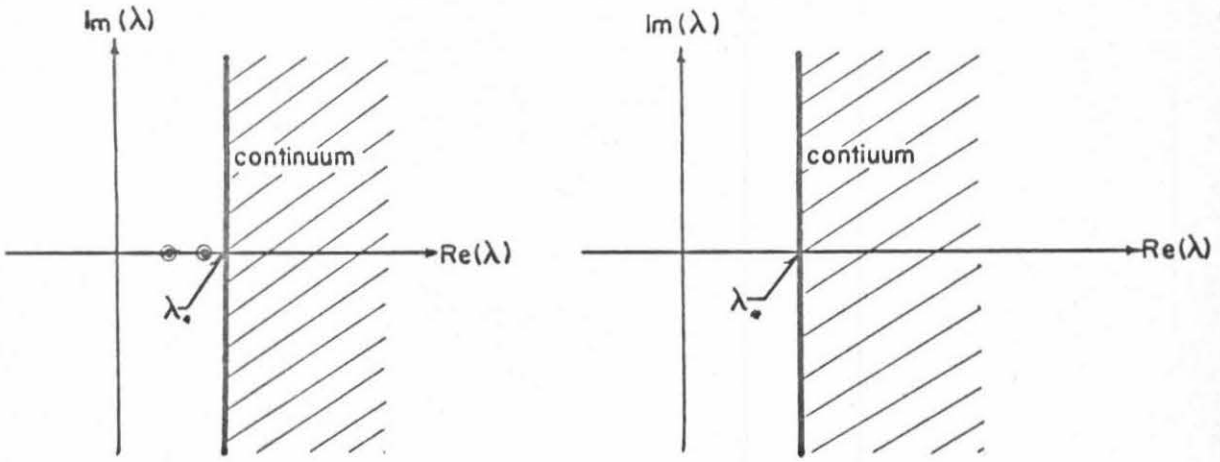

Figure I-2a. The Eigenvalue Spectrum of Albertoni and Montagnini[11] for a "Large" and a "Small" System.

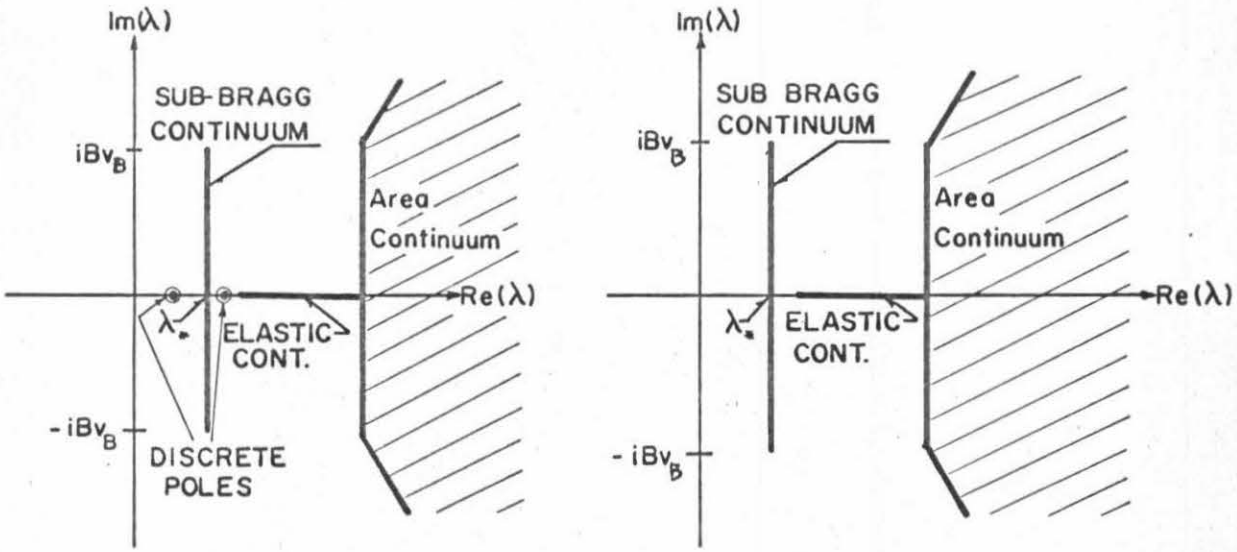

Figure I-2b. The Eigenvalue Spectrum of Conn and Corngold[15] for a "Large" and "Small" System.

For systems with $B^2 > B_*^2$, the discrete term vanishes, but the weighting function $A(\lambda)$ is sharply peaked for a portion of the range $B^2 > B_*^2$. Although the representation I-33 is certainly not adequate for the complicated area continuum of the more general theories, it seems adequate to interpret most of the experimental results. The peaking in the weighting function gives rise to what has been termed pseudo-exponential decay. Conn[17] has extended this analysis using asymptotic reactor theory and simple modeled kernels for graphite and beryllium, finding that experimentally it is probably very difficult to distinguish pseudo-exponential from true exponential decay for a limited range of bucklings.

Computation of effective decay constants which vary with time after the end of the burst is useful for comparison with experimental results. Wood[18, 19] has performed numerical computations for $\lambda_{eff}(B^2, t)$ of beryllium using a multi-phonon scattering kernel. Ardente and Rossi[20] used a simple model in a numerical scheme with a multi-phonon scattering kernel to obtain results for $\lambda_{eff}(B^2, t)$ for graphite and beryllium. Ritchie et al.[21] have performed multi-group diffusion theory calculations for beryllium oxide using a scattering kernel based on Sinclair's phonon frequency distribution to obtain $\lambda_{eff}(B^2, t)$.

Only a partial review of the theory has been attempted here. More complete reviews can be found in Williams[4] and Parks et al.[5]

C. Review of the Experimental Work

The results of several theories indicate that the dispersion curve $\lambda(B^2)$ can be accurately described by the first few terms of an expansion

$$\lambda(B^2) = \langle v \Sigma_a \rangle + D_o B^2 - CB^4 + FB^6 + \ldots . \quad \text{(I-34)}$$

The coefficient C is the diffusion cooling term which represents the preferential leakage of higher energy neutrons, an effect observed by von Dardel[2] in his early work. Most pulsed neutron experiments have been designed to obtain the coefficients in I-34 experimentally. The advantage of the pulsed technique is that the time of neutron capture relative to the source burst can be measured extremely accurately, allowing quite precise determination of the asymptotic decay constant.

Antonov et al.[22] was the first to report results for graphite in 1955. Beckurts[23] later reported values of D_o and C in disagreement with Antonov. Since then there has been almost a continuous production of experiments to supply the coefficients of equation I-34. The results have been characterized by disagreement which is not attributable to the assigned experimental error. A limited collection of the results may be seen in Table I-1. The spread in results for D_o and C reflects the non-uniqueness of the $\lambda(B^2)$ curves from the various experiments. Evidence of this spread of results may be seen in Figure I-3 . The experiment-

TABLE I-1.

Diffusion Parameters of Graphite (Density 1.6 gm/cm^3) Obtained from Polynomial Fits to $\lambda(B^2)$ Data*

Author	Year	Maximum B^2 (Cm^{-2})	D_o X 10^{-5} Cm^2 sec^{-1}	C X 10^{-5} Cm^4 sec^{-1}	F X 10^{-7} Cm^6 sec^{-1}
Antonov et al. (22)	1955	.04129	2.07 ± 0.03	12.5 ± 2.0	. . .
Beckurts (23)	1956	.0055	2.13 ± 0.02	16.3 ± 2.5	. . .
Klose, Küchle, and Reichardt (24)	1962	.005 .012	2.13 ± 0.02 2.11 ∓ 0.02	26. ± 5. 16. ∓ 5.	. . . -20 ± 10.
Starr and Price (25)	1962	.0189	2.14 ± 0.01	39. ± 4.	. . .
Davis, DeJurgen, and Reier (26)	1965	.0053 .012	2.187 ± .008 2.20 ∓ .009	30. ± 1. 44.3 ∓ 4.	. . . 12.7 ± 5.
Yamamuro et al. (27)	1966	.0189	2.05 ± .02	15.1 ± 1.8	. . .
Hanna and Harris (28)	1968	.0253	2.215 ± .019	37.46 ± 1.22	. . .
Bull, Dance, and Connolly (29)	1970	.013206 .006824	2.22 ± .02 2.19 ∓ .06	38.4 ± 1.6 33.8 ∓ 6.7	. . . . . .
Blumentritt and Fährmann (60)	1968	.0173	2.17 ± .05	32.1 ± 8.0 42.6 ∓ 12.0	. . . 10 ± 8
Hüls (53)	1970	.0062	2.164 ± .023	42.9 ± 2.4	. . .

* The data of the present work does not include enough results for small B^2 to justify this type of data fitting.

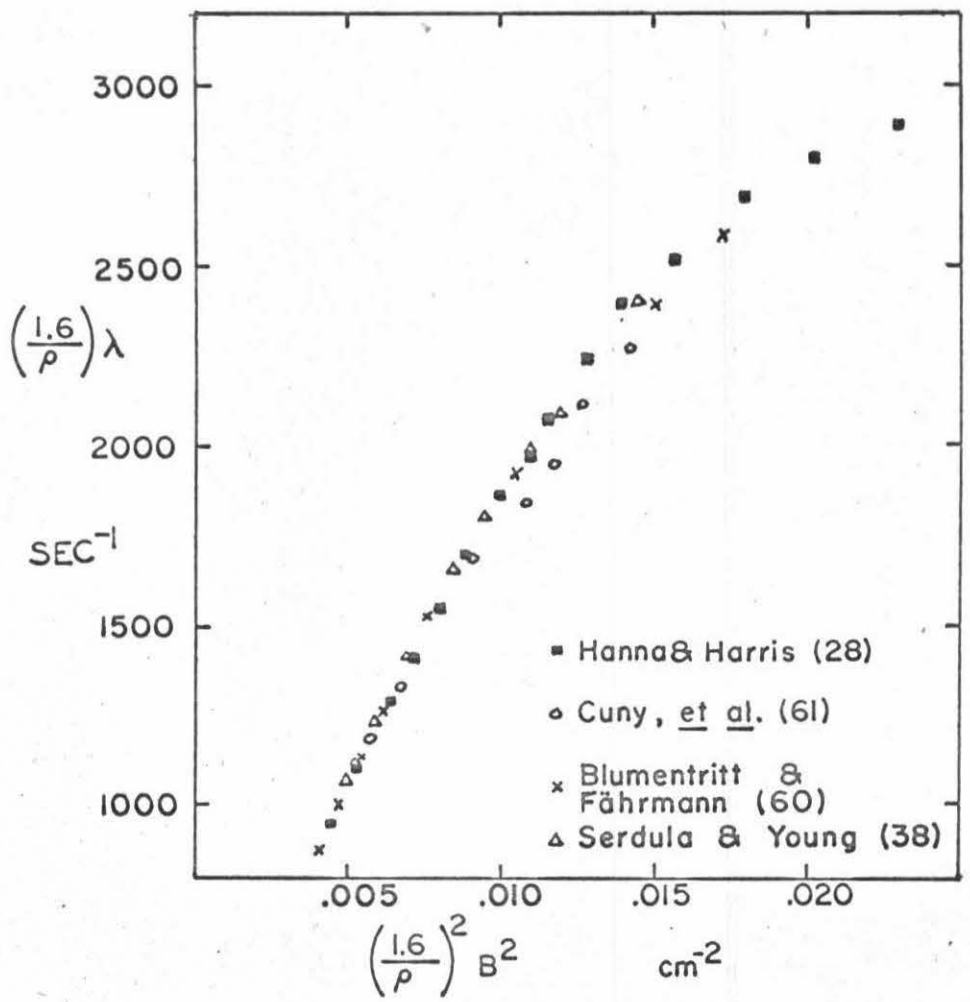

Figure I-3. Part of the Experimental Dispersion Curve for Several Authors.

ally generated dispersion curve $\lambda(B^2)$ is apparently sensitive to the type of analysis used, especially the delay time between the source burst and the beginning time for the exponential fit to the data, to the type of shielding from roon-return neutrons used, to how coarsely the time intervals after the neutron pulse are discretized, to the energy sensitivity of the detector, and to the detector placement. The nature of the graphite, that is, the density and average crystal size, also effects the result.

Part of the problem in obtaining the $\lambda(B^2)$ curve experimentally is in determining whether an asymptotic exponential decay is ever established, since the theoretical value of λ_* is not well established.[17] Recent results indicate that the onset of the region of non-exponential decay may be hard to discover experimentally. Hanna and Harris[28] using 17 channel analysis found discrete exponentials with decay constants up to almost 3000 sec^{-1} for graphite. On the other hand, Bull et al.[29] using a 256 channel analyzer found that they were probably not measuring a discrete term above 1600 sec^{-1}. Since both groups used reasonable shielding and a minimum of two milliseconds waiting time, the discrepancy probably indicates that the deviation from exponential decay is quite small and only shows up with the finer time mesh. Agreement between their quoted values for D_o and C leads one to suspect that the other critical facets of the experiment were similar.

The dispersion curves for the other two polycrystalline

moderators, beryllium and beryllium oxide, also present an anomalous spread of results. Ritchie[30] has recently published an extensive study of BeO in which he has found evidence of non-exponential decay in the range of λ greater than about 3600 sec^{-1}.

Fullwood[31] graphically displayed non-exponential die-away in beryllium by comparing the beryllium decay with an "equivalent" polyethylene system in the same environment. Zhezherun,[32] however, used a chopped beam of thermal neutrons and claimed to obtain exponential decays for all sizes of Be assemblies.

Another important class of pulsed neutron experiments has been directed toward measurement of the rate at which the average neutron energy approaches an asymptotic value. Usually this phenomenon is described by[33]

$$\bar{E}(t) - \bar{E}(t=\infty) \sim e^{-t/\tau} \quad . \qquad \text{(I-35)}$$

The quantity τ is called the thermalization time and the quantity of interest in the experiments is the value of τ for an infinitely large moderator. Theoretically, τ is identified with the reciprocal of the first higher energy harmonic of the fundamental spatial mode, if it exists.[14]

There are several methods for obtaining τ. Starr, Honeck, and De Villiers[34] used detectors of different energy sensitivity to determine the time dependence of the average neutron velocity in several sizes of graphite stacks. Hanna and Harris[35] recently used a silver transmission technique (examining the ratio

of detector response with and without a silver filter) to obtain $\tau(B^2)$. The values for $\tau(B^2)$ are extrapolated linearly to $B^2 = 0$ to estimate the infinite medium result τ_{th}. Table I-2 shows that the results of the various authors for τ_{th} are in considerable disagreement. Recent work by Polley and Walker[36] using the Cd/Hg reaction ratio measured with a Ge(Li) detector in a large graphite stack indicates that the model given by equation I-35 is inadequate for graphite and that a unique τ_{th} probably does not exist.[14]

Very little work has actually been reported on measurements of time dependent spectra in finite moderating assemblies. Bernard et al.[41] and Poole et al.[42] have made these measurements for graphite, but their results do not include neutrons in the low energy range where the graphite total cross section changes very rapidly with energy. Gaerttner et al.[43] performed time dependent measurements of the energy distribution for beryllium stacks. Neutron populations in assemblies in the range exceeding B^2 showed no indication of attaining an asymptotic energy distribution and the effects of the Bragg peaks in the total cross section were quite evident in the energy distributions.

Experiments designed to measure time dependent spatial distributions have been important for two principle reasons. The first is that the value of the extrapolation length Z_o can be determined and the proper buckling assigned to the system. These measurements also allow isolation and observation of the decay of

TABLE I-2

The Thermalization Time For Graphite

Author	Year	B^2 Range	Method	(microseconds)
Beckurts (23)	1956	$\leq .0055$	Ag Filter Transmission	200 ± 50
Starr and deVilliers (37)	1962	(.001765 - .01320)	Mean Velocity Measurement	525 ± 125
Serdula and Young (38)	1965	(.005 - .0145)	Ag Filter Transmission	750 ± 200
Kaneko and Sumita (39)	1965	. . .	Filter Transmission	296 ± 50
Purica, et al. (40))	1967	(.0014 - .012)	Frequency Characteristics	694 ± 57
Hanna and Harris (35)	1969	(.003 - .0253)	Ag Filter Transmission	660 ± 115

individual spatial modes, information which is especially important in large systems often rich in higher spatial harmonics. Light water systems have extensively studied using this technique. In a classic experiment, Lopez and Beyster[44] measured $Z_o(B^2)$ and determined values for the diffusion parameters of water from the decay of the fundamental spatial mode.

Time dependent spatial harmonic analysis for large graphite systems has been reported by Hanna and Harris[28] and by Chwaszczewski and Mikulski.[45] Davis et al.[26] have measured Z_o for large graphite systems by measuring the flux distribution at long times after the pulse when only the fundamental spatial mode persists. Klose et al.[24] have determined Z_o by treating it as a free parameter in fitting a curve to (λ , B^2) data. Ritchie[30] has provided both harmonic analysis of a neutron pulse and $Z_o(B^2)$ for beryllium oxide, while Andrews[46] has supplied the necessary data for beryllium.

D. Motivation for This Thesis

Except for detailed time-energy distributions, it is readily evident that a great many experimental results for transient neutron populations in graphite have already been compiled. With the possible exception of a couple of thermalization experiments,[36, 47] the existing results for graphite do not prove a very adequate check on some of the exciting theoretical developments of the 1960's. The reason for this inadequacy is not that the experiments are in

any way faulty, but rather that they have been specifically designed to measure thermalization and diffusion parameters.

The principal void to be filled in the experimental results is the empirical determination of the buckling ranges characterized by exponential, pseudo-exponential, and non-exponential decay of transient neutron populations. In addition, the extension of Z_o measurement into the range of probable non-exponential decay is needed. Finally, a check on the ability of a simple theory to provide an effective decay constant when a discrete λ does not exist will be useful.

II. MEASUREMENT OF EFFECTIVE DECAY CONSTANTS

Since the diffusion parameters of graphite, determined by the pulsed source method, have been published by many competent authors,[62] it seems rather obvious that the world does not need another set of these parameters. However, since the dispersion in the parameters may be due to the non-existence of an asymptotic decay mode when the apparent decay constant exceeds some critical value, knowledge of the regions of exponential, pseudo-exponential, and non-exponential decay seems essential to the interpretation of these results. We have performed experiments in which the decay of the neutron populations exhibits these types of behavior for reasonably well defined ranges of the graphite stack size and apparent decay constant. Other experiments, in which the spatial distribution of the neutrons fails to achieve an asymptotic mode are reported in the third chapter.

In order to tie the critical decay constant to the theory discussed in Chapter I, we shall identify $\lambda_* = [v\Sigma_s(v)+v\Sigma_a(v)]_{min}$ as the critical decay constant. The theoretical value of λ_* has not been well established.[17] The most quoted value, based on old cross section measurements in the sub-Bragg energy range, is $\lambda_* = 2600\ sec^{-1}$.[4] The kernel of Ghatak and Honeck,[49] based on Parks' model for graphite, yielded λ_* approximately equal to $1100\ sec^{-1}$. Values based on other kernels have been consistently lower than $2600\ sec^{-1}$. Conn[50] has recently included

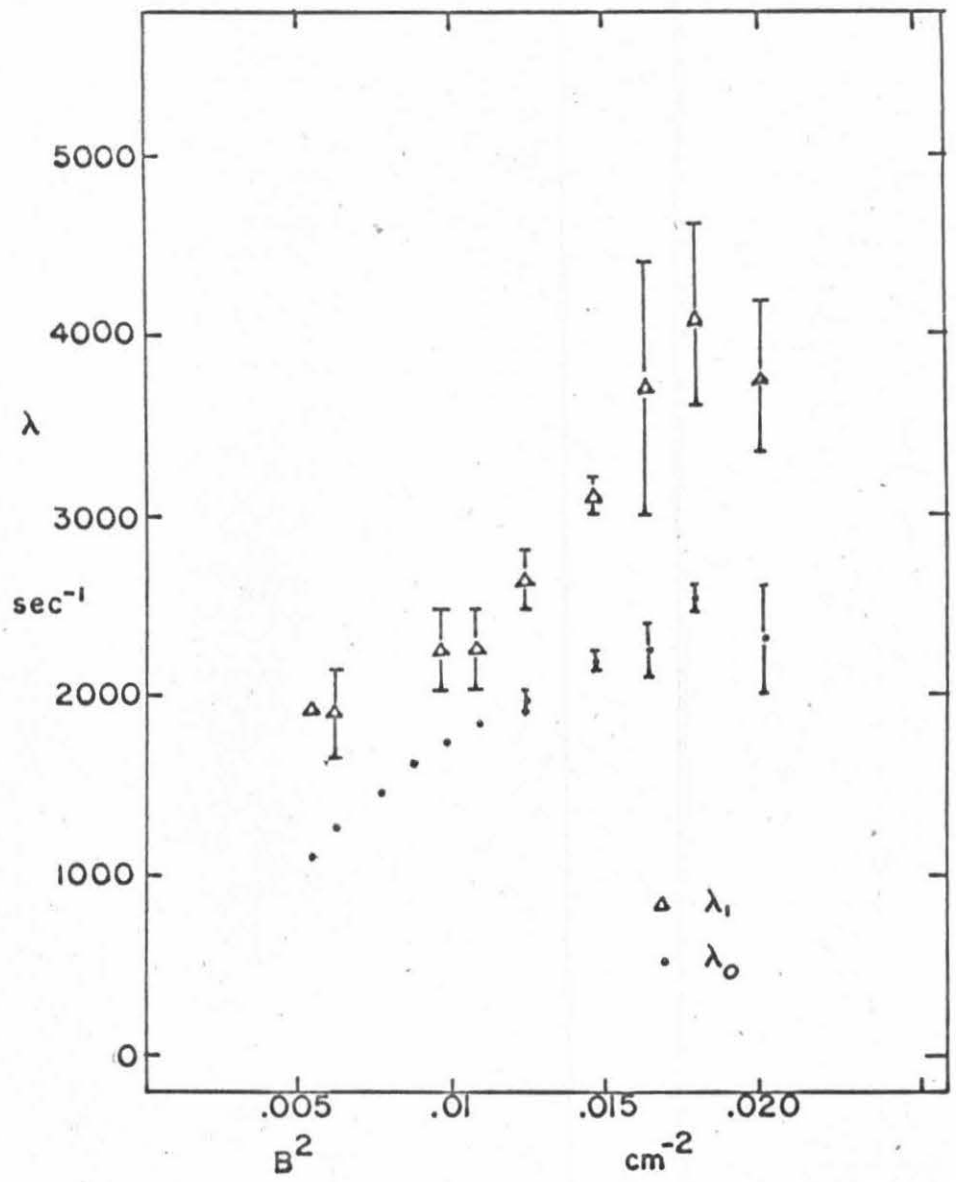

Figure II-1. The Results of Shapiro[70] for Fitting Two Exponentials to the Decay Data.

the inelastic coherent contribution to the total cross section in a kernel to compute λ_* as 1811 sec^{-1}. However, the theoretical models of the scattering kernel are not very accurate in the sub-Bragg energy region, so that the theoretical values for λ_* are just first order estimates. The work of Shapiro,[70] in which he describes the decay of the detector response by a sum of two exponentials, gives an experimental estimate of λ_* in the neighborhood of 1800 sec^{-1}. As mentioned in Chapter I, Bull et al.[29] have estimated to be 1600 sec^{-1} based on their experiments. Corngold and Michael[51] used a perturbation theory solution due to Takahashi[52] to obtain an upper bound on C based on the 2600 sec^{-1} value for λ_*. Their expression

$$C < \frac{1}{|\lambda_*|} \left[< 0 \,|\, (vD(v))^2 \,|\, 0 > - \{ < 0 \,|\, vD(v) \,|\, 0 > \}^2 \right] \qquad \text{(II-1)}$$

can be inverted and an experimental value supplied for C to yield a bound for λ_*. If we use C due to Hanna and Harris,[28] λ_* is bounded above by 1735 sec^{-1}.

Information about the value of λ_* is not readily available from the experiments designed to determine the diffusion parameters, for the data one collects in those experiments is specifically geared to the determination of an asymptotic decay constant. The value of the decay constants can be determined extremely accurately from data which is much less detailed than one needs to detect subtle changes in the fitted value of the decay constant

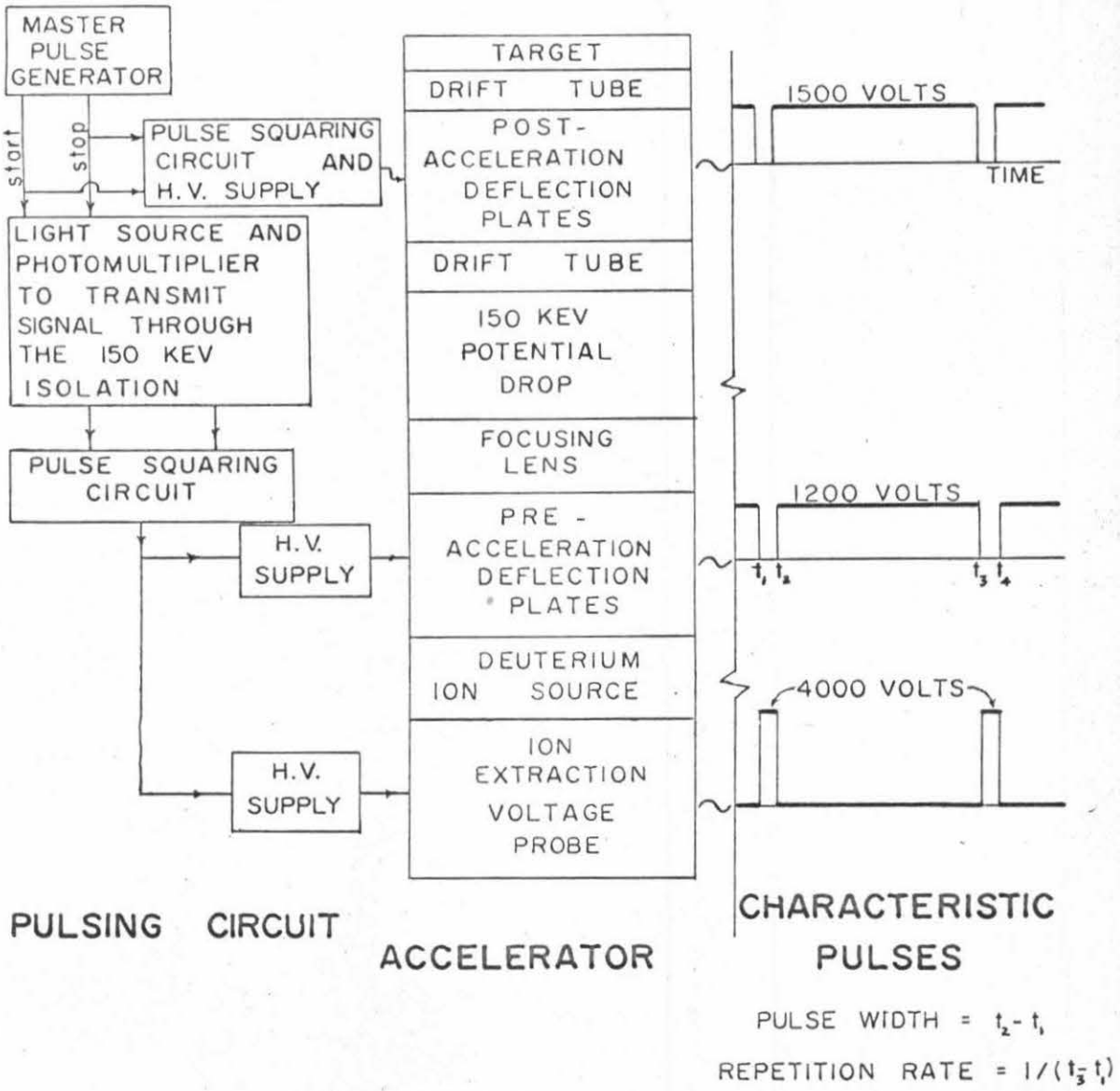

Figure II-2. Block Diagram of the Pulsing System.

at increasing times after the source burst. Hüls[53] has obtained some very recent data of fine time mesh and for very long times after the experiment which indicate non-exponential decay in his graphite for a buckling of .006723 cm^{-2} (decay constant about 1350 sec^{-1}) for times greater than 6.5 milliseconds after the source burst. The data we have obtained at Caltech is in minor disagreement with that of Hüls. Our data indicate λ_* in the neighborhood of 1600 sec^{-1}, which corresponds approximately to a buckling of .0085 cm^{-2}.

Unfortunately, values of B_*^2 corresponding to λ_*, will vary from experiment to experiment due to variations of up to 10 percent in the density of the graphite. To facilitate future discussion, we shall define a critical buckling, $B_c^2 = .0085\ cm^{-2} \sim B_*^2$, and give other values of B^2 in units of B_c^2.

A. Apparatus

Neutrons were produced for this experiment with a Texas Nuclear Corporation model 9505 neutron generator, which is a 150 KEV linear accelerator. High energy (14.7 MEV) neutrons result from the T(d, n) reaction as deuterium ions are accelerated into a tritum target.[54]

$$_1H^2 + {}_1H^3 \rightarrow ({}_2He^5) \rightarrow {}_0n^1 + {}_2He^4 + 17.6\ MEV\ . \quad (II\text{-}2)$$

The tritium targets consist of five curies/in^2 of tritium coated on a copper disc. Some neutrons are also produced by the D(d, n)

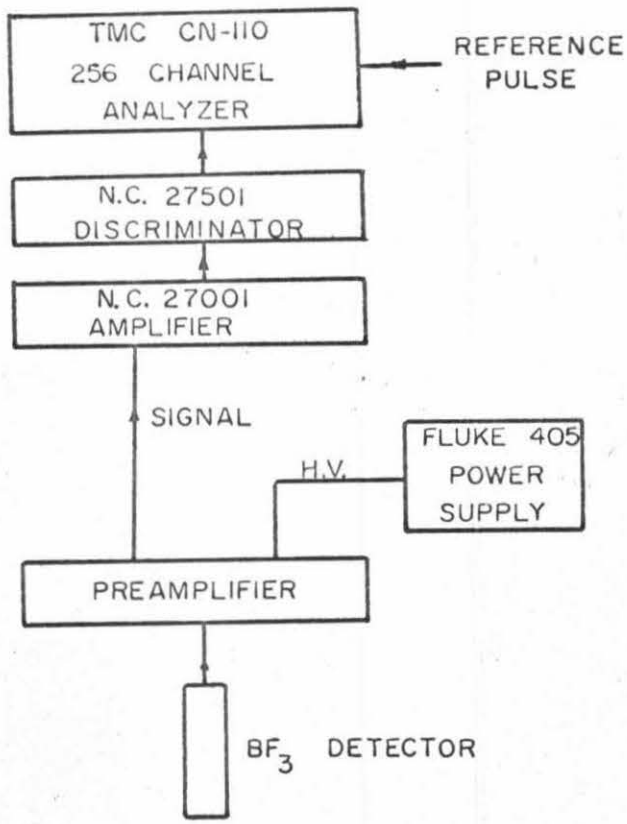

Figure II-3. Block Diagram of the Detection System

reaction,

$$_1H^2 + {}_1H^2 \rightarrow ({}_2He^4) \rightarrow {}_0n^1 + {}_2He^3 + 3.25 \text{ MEV} \qquad \text{(II-3)}$$

because of the residual deuterium gas in the accelerator system. The system is capable of producing more than 10^{11} neutrons/second at a maximum beam current of one milliampere.

The system is capable of producing source pulse widths which are continuously variable from one microsecond to 10^4 microseconds and repetion rates continuously variable from 10 to 10^5 pulses per second. The standard system is equipped with pre-acceleration and post-acceleration deflection plates to prevent the ion beam from reaching the target between pulses. The deuterium ions are transferred from the deuterium plasma bottle to the focusing and accelerating section by means of an "extraction potential" of three to five kilovolts. The unique feature of our accelerator was the addition of a pulsing unit to the extraction voltage. The "dark current" at the target between pulses was virtually eliminated, within detectable limits, with this triply pulsed system.

The thermal neutron detectors were standard one inch diameter, BF_3 (96% B^{10} enriched) filled proportional counters, with an active length of about 4 inches. Both Reuter-Stokes detectors with 70 cm Hg filling pressure and Nuclear Chicago detectors with 40 cm filling pressure were used. DC power was supplied by a model 405 Fluke power supply. Detector pulses were

amplified by a preamplifier and a Nuclear Chicago model 27001 linear amplifier and fed into a model 27501 Nuclear Chicago integral discriminator.

The heart of the data collection system was the Technical Measurement Corporation model CN-110 256 channel pulse analyzer system with the model 212 pulsed neutron logic unit. The reference time for the TMC multi-channel analyzer was the end of the pulse from the TNC pulsing system. After an adjustable waiting time, counts from the discriminator were accepted and allocated to the time channels of widths adjustable in non-equal discrete steps from 10 to 2560 microseconds. A storage time of 10 microseconds was required after each analysis channel. The time interval covered in each experiment was sufficient to allow about 100 channels for an accurate determination of the background. Data were printed out after each 50,000 pulses in order to minimize wasting data due to transient, external electronic problems.

Nuclear grade graphite from the Hanford project was borrowed from the AEC for use in this experiment. Most of the graphite stacks were formed from blocks of dimensions 3.75" x 3.75" x 12". The stacks ranged in size from 12" x 15" x 15" to 36" x 26.25" x 26.25" corresponding to bucklings in the range .018 cm^{-2} to .0051 cm^{-2} or (2.12 to 0.6) B_c^2. Temperature in the graphite was maintained at 21 $\pm$ 2°C. The average density of the stacks was 1.709 $\pm$ .003 grams/cm^3.

The graphite was shielded from room-return neutrons by

a cover of 0.03 inch cadmium sheet and 0.25 inch thick boral plate. The entire assembly, except for a slot allowed for the accelerator drift tube, was surrounded by 8.0 inch thick boxes of paraffin. It was found experimentally that this combination of shielding together with the triply pulsed accelerator allowed backgrounds of about one count per channel even for experiments of several million pulses lasting several days. There was a high energy component of the background for short times after the experiment with a fast decay constant ($\sim$ 5000 sec^{-1}), but the addition of the paraffin shielding reduced the amplitude significantly so that this contribution to the background had vanished by one-half millisecond after the pulse. Since the measuring times of interest in these experiments were greater than one millisecond, the transient background presented no problem. In the range 100 - 500 microseconds, the transient background contributed less than 0.01 percent of the total count rate.

B. Data Collection Procedure

The BF_3 detectors were placed inside the cadmium shielding on a side of the stack adjacent to the source target. For the smaller stacks, a single detector was centered on the adjacent face. For the three largest stacks ($B^2 \leq .747 B_c^2$), the four detector arrangements shown in Figure III-6 was used to help minimize the effect of the higher spatial harmonics. These detector arrangements are shown schematically in Figure II-4. Simple diffusion theory

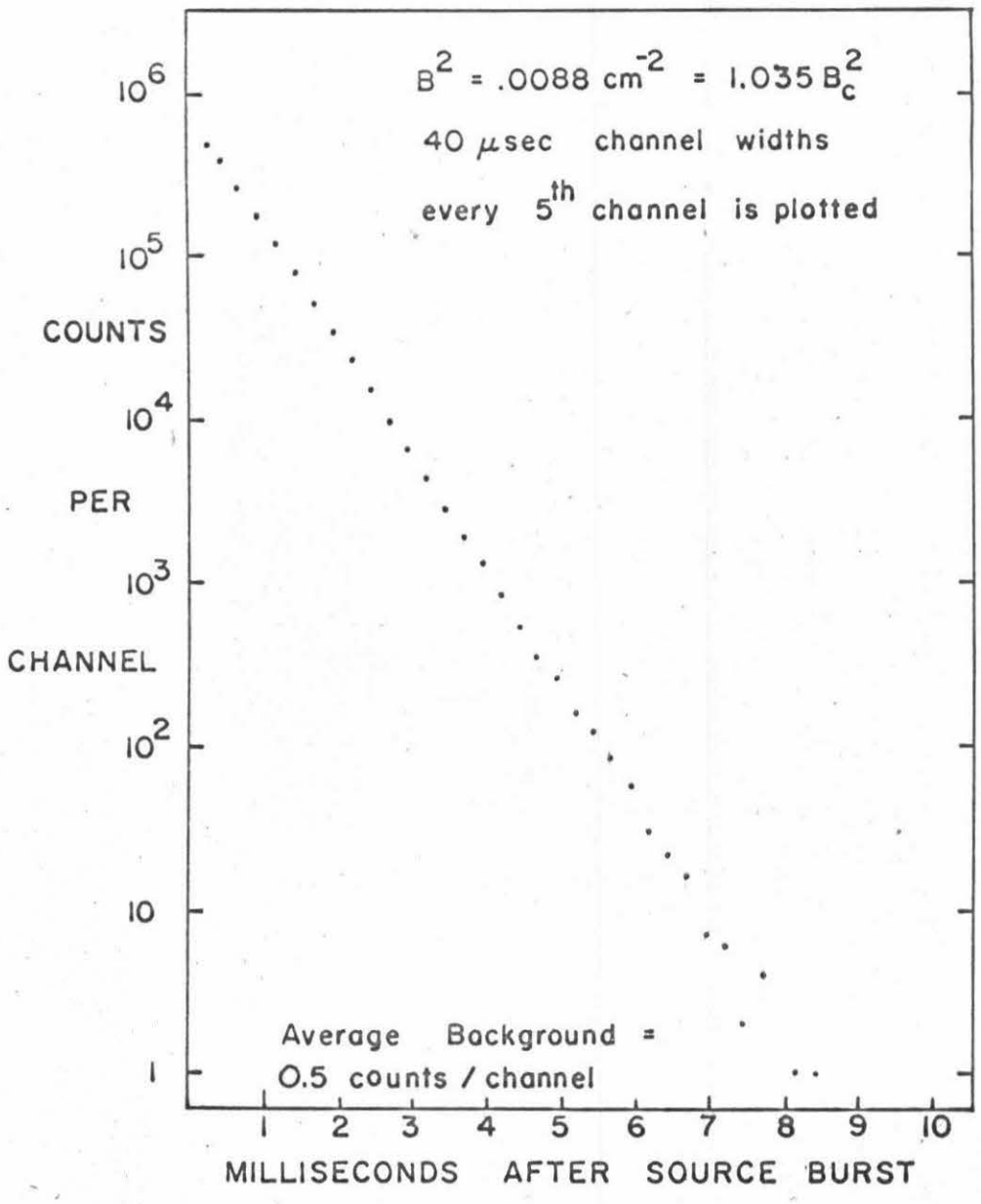

Figure II-4. Sample Multi-channel Analyzer Data

predicts that one can eliminate the most important higher spatial harmonics by clever placement of the source and the detectors.[9] However, the spatial dependence of the source is considerably complicated by the high energy albedo from the shielding material, which makes elaborate efforts to eliminate the spatial harmonics unjustified.

After a typical waiting time of 500 microseconds, the number of counts in each of 255 discrete time intervals of 40 or 80 microseconds was collected by the TMC multi-channel analyzer for each source burst. Except for the smallest two graphite stacks, good "statistics" were obtained for more than five milliseconds after the source burst. For stacks corresponding to $B^2 < 1.035 B_c^2$, the data were meaningful for more than nine milliseconds.

C. Data Analysis

The raw data was analyzed on the IBM 360/75 by two computer codes. The first was a modified version of the FRANTIC code[55] developed at the Massachusetts Institute of Technology Laboratory for Nuclear Science for analysis of exponential growth and decay curves. The second was a simple least squares program to fit the data to an exponential plus a constant background term.

The FRANTIC code corrects the raw data (C_i) from the i^{th} channel for detector dead time (τ) losses by the formula:[56]

$$C' = \frac{C}{1 - C\frac{\tau}{T}} \qquad \text{(II-4)}$$

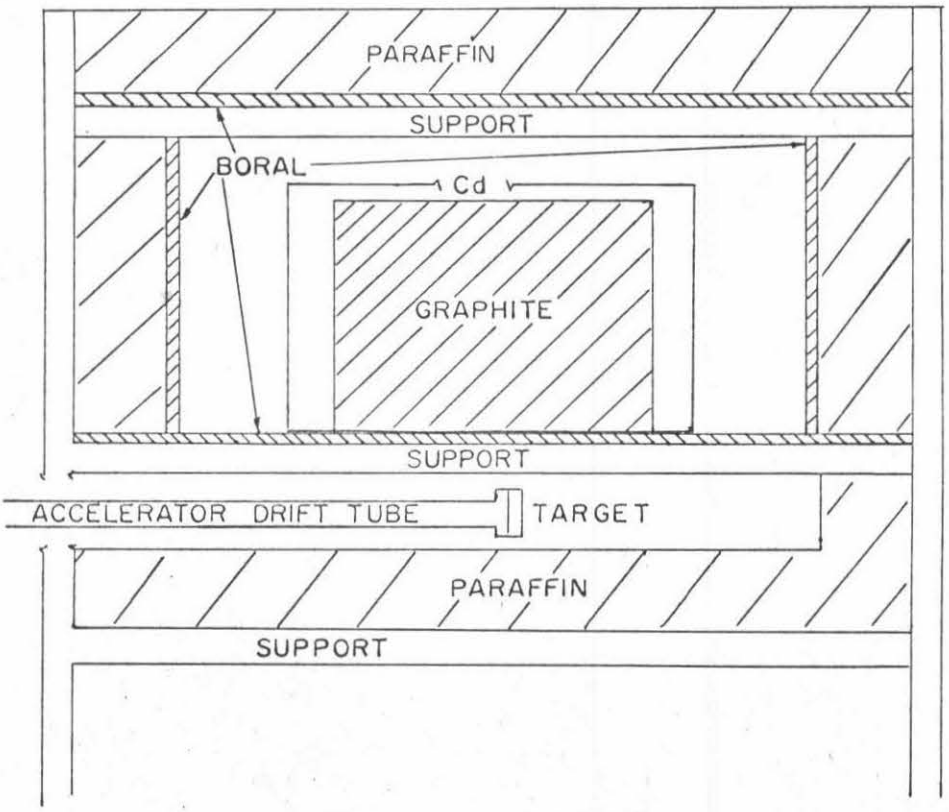

Figure II-5. Schematic of the Shielding System

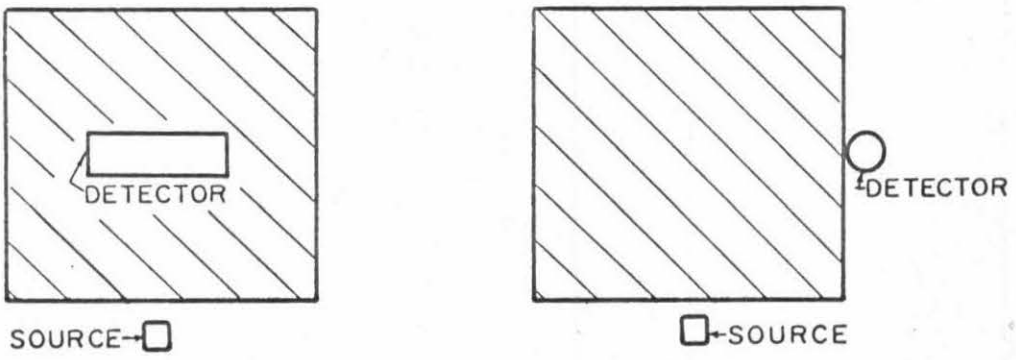

Figure II-6a. Schematic of the One Detector Arrangement

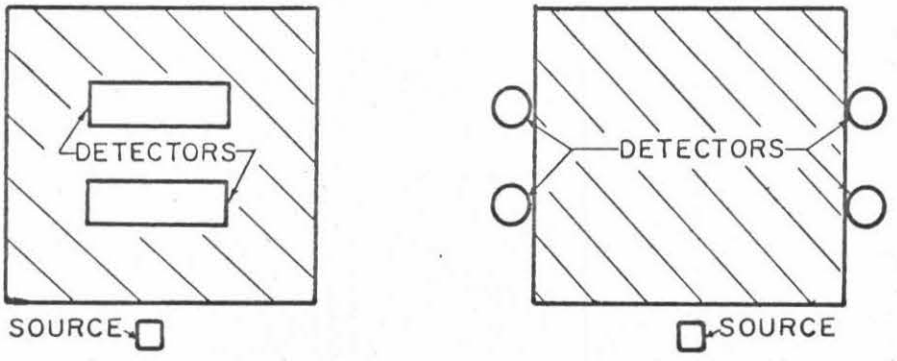

Figure II-6b. Schematic of the Four Detector Arrangement for Large Assemblies

T, the total counting time, is the product of the channel width and the number of pulses. The corrected data are forced to fit the form

$$C'(t) = \sum_{j=1}^{K} A_j e^{-\lambda_j t} \qquad \text{(II-5)}$$

where the number of components K is variable from one to ten. Any of the parameters A_j, λ_j may be held fixed during the fitting procedure. The free parameters are determined by minimizing the variance

$$\text{VARIANCE} = \frac{1}{D} \sum_{i=m}^{n} Wi \left[C_j' - \sum_{j=1}^{K} A_j e^{-\lambda_j t_i} \right]^2 \qquad \text{(II-6)}$$

over channels n through m. D is the number of degrees of freedom which is equal to total number of channels used in the fit less the number of parameters being fit. The time associated with each channel is t_i. The weighting function w_i is set equal to the estimated variance in the data C_i. The minimizing procedure is iterative because of the way that λ_j appears in the expression. The background is fit by fixing λ_m equal to zero. The output includes the parameters A_j, λ_j, the variance of fit, and a chi-squared analysis. Giraudbit[57] gives a more complete description of the modified FRANTIC code.

FRANTIC was used to fit two exponential components plus a background term to the data. For the large stacks ($B^2 < B_c^2$), the amplitude of the component with the larger λ became small

enough to make the fitting procedure difficult. For the largest stacks, the amplitude was negative, which made the interpretation difficult because of possible contamination of the data by higher spatial modes. The data were then fit to one exponential plus background over the entire 255 channels and the process repeated, each time dropping the initial five channel of the preceeding fit. This yielded a "deletion profile" which is a common method of analysis for this type of experiment. One examines the λ's obtained in this process to see if they become constant after some waiting time following the source burst.

The second code, FITIT, performed analysis which could have been done with FRANTIC, but was more specialized and required less running time on the computer with much simpler input and output. The data was corrected for dead time losses and the background, obtained from the FRANTIC runs, was subtracted. The corrected data was then described by a single exponential term

$$C_i' \sim A e^{-\lambda t_i} \quad . \tag{II-7}$$

By taking the logarithm of the data, a linear least squares fit could be performed.

$$F_i = \log(C_i') \; ; \quad D = \log(A) \quad . \tag{II-8}$$

The function $L(D, \lambda)$,

$$L(D, \lambda) = \sum_{i=n}^{m} W_i \left[F_i - D + \lambda t_i \right]^2 \tag{II-9}$$

was minimized by setting the derivatives with respect to D and λ equal to zero. This results in two linear, coupled equations for D and λ .

$$\left(\sum_{i=n}^{m} W_i\right) D - \left(\sum_{i=n}^{m} W_i t_i\right)\lambda = \sum_{i=n}^{m} W_i F_i$$

$$- \left(\sum_{i=n}^{m} W_i t_i\right) D + \left(\sum_{i=n}^{m} W_i t_i^2\right)\lambda = \sum_{i=n}^{m} W_i t_i F_i \quad . \tag{II-10}$$

Thus, λ appears as the quotient of sums of known quantities.

$$\lambda = \frac{\left(\sum_{i=n}^{m} W_i\right) \cdot \left(-\sum_{i=n}^{m} W_i t_i F_i\right) + \left(\sum_{i=n}^{m} W_i t_i\right)\left(\sum_{i=1}^{m} W_i F_i\right)}{\left(\sum_{i=n}^{m} W_i\right) \cdot \left(\sum_{i=n}^{m} W_i t_i^2\right) - \left(\sum_{i=n}^{m} W_i t_i\right)^2} \quad . \tag{II-11}$$

The fit was taken over four to twelve channels, depending on the "statistics" of the data in the particular time region of the fit. In this manner, the effective decay constant, $\lambda_{eff}(t)$, was determined as a function of time after the source burst. Fitting the data with this procedure exhibited the tendency of the decay constant to decrease better than the "deletion profile technique." This procedure requires that the effective decay constant change very little over the range of the fit, hence the data must be reasonably detailed and the counting statistics good over a long

time interval after the burst in order to insure an accurate fit. The background should be insignificant so that the corrected data do not suffer from uncertainties in the background.

D. Results

The results of these experiments on ten graphite stacks indicate that a range of buckling exists where the decay is described by a well defined exponential over most of the measuring interval and another range in which the decay of the neutron population is definitely non-exponential. The two ranges are joined by a region of buckling in which the decay constant appears to establish a plateau for a portion of the measuring time, but for later times the fitted value of $\lambda_{eff}(t)$ appears to drift toward a lower value. These trends are shown on the graphs of $\lambda_{eff}(t)$ on the following pages.

The results may be summarized as follows: For $B^2 < 1.035B_c^2$, no monotonic downward drift of the measured decay constant was noted over any significant range of the measurement period from two to nine milliseconds. The apparent increase in λ_{eff} after 6 milliseconds in $0.747\,B_c^2$ and $0.905\,B_c^2$ was independent of the detector placement. For the range $1.165B_c^2 < B^2 < 1.471B_c^2$, a reasonable decay constant can be assigned to the systems, but there exists a perceptible decrease in the fitted decay constant. For the systems with $B^2 > 1.741B_c^2$, the decay was definitely non-exponential over the whole range of fit. Table II-1 lists the

TABLE II-1

BUCKLING	λ_{eff}(2.0 milliseconds)	% DRIFT IN λ_{eff}(>2.0 msec.) PER MILLISECOND (±50%)
1.165 B_c^2	1830 sec^{-1}	2.6
1.318 B_c^2	1956 sec^{-1}	1.7*
1.471 B_c^2	2231 sec^{-1}	4.0
1.741 B_c^2	2466 sec^{-1}	8.0
1.941 B_c^2	2873 sec^{-1}	13.4
2.118 B_c^2	2909 sec^{-1}	17.7

* value obtained from the "deletion profile" curve.

The apparent drift in the decay constants for times greater than two milliseconds for those stacks where any monotonic drift was perceptible.

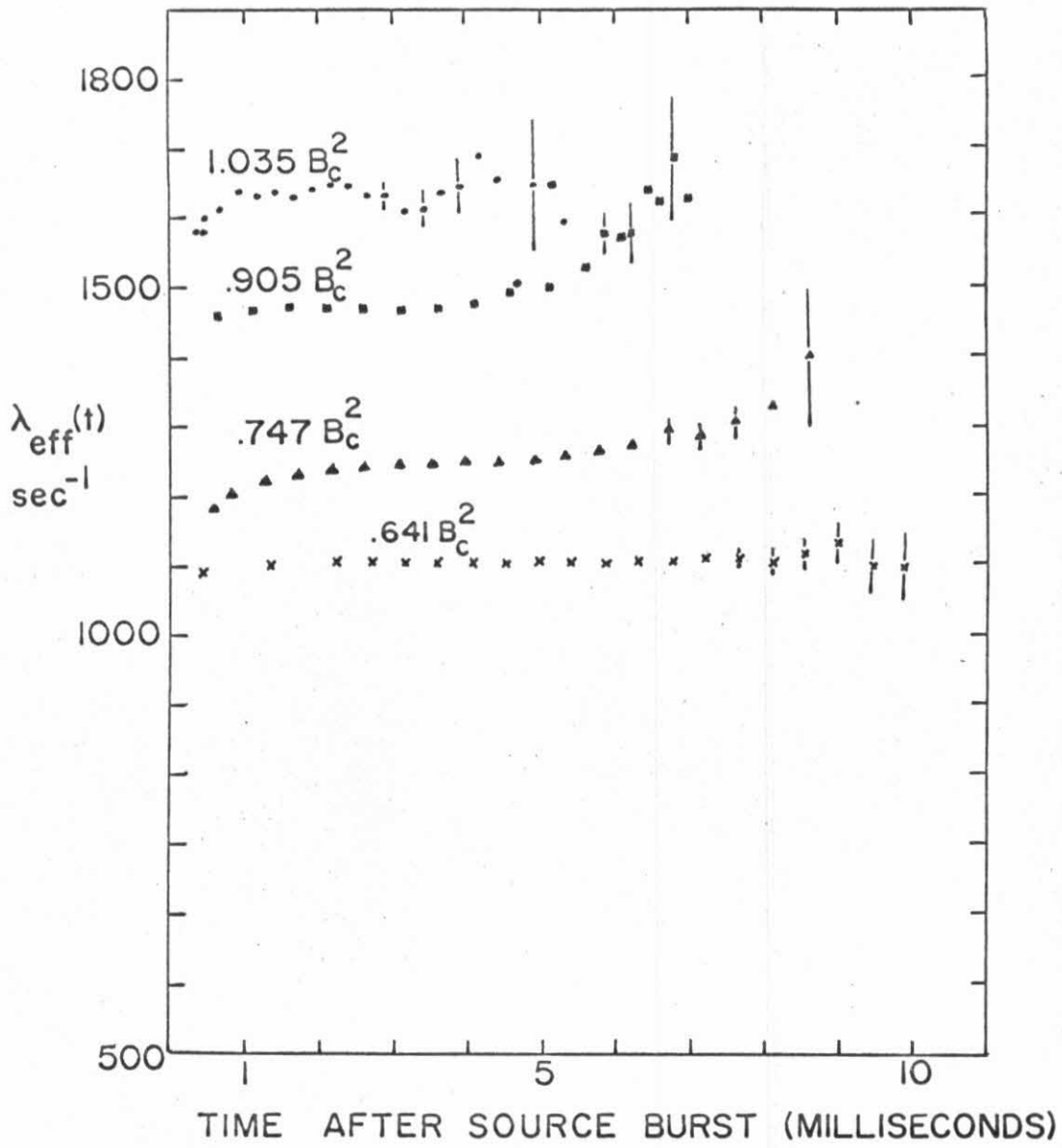

Figure II-7. Effective Decay Constants for the Four Largest Graphite Stacks.

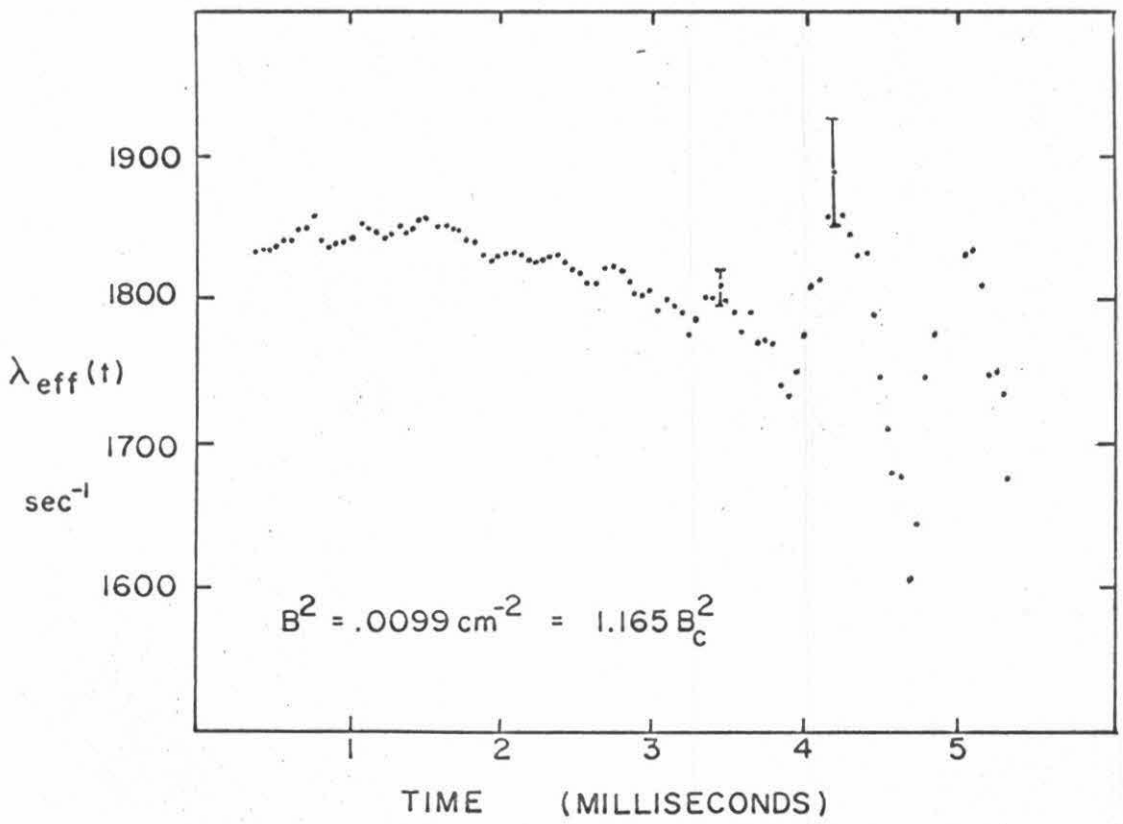
1900
1800
$\lambda_{eff}(t)$
1700
sec^{-1}
1600
$B^2 = .0099\ cm^{-2} = 1.165\ B_c^2$
1
2
3
4
5
TIME (MILLISECONDS)

Figure II-8.

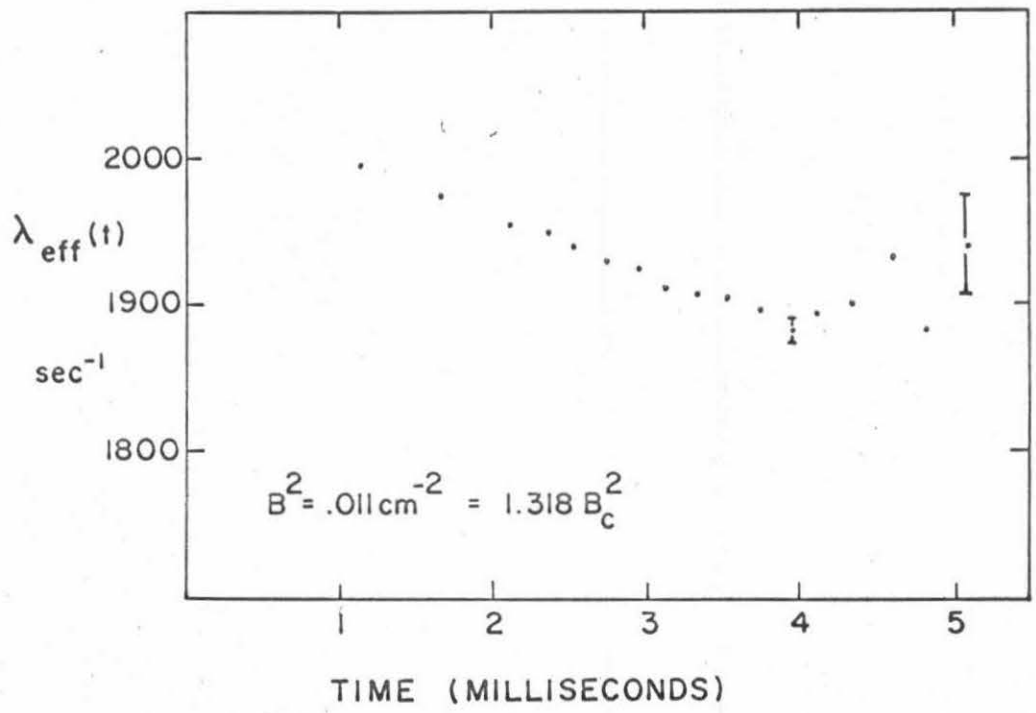

Figure II-9. Deletion Profile

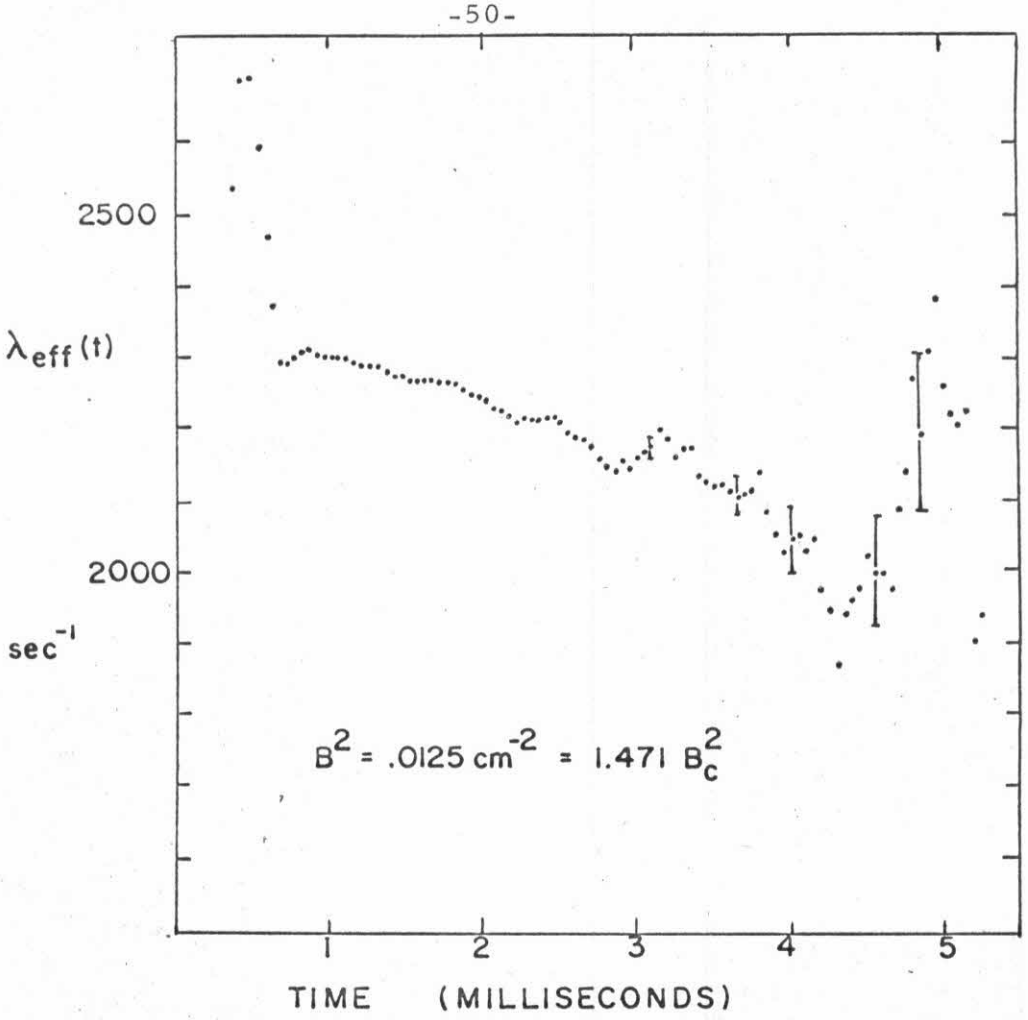
2500
2000
$\lambda_{eff}(t)$
sec^{-1}
$B^2 = .0125\ cm^{-2} = 1.471\ B_c^2$
1
2
3
4
5
TIME (MILLISECONDS)

Figure II-10.

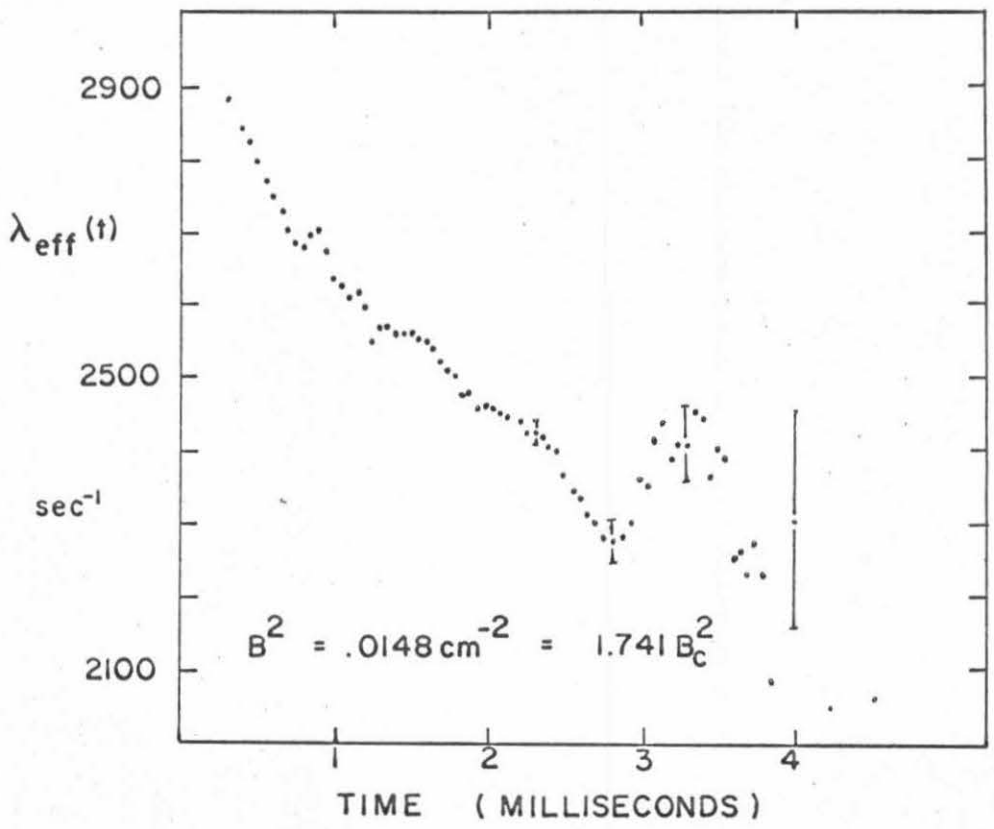
2900
2500
2100
$\lambda_{eff}(t)$
sec^{-1}
$B^2 = .0148\,cm^{-2} = 1.741\,B_c^2$
1
2
3
4
TIME (MILLISECONDS)

Figure II-11.

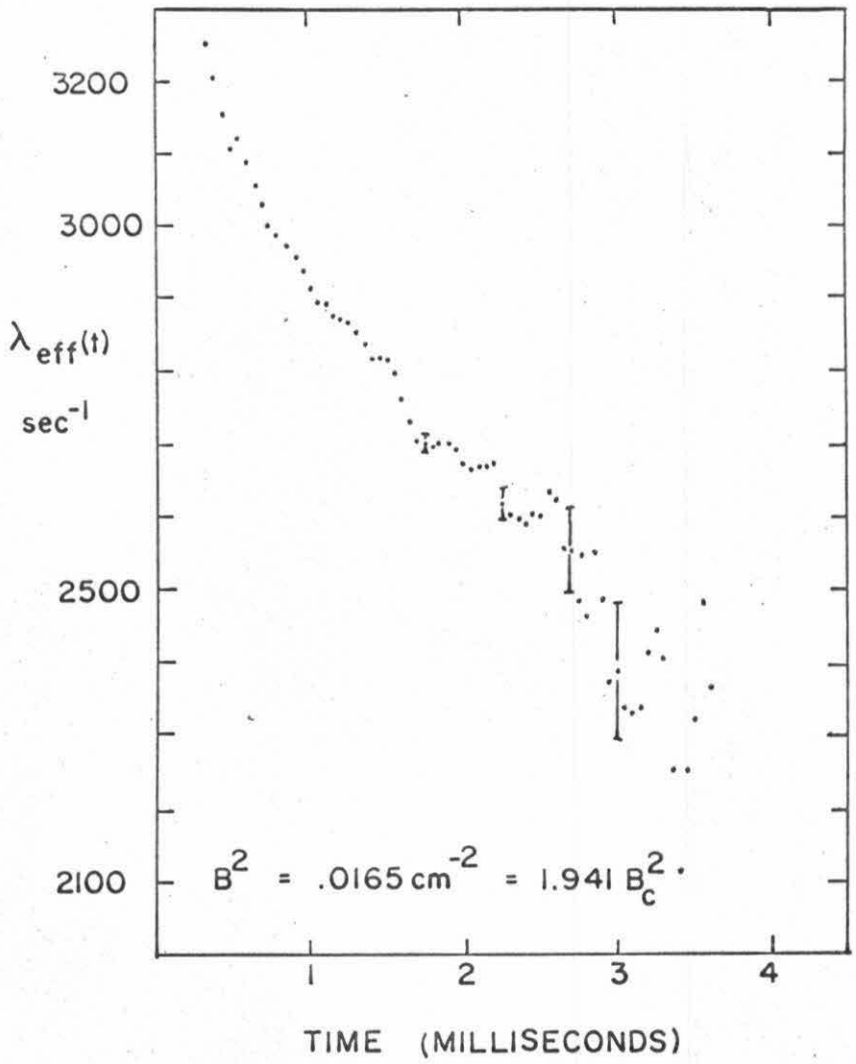
3200
3000
$\lambda_{eff(t)}$
sec^{-1}
2500
2100
$B^2 = .0165\,cm^{-2} = 1.941\,B_c^2$.
1
2
3
4
TIME (MILLISECONDS)

Figure II-12.

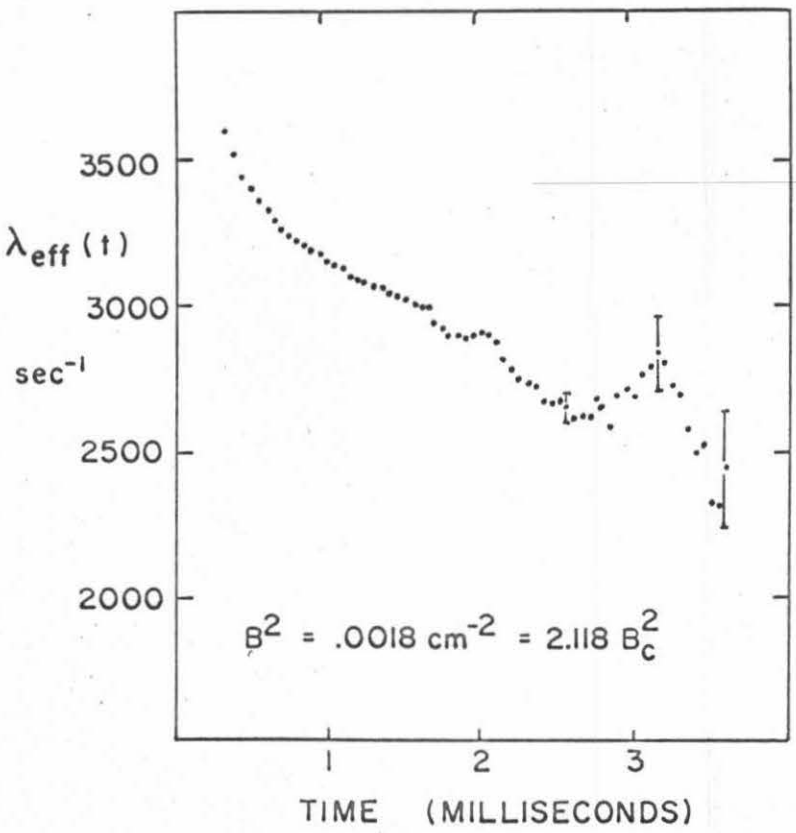
3500
λ_{eff} (t)
3000
sec^{-1}
2500
2000
B^2 = .0018 cm^{-2} = 2.118 B_c^2
1
2
3
TIME (MILLISECONDS)

Figure II-13.

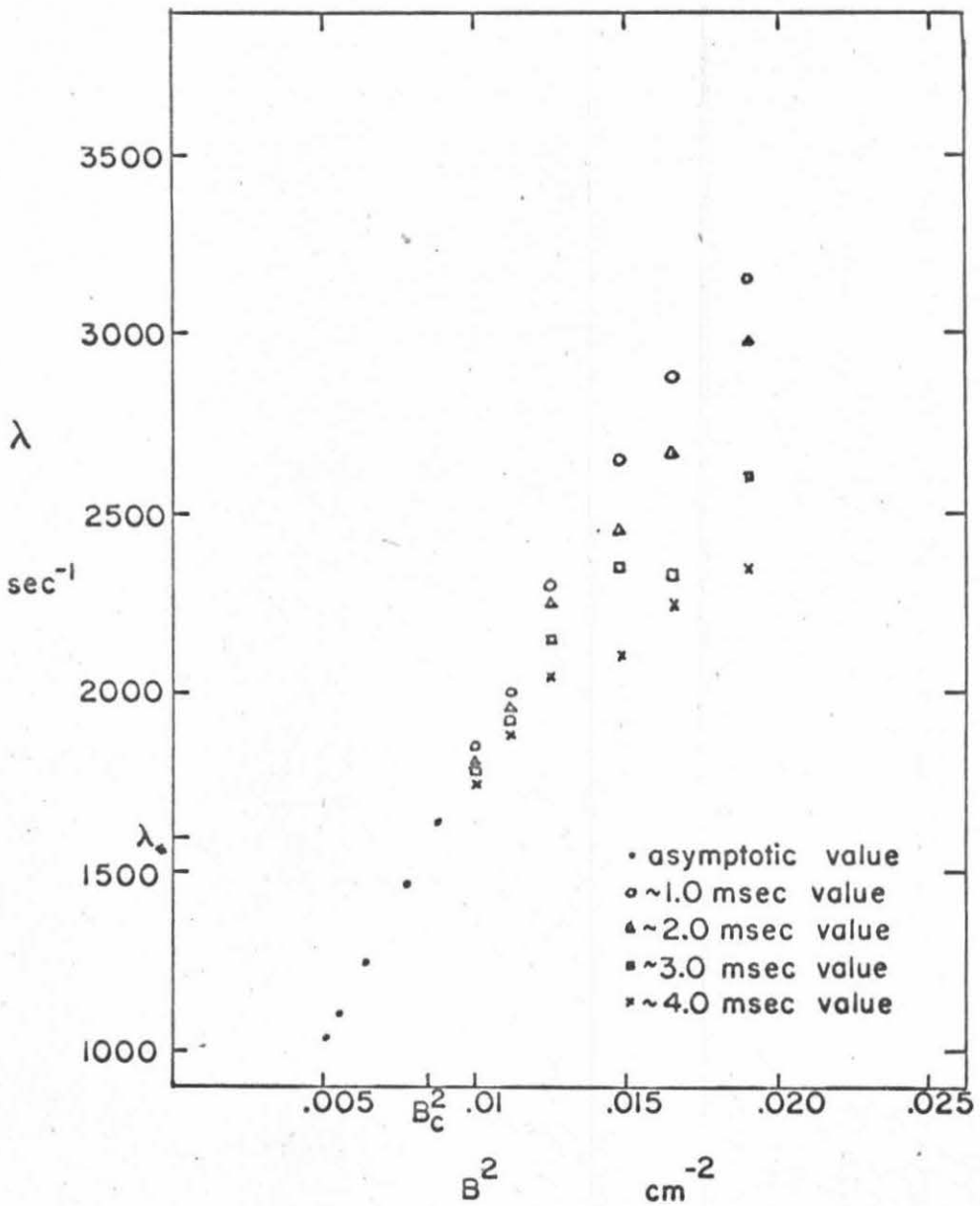

Figure II-14. The Experimental Dispersion Curve.

percent change per millisecond of the pseudo-exponential and the non-exponential decays.

The effective decay constants all exhibit oscillations for long times after the source burst. These oscillations, which have been observed by other experimenters, are as difficult to explain as they are interesting. One proposed explanation has been that the oscillations were related to channel drift for the time - of - flight units which were used in the multi-channel analyzers.[58] However, use of pulsed neutron logic units, which are not subject to significant channel drift, in modern experiments has apparently negated this argument. One still entirely plausible explanation is that the oscillations are inherently connected to the fitting procedure when the counting statistics fall below some critical value.

Since the nature of the oscillations has not been positively identified, let us consider a more interesting conjecture. If we re-examine the analysis of Conn and Corngold,[15] we see that the transform plane has branch points with imaginary parts equal to $\pm iBv_B$, where v_B is the Bragg velocity. For $B^2 = 0.747B_c^2 = 0.00635\ cm^{-2}$, the frequency Bv_B is about 4640 sec^{-1}, while the frequency of the oscillations in the fit, though poorly defined, is about 3600 sec^{-1}. For $B^2 = 1.165B_c^2 = 0.0099\ cm^{-2}$, the approximate frequency of oscillation is 8970 sec^{-1}, while Bv_B is about 5900 sec^{-1}. The correlation at the other bucklings is also "ballpark" considering the crudeness of the data. The data of

Hüls[53] exhibit these oscillations in the same range of buckling with about the same frequencies. The onset of the oscillations occurs at about the same time after the source burst although the counting statistics and the width of the channels are quite different for the two sets of data.

The frequency of the oscillations cannot be resolved well enough to draw any definite conclusions, but the above speculation is interesting. While the oscillatory behavior appears rather naturally in the theoretical solutions, the physical interpretation has not been suggested. If the oscillations are not some quirk of the data collection and analysis, this question will have to be given some more consideration.

III. MEASUREMENT OF TIME DEPENDENT SPATIAL DISTRIBUTION

The time dependent detector response was measured as a function of one spatial dimension for four graphite stacks varying in size from 66.68 cm X 66.68 cm X 91.44 cm to 47.63 cm X 28.58 cm X 60.96 cm, representing the buckling range 0.6 B_c^2 to 1.847 B_c^2. The largest dimension of the stack was arranged so that it was colinear with the direction of the ion beam in the accelerator drift tube. The measurements were made along the central axis in order to accentuate only those higher spatial harmonics in the measured direction. We measured the higher order decay constants associated with the spatial harmonics and we isolated the fundamental spatial mode and examined it in detail. Measurement of the extrapolation length Z_o for these assemblies as a function of time after the source burst was also made.

A. Experimental Apparatus and Procedure

The experimental equipment was basically the same as that described in Chapter II for the measurement of effective decay constants. The principal difference was that the source strength, which varied considerably over the measuring times of 75 to 125 hours, had to be monitored in order to normalize the data taken at different detector positions. The source monitor detector was a thermal neutron (BF_3) detector identical to the one used to measure the distribution in the graphite stack. The monitor detector was

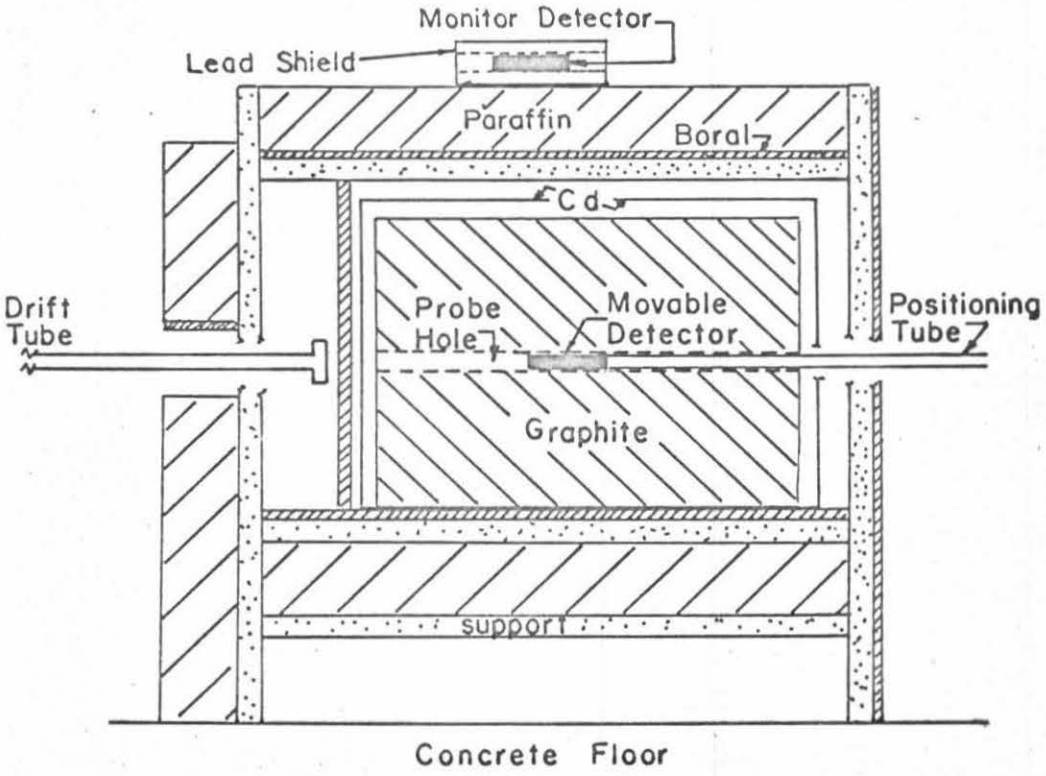

Figure III-1. Experimental Arrangement

placed in a lead gamma ray shield above the graphite-paraffin system. It required an extra preamplifier, amplifier, discriminator, and scaler system, but the high voltage was taken from the same supply that fed the in-stack detector in order to minimize systematic error due to voltage variation between the two detectors. The amplifier-discriminator systems for the two detectors were housed in the same modular power supply to help reduce the systematic error due to relative drift in the power supplies. The problem of normalizing the source strength without introducing significant systematic error makes these experiments about an "order of magnitude" more difficult than the effective decay constant measurements.

We examined the time response of the monitor detector with the multi-channel analyzer. Less than ten percent of the total monitor count was accumulated during the source pulse and the following 200 microseconds. The effective decay constant of the monitor count rate was about 820 reciprocal seconds and the amplitude was sufficiently low enough that there were no saturation problems or significant dead time losses. The normalization by this monitoring system was found to be consistently repeatable to within about 1.5σ, where σ is one standard deviation based on the Poisson statistical uncertainty in the counting rates only.

The source strength was also monitored by the high energy (14 MEV) neutron induced $O^{16}(n, p)N^{16}$ reaction in the cooling water of the tritium target source. The N^{16} decays with a 7.4 second half life and gives off a high energy gamma ray. The cooling water

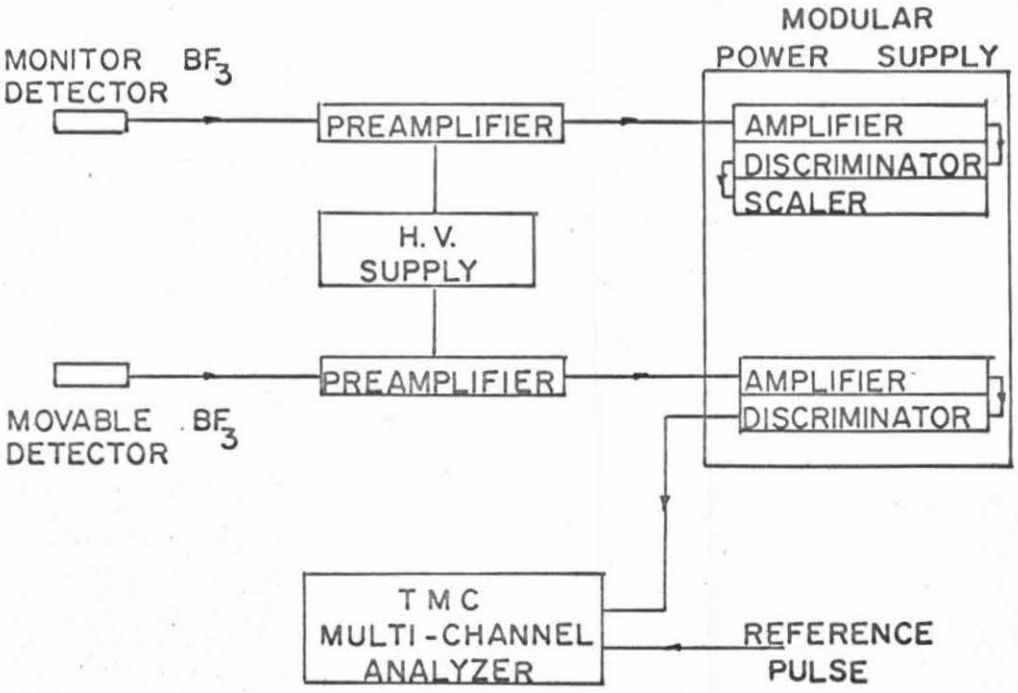

Figure III-2. Block Diagrams of the Detector System

returning from the target was passed around a Geiger tube, well shielded by lead and concrete, and the N^{16} gamma was detected. This system, which was sensitive only to neutrons at the source energy and therefore rather insensitive to any changes in the external environment, was superior to the other monitoring system in principle. However, due to the short half life of the reaction product, it was necessary to regulate the flow rate of the water very accurately. This problem, as well as a high gamma background due to other reactions and an intrinsically low counting rate, made this procedure quite difficult in practice. The first system proved more accurate and was used to normalize the data from these experiments.

The detectors used in the experiments had an active length of about four inches. The movable detector was positioned in the stack by a thin-walled aluminum tube. The 1.1 inch diameter probe hole for the movable detector was co-linear with the accelerator drift tube and target. As shown in Figure III-3, a small collimated beam of thermal neutrons was used to determine the sensitivity of the movable detector as a function of the position in the active volume. The most sensitive position was in the center of the active volume and the sensitivity could be approximately described by

$$S(Z) = 0.0842 + 0.0222 \sin\left(\frac{\pi Z}{10.16}\right) \qquad \text{(III-1)}$$

where Z is the distance in centimeters from one end of the active volume. The location of the detector in the stack was defined to be

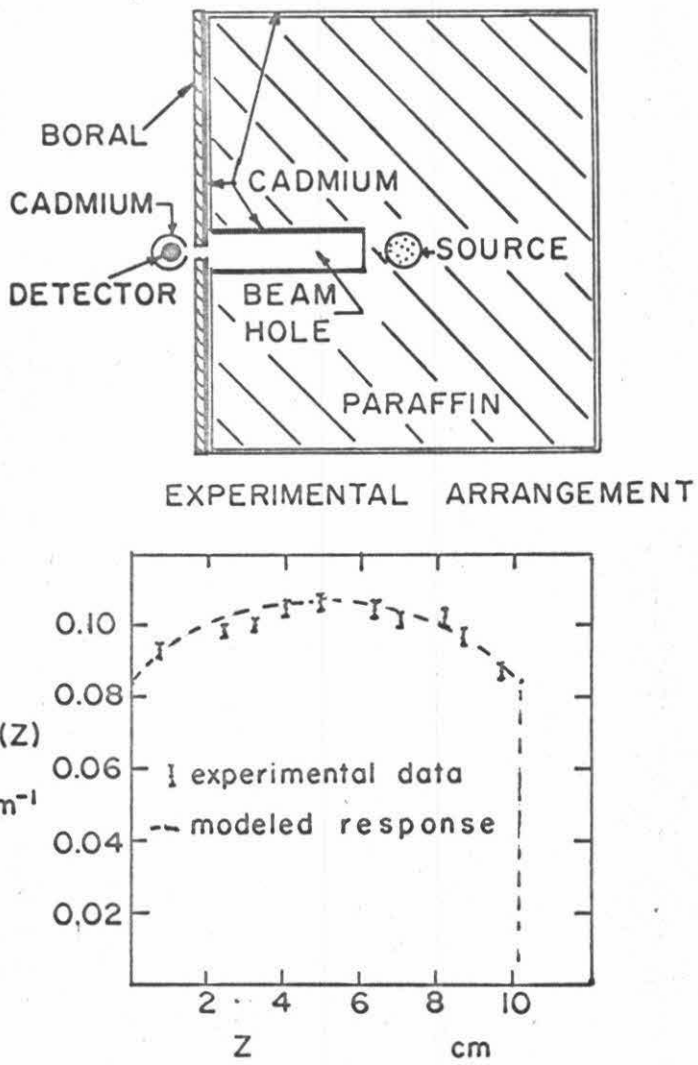

Figure III-3. Schematic of Experiment to Determine Relative Sensitivity in the Detector and Graph of the Results

the position of the center of the active volume, except for calculations in which we specifically accounted for the finite detector volume.

The analysis of the experiment explicitly assumes a diffusion theory solution for the spatial distribution of the neutron density:

$$n(\underline{r}, t) = \sum_{j,k,m} A_{j,k,m}(t) \sin\left(\frac{j\pi x}{a+2Z_o}\right) \sin\left(\frac{k\pi y}{b+2Z_o}\right) \sin\left(\frac{m\pi z}{c+2Z_o}\right) . \qquad \text{(III-2)}$$

(The quantities a, b, and c are the dimensions of the graphite stack.) Since the detector response is only measured in the z direction, one has to be certain that the distribution in the transverse directions is adequately described by the fundamental mode, that is, $j = k = 1$. To check this, we irradiated thin, coin-shaped, cadmium-covered indium discs spaced 3.75 inches apart along the three axes of the graphite volume ($B^2 = 0.00635\ cm^{-2} = 0.747\ B_c^2$) with the steady state 14 MEV neutron source. The cadmium shielded the indium absorbers from the thermal neutron population, therefore the indium foils were activated by the epithermal neutrons, principally neutrons captured in the 1.46 ev resonance of the indium cross section. The foils were spaced far enough apart so that there was no significant neutron density depression at the site of one foil due to the strong absorption in another foil. After about two hours of activation, the beta decay rate of the indium foils was counted in a gas flow proportional counter. These data yielded rather directly the relative

amplitude of the epithermal neutron density at each of the points of activation.

Though it is the spatial distribution of the thermal neutrons which is of interest in the pulsed experiments, the distribution of the epithermal neutrons represents a worse case as far as the relative amplitude of the higher spatial harmonics is concerned. The slowing down time to 1.46 ev for 14 MEV neutrons in graphite is less than 30 microseconds,[39] while the (non-existent) thermalization time is of the order of 500 microseconds.[38] The significance is that the epithermal distribution has less chance to relax to an asymptotic distribution, hence the higher spatial harmonics are enhanced.

A function of the form of III-2, with no time dependence, was least-squares fit to the activation data in order to obtain the relative amplitudes of the coefficients A_{jkm}. The results for the 1.46ev neutron distribution, with the source adjacent to one face of the stack in the center of the x-y plane, are:

TERM	$\lvert A_{jkm}/A_{111}\rvert$
A_{211}	0.0096 ± 0.0011
A_{311}	0.0521 ± 0.0011
A_{121}	0.0056 ± 0.001
A_{131}	0.0508 ± 0.001
A_{112}	0.579 ± 0.001
A_{113}	0.139 ± 0.001

Hence, the only harmonics with significant amplitude are in the z direction as was desired. The non-zero amplitudes of the coefficients A_{211} and A_{121} are due to the skew-symmetric, high energy albedo from the surrounding shielding.

It should be pointed out that the analysis of these experiments assumes that the detector response is an integral over the neutron distribution function of the form

$$D_r(Z,t) = \int_o^\infty v\Sigma_d(E)\, n(Z,E)\, dE \quad , \qquad \text{(III-3)}$$

while the actual measured detector response samples the neutron current in preferred directions due to the finite size of the detector and to the void channel in which the detector is located. We improved the experiment for the smallest stack (which should be the worst case) by filling the void with graphite plugs, but the neutron current was still not sampled isotropically because the detector appeared "thicker" to neutrons traveling in certain preferred directions. The results (see Table III-1) were insignificantly altered.

B. Analysis of the Data

Since the neutron distribution was only measured in one dimension, we effectively only considered terms in the expansion III-2 with j = k = 1. Therefore it is more convenient to consider the one dimensional expansion,

$$n(Z,t) = \sum_m A_m(t) \sin\left(\frac{m\pi Z}{c+2Z_o}\right) \quad . \qquad \text{(III-4)}$$

The analysis of the experiments was designed to determine the coefficients $A_m(t)$ and the extrapolation length Z_o, which was actually a function of time and buckling. Furthermore, the coefficients were assumed to have the form $A_m(t) = A_m e^{-\lambda_m t}$, and the decay comstamts λ_m were determined. The buckling associated with the spatial modes of the rectangular parellelepiped assemblies was prescribed by

$$B_m^2 = \left(\frac{\pi}{a+2Z_o}\right)^2 + \left(\frac{\pi}{b+2Z_o}\right)^2 + \left(\frac{m\pi}{c+2Z_o}\right)^2 . \qquad \text{(III-5)}$$

(See Chapter I.) The lowest value, B_1^2, is the buckling, B^2, used to identify the assemblies when the effective decay constants are measured as described in Chapter II.

The data were subjected to a three-fold analysis. First, the multi-channel data from each of the 12 - 15 spatial locations was corrected for dead time losses and background and fit to a function of the form $A_1 e^{-\lambda_1(Z_k)t} + A_2 e^{-\lambda_2(Z_k)t}$ by a simple computer code (PULSE). Then a harmonic analysis was done on the data from the spatial measurements for each of the time channels by another computer code (MYCODE), thus obtaining up to five of the coefficients $A_m(t_i)$ for fixed Z_o. MYCODE also fit the associated decay constants λ_m to the reduced data $(A_m(t_i), i=1, N)$. Finally, in a third code (LENGTH), Z_o and the coefficients A_m were treated as free parameters in fitting the data to the functional form III-4, so that Z_o was obtained as a function of time (or channel) for each graphite stack. The "best" value of Z_o was fed back

into MYCODE as a fixed parameter.

The first line of analysis, the PULSE program, was really uninteresting as far as the information obtained was concerned. The quantities $\lambda_1(Z_k)$ and $\lambda_2(Z_k)$ could not actually be identified as the decay constants associated with the coefficients A_1 and A_2 in the expansion III-4, but they did serve as a check on the reasonableness of the MYCODE results. The fitting procedure was in fact a little better than a graphical one. The long time ($t > \sim 3.0$ msec), background subtracted, dead-time loss-corrected data were least-squares fit to the function $A_1 e^{-\lambda_1(Z_k)t}$. Once A_1 and $\lambda_1(Z_k)$ were determined, an amount $A_1 e^{-\lambda_1(Z_k)}$ was subtracted from the short time data and this difference was fit to $A_2 e^{-\lambda_2(Z_k)t}$ by the least squares procedure. The data were weighted by the reciprocal of the statistical variance in the least squares procedure. The values $\lambda_1(Z_k)$, $\lambda_2(Z_k)$ obtained by this procedure were reasonably constant as a function of position in the stack, but of course the amplitudes A_1, A_2, and the ratio A_2/A_1 varied considerably. The results of this procedure were checked for several cases by analyzing the data with the much more accurate (and correspondingly more complicated and expensive) FRANTIC code. (See Chapter II.) The agreement was fairly good except for one or two isolated spatial positions.

MYCODE performed several sets of operations on the detector response data ($D(z_k, t_i)$, $i = 1, N$, $k = 1, M$), where N is the number of time channels (30-50) and M is the number of spatial

positions (12-15). The raw data was corrected for dead time losses as described in Chapter II and the average background per channel, determined from the last 5 - 10 of the 64 - 128 analysis channels, was subtracted. The data were normalized to the same source strength for each spatial position by multiplying by the ratio $M_o/M_1(k)$, where $M_1(k)$ is the number of counts accumulated by the monitor detector when the movable detector was at the $k^{\underline{th}}$ position and M_o is an arbitrary number chosen so that the ratios are approximately equal to one. Since we desired the data in the form III-4, the coefficients $A_m(t_i)$ were determined by minimizing the function

$$L_i = \sum_{k=1}^{M} \frac{1}{W_{ki}} \left[D(Z_k, t_i) - \sum_{m=1}^{P} A_m \sin\left(\frac{m\pi Z_k}{c+2Z_o}\right) \right]^2 . \qquad \text{(III-6)}$$

This involves solving the set of linear, algebraic equations

$$\frac{\partial L_i}{\partial A_m} = 0 , \quad m = 1, P \qquad \text{(III-7)}$$

where P is the number of terms retained in the expansion III-4. In practice, it was found that no more than three terms were needed to describe the spatial distribution. The weighting factor w_{ki} was chosen to be the reciprocal of the variance in the data. The variance consisted of the Poisson statistical uncertainty in the counting rate and three times the statistical uncertainty due to the normalizing

ratio. The large variance in the normalizing factor was chosen to allow for small systematic errors due to the long counting times. The uncertainties in the coefficients were also obtained from the least-squares fit.

A least-squares fit was performed on the reduced data $A_m(t_i)$, weighted by the reciprocal of the variance $\sigma^2(A_m(t_i))$, to obtain the associated decay constants λ_m and the uncertainties $\sigma(\lambda_m)$.

The finite volume of the detector was also taken into account by the MYCODE program. When the above procedure was completed, the normalized, corrected data was fit to functions of the form $A_m \int_{Z_i}^{Z_i+\ell_o} S(Z) \sin\left(\frac{m\pi(Z-Z_i)}{c+2Z_o}\right) dZ$, where Z_i is the position of the beginning of the active volume, ℓ_o is the length of the active volume, and S(Z) is defined by III-1. These functions just correspond to a weighted integration of the neutron density (III-4) over the active length of the detector. The decay constants for the resulting coefficients were fit in the manner described above. The decay constants determined from the two sets of expansion coefficients differed at most by one percent.

The sensitivity of the fitted decay constants was checked for variations in the dead time corrections and for uncertainties in the detector position, but no significant changes were noted for reasonable introduction of error by these means.

The LENGTH program was similar to the MYCODE program, except that the extrapolation length Z_o was treated as a free parameter to be determined in the least-squares fit. This added an extra equation,

$$\frac{\partial L_i}{\partial Z_o} = 0 \quad , \qquad \text{(III-8)}$$

to the set of equations III-7, and made the equations non-linear so that they had to be solved by an iterative technique. The feature of allowing for the finite volume of the detector was dropped after it was determined that the results were not influenced for times greater than one millisecond after the source pulse. Artificial data was put into the LENGTH program to determine that the result for Z_o was accurate to about 1.5 percent, exclusive of any error introduced by the data.

C. Results

The results of these experiments, the variations of the coefficients A_n with time, the fitted values of the decay constants λ_n, and the variations of Z_o with buckling and time after the pulse, are best seen in the tables and graphs on the following pages. However, several significant and surprising features should be mentioned. Some of the explanations and/or comments are reserved for Chapter V.

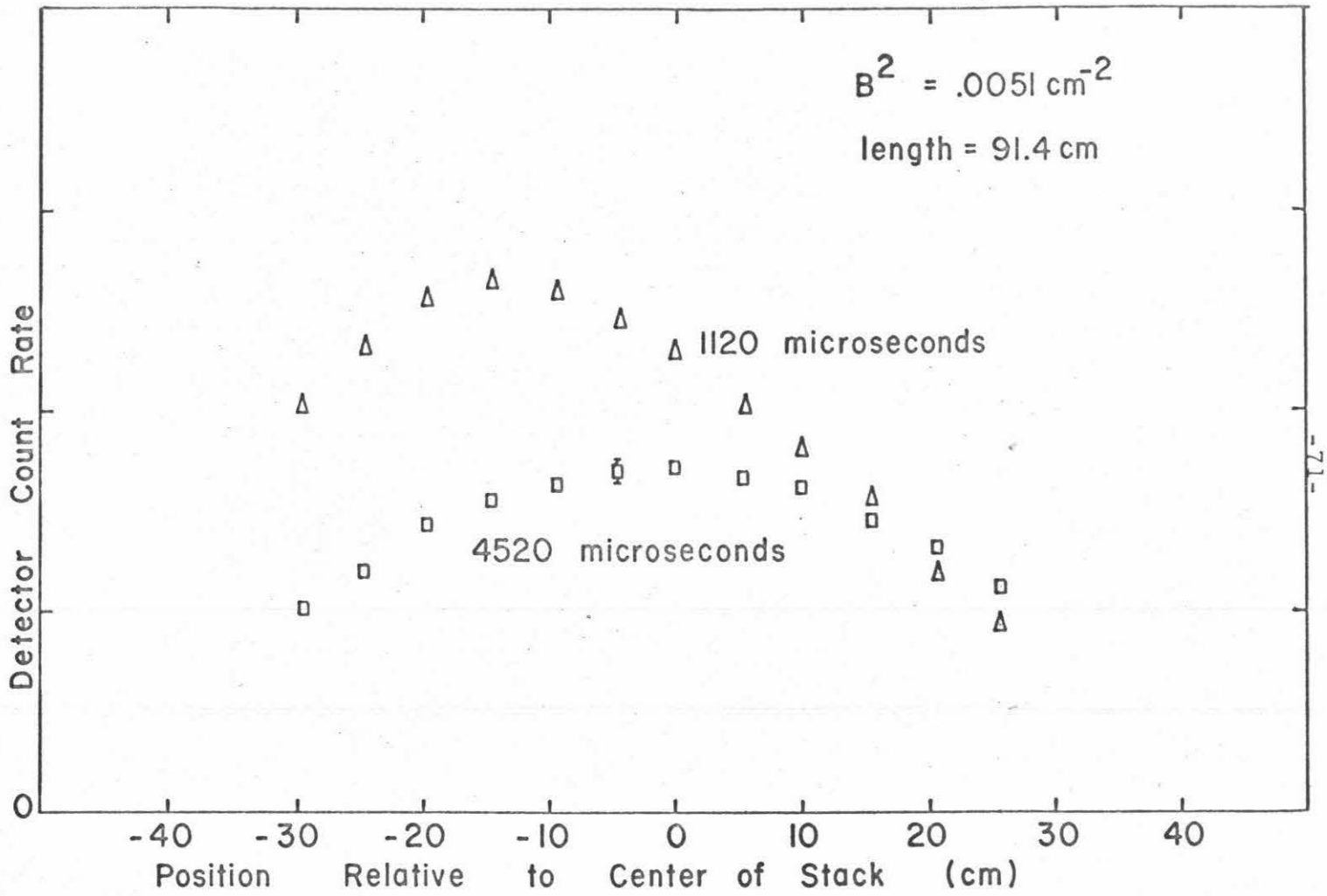

Figure III-4. Shape of the Neutron Density in the Stack

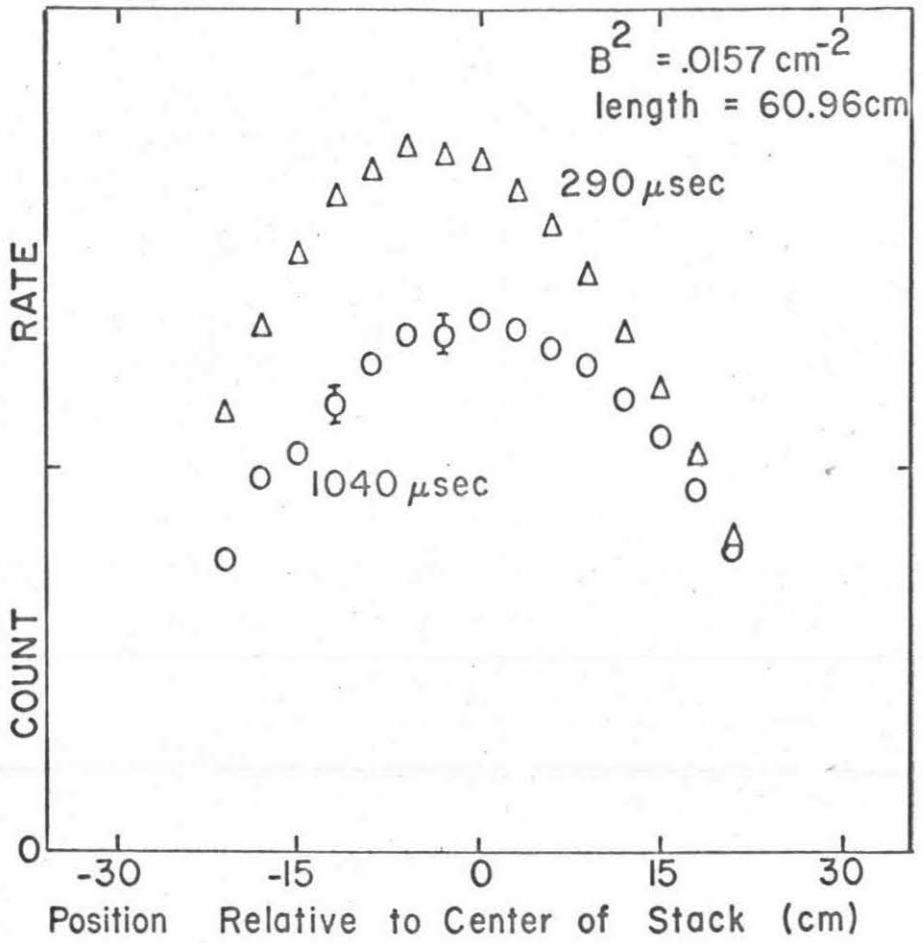

Figure III-5. Shape of the Neutron Density in the Stack

Table III-1 lists some of the results from the MYCODE analysis of the data. It should be pointed out that the decay constants λ_2 exceeded the critical value of 1600 sec^{-1} so that they were not really well defined. The tabulated uncertainties are very conservative and are based on the MYCODE output and on the dispersion of the PULSE code results about the values computed for the λ_n by MYCODE. (See Figure III-12.) As indicated in the table, filling the probe channel with graphite plugs made no significant change in the decay constant results for the smallest graphite stack.

The most significant result concerning the decay constants associated with the spatial modes is that the decay constants of the second spatial modes is that the decay constants of the second spatial mode do not fall on the dispersion curve $\lambda(B^2)$ of the fundamental mode. These decay constants exceed the critical value of 1600 sec^{-1}. This phenomenon was also noticed by Ritchie[30] in his study of BeO. The results of Hanna and Harris[28] for very large graphite stacks, in which the decay constants λ_2 were well below the critical value of 1600 sec^{-1}, indicate that the decay constants for the higher modes fall pretty well on the fundamental dispersion curve. These results are more clearly seen on the master $\lambda(B_n^2)$ plot in Figure III-13.

Figures III-6 through III-9, which show the time dependence of the coefficients $A_n(t_i)$ for the four cases, all exhibit the peculiar long time behavior of the A_2 coefficient. The curve of log $(A_2(t_i))$ versus t_i is reasonably linear until A_2 drops to about two or three

TABLE III-1

Decay Constants of the Spatial Modes of Four Graphite Assemblies

Dimensions (cm)	Fundamental Buckling	Spatial Mode (n)	Central Time of Fitting Interval (μ sec)	λ_n (sec^{-1})
(66.68 X 66.68 X 91.44)	$0.6\ B_c^2$	1	4860	1059 ± 60
		2	2310	1794 ± 180
		3	2230	2814 ± 1000
(47.63 X 47.63 X 91.44)	$1.0\ B_c^2$	1	5200	1630 ± 150
		2	2310	2479 ± 243
(47.63 X 47.63 X 60.96)	$1.165\ B_c^2$	1	3260	1865 ± 400
		2	1100	3867 ± 1000
(47.63 X 28.58 60.96)	$1.847\ B_c^2$	1	2085	2656 ± 200
		2	645	4759 ± 600
same*	$1.847\ B_c^2$	1	2085	2672 ± 100
		1	2625	2504 ± 100
		2	645	4678 ± 500
		2	1185	4571 ± 700

* graphite plugs filled the probe channel on each side of the movable detector

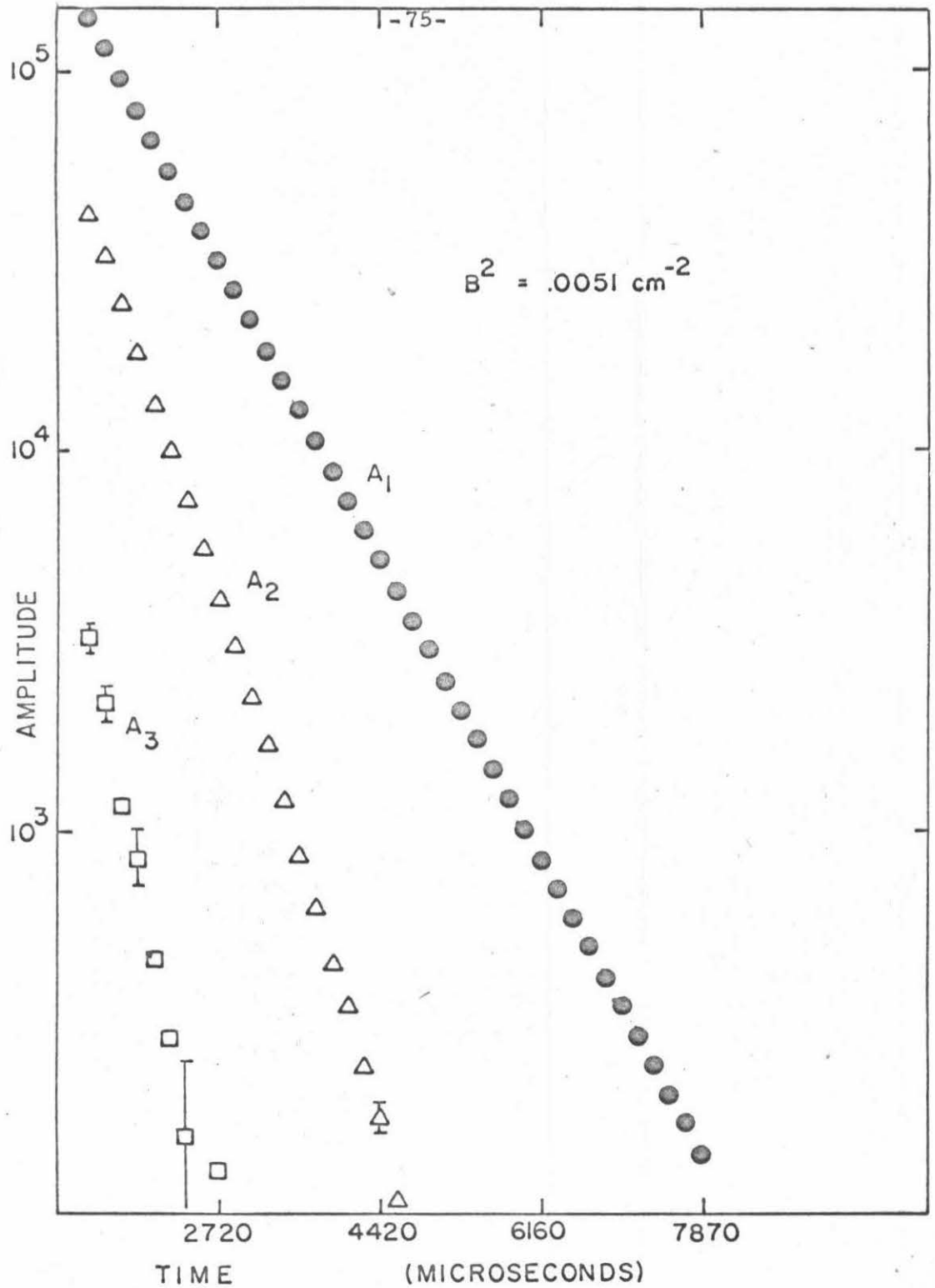

Figure III-6. Amplitudes of the Expansion Coefficients at Various Times after the Pulse.

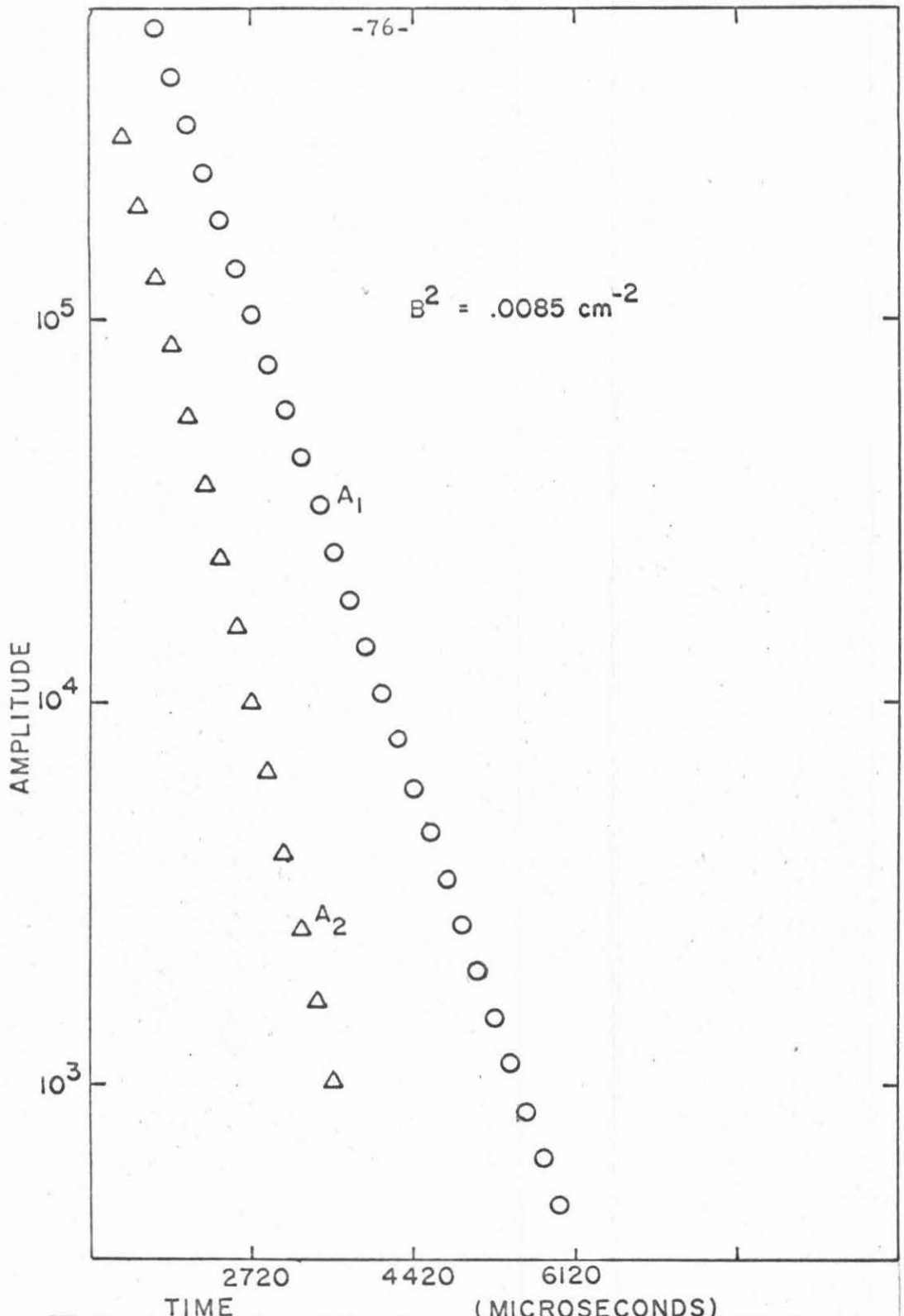

Figure III-7. Amplitudes of the Expansion Coefficients at Various Times after the Pulse.

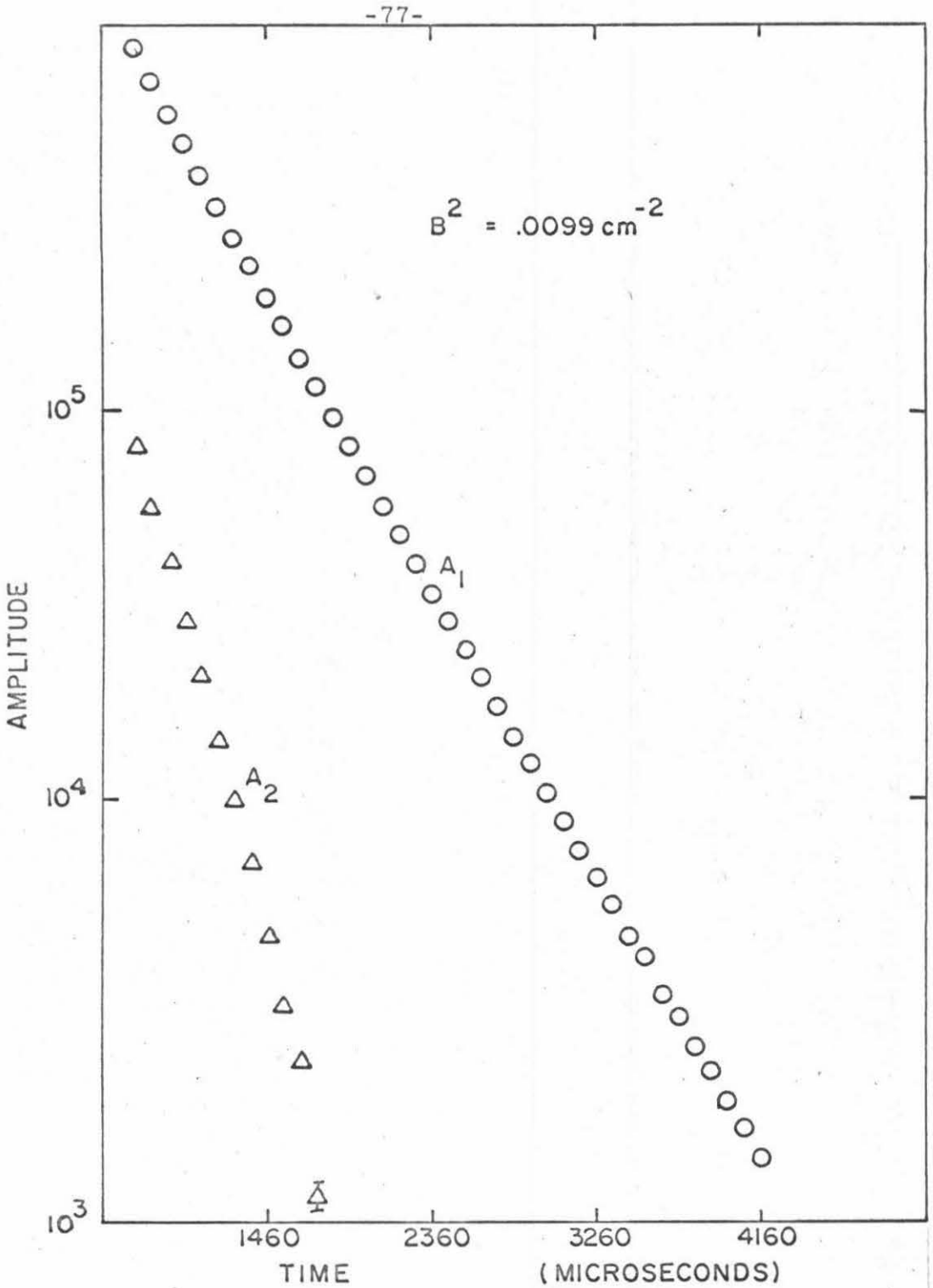

Figure III-8. Amplitudes of the Expansion Coefficients at Various Times after the Pulse.

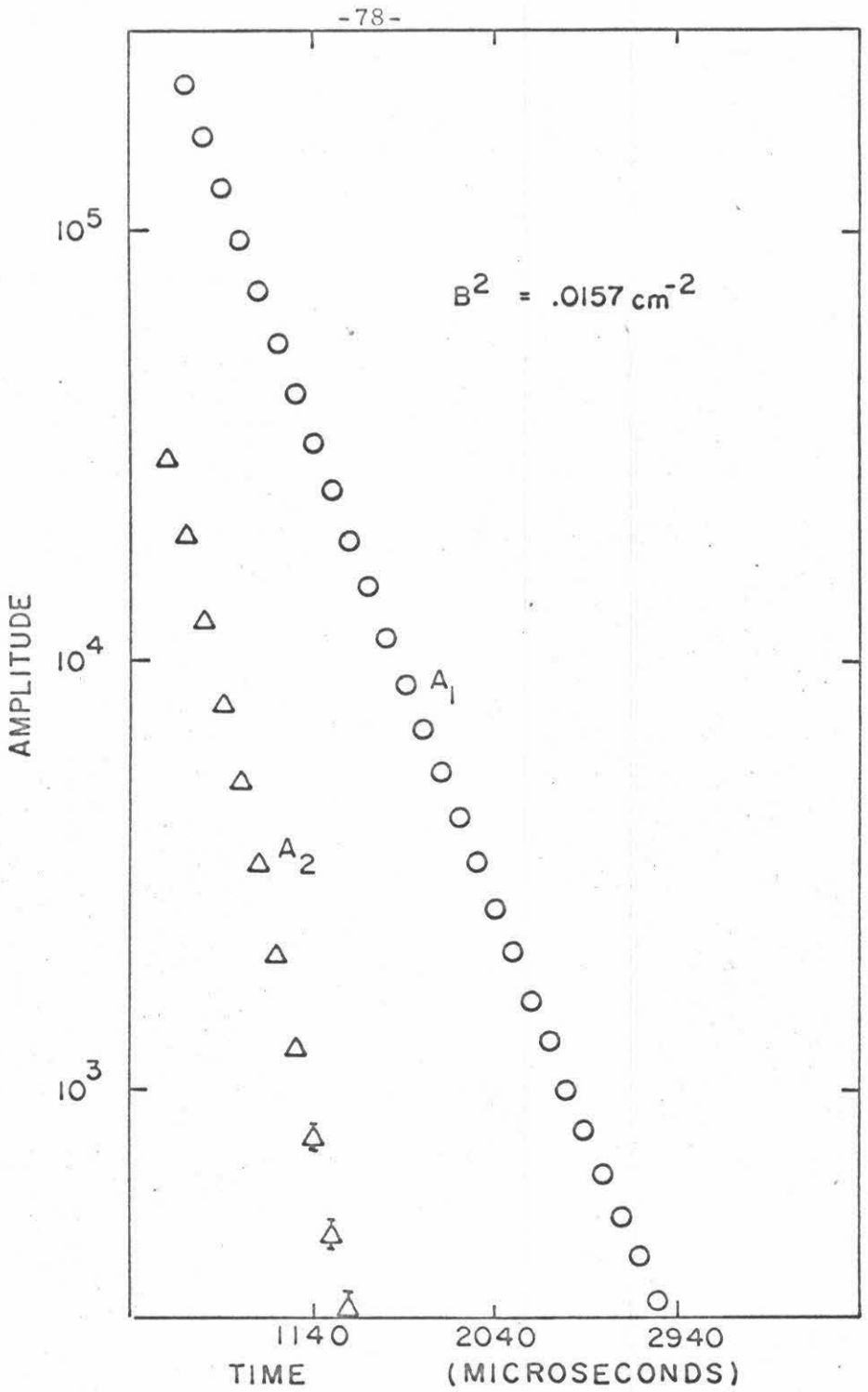

Figure III-9. Amplitudes of the Expansion Coefficients at Various Times after the Pulse.

percent of the total signal; at that point the slope of the curve becomes more negative. Apparently the statistics are not good enough for the program to resolve the second component in that time region. Ritchie[30] also observed this behavior, but was able to attribute part of it to inaccuracies in determining the center of his BeO stack. However, translation of his coordinate system by four times the estimated uncertainty in determining the central position failed to completely eliminate this tendency. We also observe that shifting the coordinate system by amounts up to twice the estimated uncertainty in the detector position (about 0.05 cm) does not significantly effect this tendency for our graphite stacks.

Figures III-10 and III-11 show the computed values of Z_o as a function of time after the source pulse for the largest and the smallest stack. The data for the later time channels, when the spatial distribution could be adequately described by the fundamental mode, were summed and the summed data were fit to a single term by the LENGTH code in order to compare the results for Z_o with the results of Davis et al.,[26] who did not have the multi-channel information. Their data were from large stacks, $B^2 < B_c^2$, so that the asymptotic mode was probably well defined. Successive runs of our summed data were made, dropping the first channel in the sum each time until Z_o was relatively constant. Our large stack results, $Z_o(0.6\ B_c^2) = 1.84$ cm and $Z_o(B_c^2) = 1.85$ cm compare favorably with their average value of 1.85 cm. The

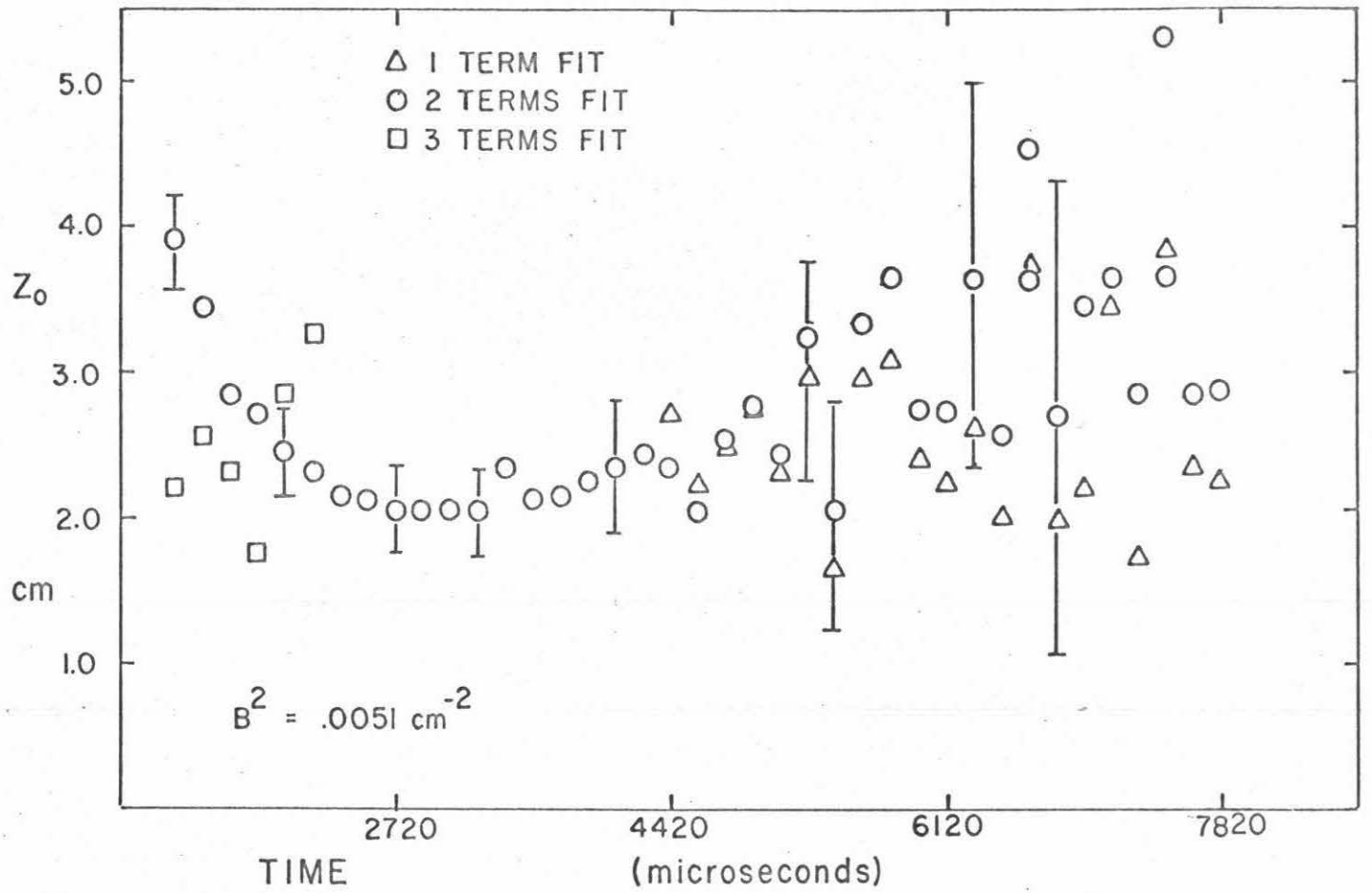

Figure III-10. Extrapolation Length at Various Times After the Pulse

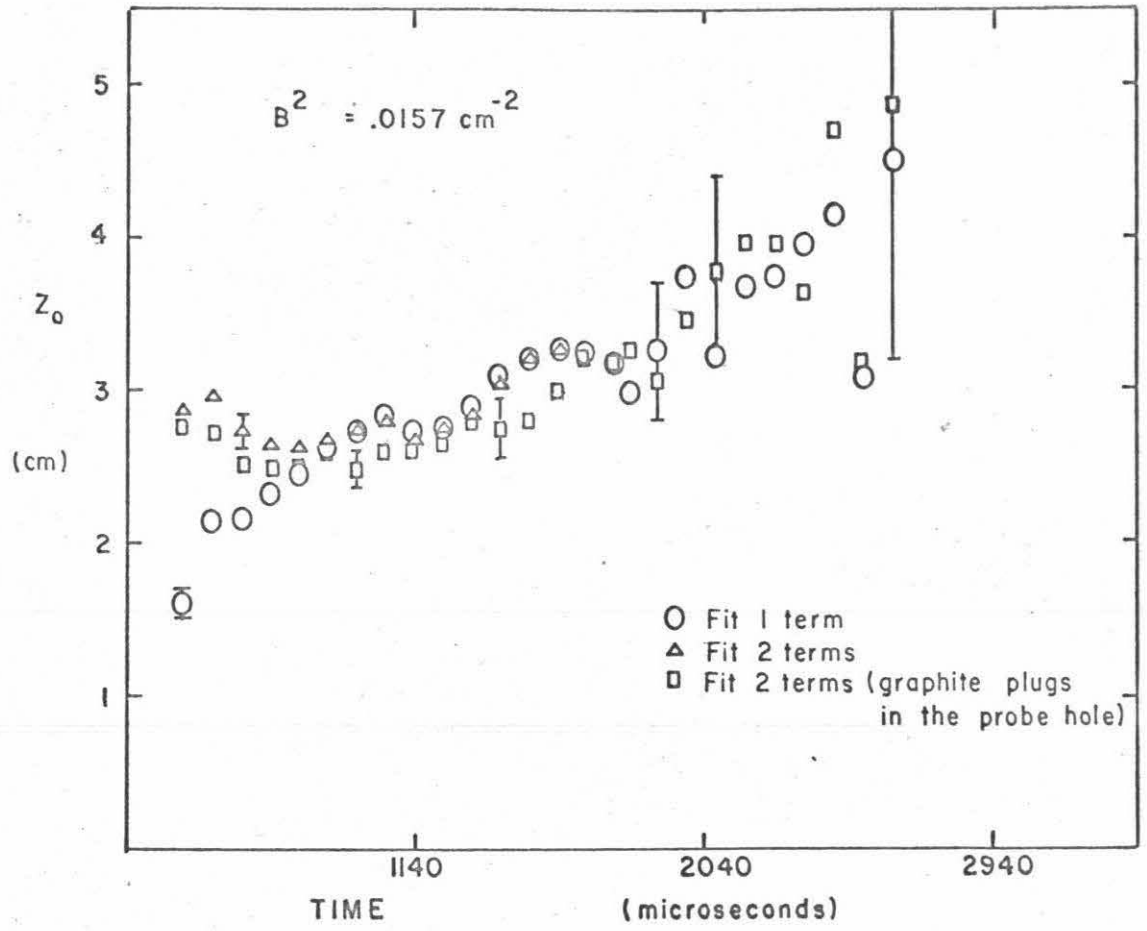

Figure III-11. Extrapolation Length at Various Times After the Pulse.

results for the smaller stacks differ considerably. The discrete data for the smallest stack indicates that the distribution tends to "flatten out", resulting in an increasing value for Z_o. Ritchie[30] also observed this behavior in his BeO data. Our measurements were made at least 15 cm from the edge of the stack in order to reduce the influence of spatial boundary transients. In light of this precaution, the observed behavior is quite strange.

TABLE III-2

Comparison of the Measured Extrapolation Length With the Results of Davis, et al. (26)

Davis, et al.		This work	
B^2 (cm^{-2})	Z_o (cm)	B^2 (cm^{-2})	Z_o (cm)
.002356	1.845 ± .025	.0051	1.84 ± .2
.003714	1.801 ± .018	.0085	1.85 ± .2
.007095	1.903 ± .043	.0099	1.72 ± .3
		.0157	3.25 ± .2*

* Fitting two terms to the earlier data yielded a lower value of 2.5 cm. (See Figure III-11.)

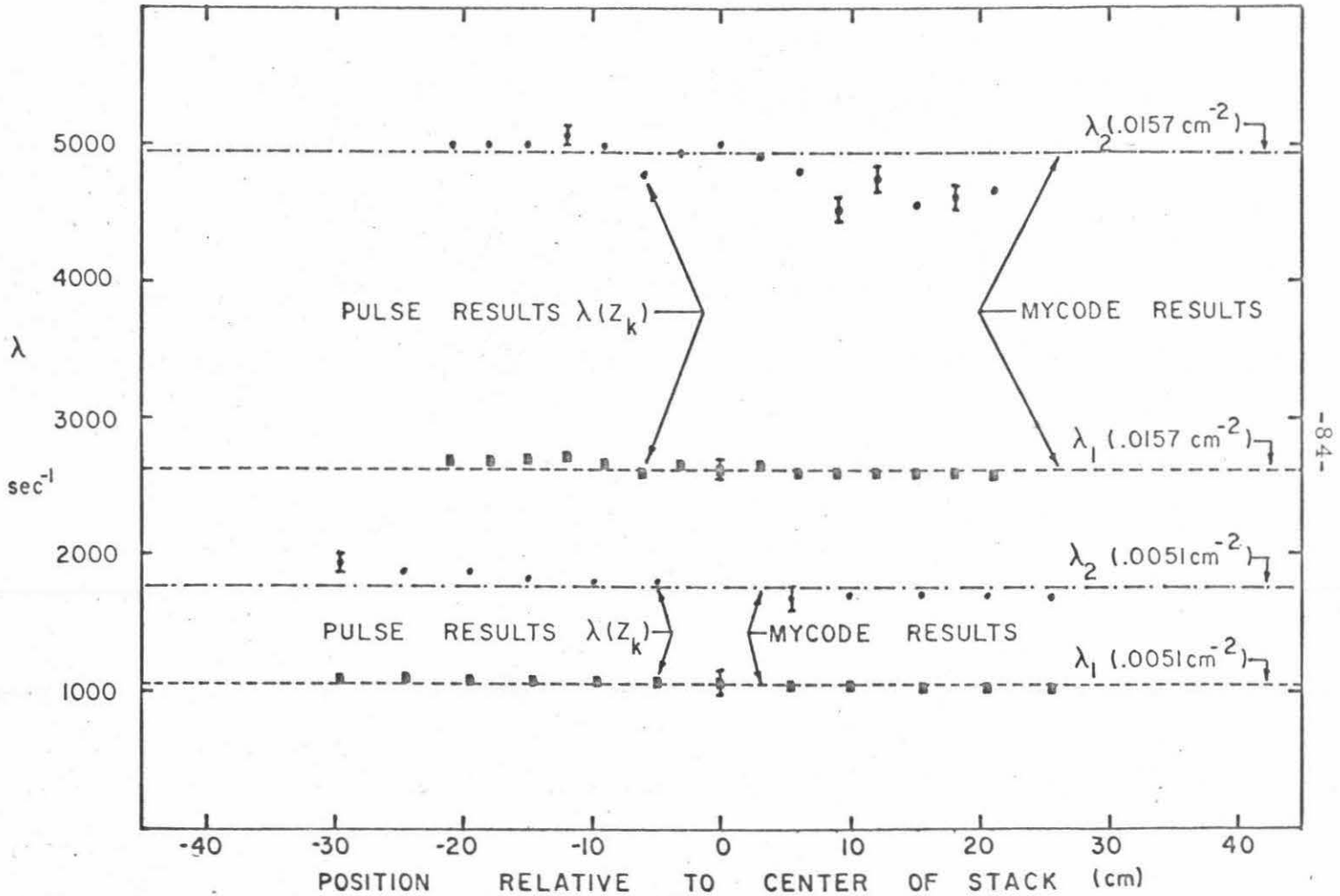

Figure III-12. Comparison of PULSE and MYCODE Results for the Largest and the Smallest Stack.

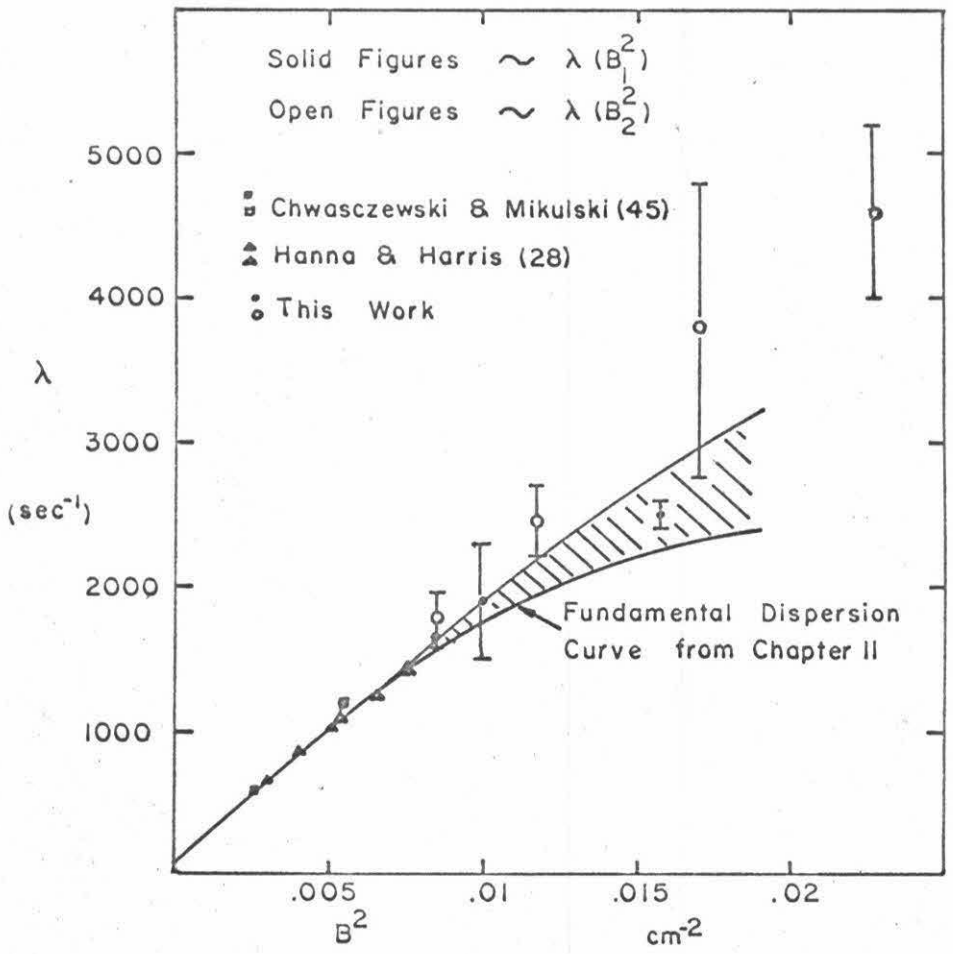

Figure III-13. Decay Constants of First Two Spatial Modes

IV. COMPUTATION OF EFFECTIVE DECAY CONSTANTS

We have used a simple theory to compute the time dependent effective decay constants $\lambda_{eff}(B^2, t)$ for the graphite assemblies which exhibited non-exponential decay as well as to compute the asymptotic decay constants for the other graphite assemblies. The essential features of the model are identical to that used by Corngold and Durgun[16] to analyze non-exponential decays in beryllium and hydrogenous moderators. We consider only the fundamental mode of the spatial distribution so that the neutron leakage through the boundaries is represented by $vD(v)B^2$ (zero-dimensional diffusion theory). A modified one-term degenerate kernel is used in the scattering integral. The effective decay constants are compared to the experimental results of Chapter II. Since the model is easily extended to beryllium, we have also compared the time dependent energy distribution with the experimental results of Gaerttner et al.[43] for two beryllium assemblies.

From Chapter I we have the diffusion equation for the fundamental spatial mode

$$\frac{\partial n_o(v,t)}{\partial t} + v\left[\Sigma_a(v)+\Sigma_s(v)+D(v)B^2\right]n_o(v,t) = \int_o^\infty dv' v' \Sigma_s(v'\to v) n_o(v',t)$$

$$t > 0, \qquad n_o(v,0) = N(v) \quad . \tag{IV-1}$$

In order to better model the experiments, we have chosen to write the equation with an initial condition rather than to include the delta function source term used by Corngold and Durgun.[16] The scattering

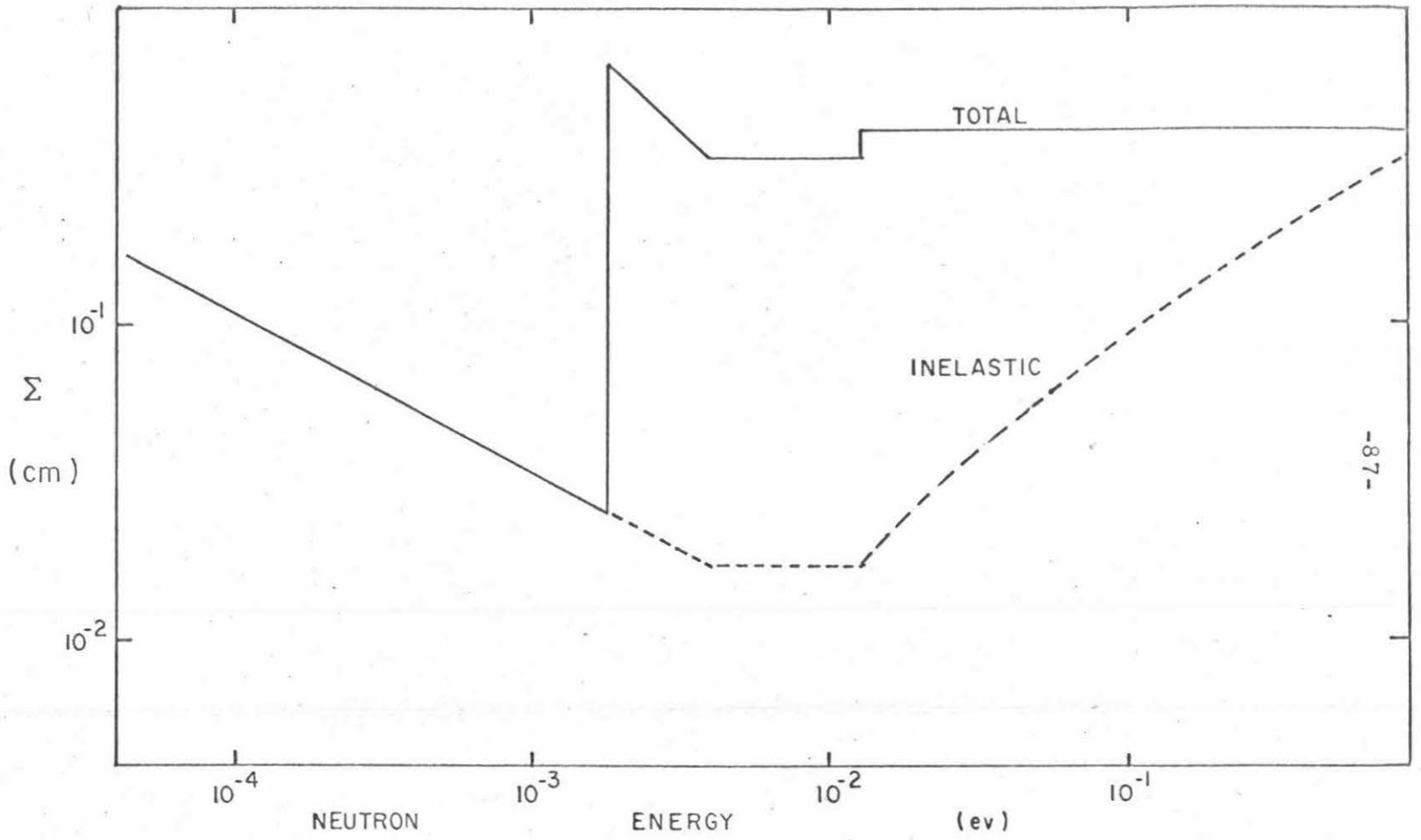

Figure IV-1. The modeled total cross sections for graphite.

kernel consists of two terms: the part due to inelastic scattering and the part due to elastic scattering.

$$\Sigma_s(v' \rightarrow v) = \Sigma_{e\ell}(v')\delta(v'-v) + \beta v \Sigma_i(v) M(v) \Sigma_i(v') \qquad \text{(IV-2)}$$

M(v) is a Maxwellian energy distribution at the temperature of the moderator and the coefficient β is the reciprocal of the Maxwellian averaged total inelastic scattering cross section.

$$\beta^{-1} = \int_0^\infty dv\, v \Sigma_i(v) M(v) \qquad \text{(IV-3)}$$

This approximation to the real scattering kernel preserves the total cross sections, $\Sigma_{e\ell}(v)$ and $\Sigma_i(v)$, and satisfies the principle of detailed balance. (See Chapter I.) The total cross sections, shown in Figure IV-1, were modeled to approximate the more exact cross sections shown in Figure I-1.

We have chosen the simplest model based on reasonable approximations that will allow us to examine some of the properties of non-exponential decay. Although we have used the model in detailed computations to compare with the experiments, one should recognize that, because of the severe approximations of the spatial distribution and the scattering kernel, no more than qualitative agreement can be expected.

If we assume that the absorption cross section is proportional to 1/v, the absorption rate $v\Sigma_a(v)$ is constant (λ_a) and can be eliminated from equation IV-1 by the ansatz

$$n_o(v, t) = n(v, t)e^{-\lambda_a t} \qquad \text{(IV-4)}$$

After integration of the delta function term, the equation for n(v, t) is

$$\frac{\partial n(v,t)}{\partial t} + v\left[\Sigma_i(v)+D(v)B^2\right]n(v,t) = \beta v\Sigma_i(v)M(v)\int_o^\infty dv'v'\Sigma_i(v')n(v',t)$$

$$n(v,0) = N(v) \qquad \text{(IV-5)}$$

The initial distribution N(v) is obtained by assuming that prior to t = 0, a steady-state distribution exists in the assembly. In the experiments, the pulse width is typically of the order of 500 - 750 microseconds which allows sufficient time to establish the thermal neutron population. Hence, the initial distribution N(v) is obtained by assuming that prior to t = 0, a steady-state distribution exists in the assembly. We solve the steady-state integral equation

$$v\left[\Sigma_a(v)+\Sigma_i(v)+D(v)B^2\right]N(v) = \beta v\Sigma_i(v)M(v)\int_o^\infty dv'v'\Sigma_i(v')N(v')+S(v) \qquad \text{(IV-6)}$$

for N(v). The source term S(v) is taken as the distribution of neutrons scattering from a Maxwellian distribution $M_o(v)$ with a mean energy in the range 0.1 - 0.7 electron volts

$$S(v) = \int_o^\infty dv'\left[v'\Sigma_{e\ell}(v')\delta(v'-v) + \beta v\Sigma_i(v)M(v)v'\Sigma_i(v')\right]M_o(v') \qquad \text{(IV-7)}$$

This form of the source is chosen only for convenience, as we do not expect the computed effective decay constants to be very sensitive to the particular form of S(v). The sensitivity of the final results to S(v) is checked by changing the mean energy of the source.

If we define the unknown constant C_o,

$$C_o = \int_o^\infty dv'\, v'\, \Sigma_i(v')\, N(v) \qquad \text{(IV-8)}$$

the formal solution to equation IV-6 may be written

$$N(v) = \frac{\beta C_o v\Sigma_i(v) M(v) + S(v)}{v[\Sigma_a(v) + \Sigma_i(v) + D(v) B^2]} \qquad \text{(IV-9)}$$

We solve for the constant C_o in terms of known quantities by multiplying equation IV-9 by $v\Sigma_i(v)$ and integrating over v. If we define the integrals

$$C_1 \equiv \int_o^\infty dv\, v\Sigma_i(v) M_o(v) \quad , \qquad \text{(IV-10)}$$

$$C_2 \equiv \int_o^\infty dv\, \frac{v\Sigma_i^2(v)\, M(v)}{[\Sigma_i(v) + \Sigma_a(v) + D(v)B^2]} \qquad \text{(IV-11)}$$

$$C_3 \equiv \int_o^\infty dv\, \frac{v\Sigma_i(v)\, \Sigma_{e\ell}(v) M_o(v)}{[\Sigma_i(v) + \Sigma_a(v) + D(v) B^2]} \quad ,$$

then, we have

$$C_o = \frac{C_1 C_2 + C_3}{1 - \beta C_1} \qquad \text{(IV-13)}$$

To facilitate the discussion of the time dependent equation, we define the removal cross section $\Sigma_R(v)$,

$$\Sigma_R(v) \equiv \Sigma_i(v) + D(v)\, B^2 \quad . \qquad \text{(IV-14)}$$

We also note that the diffusion coefficient D(v) is related to the reciprocal of the total scattering cross section (the mean free path) in a simple manner:[63]

$$D(v) = \frac{1}{3\Sigma_s(v)} \qquad \text{(IV-15)}$$

Hence, the elastic scattering is retained in the equation (IV-5) in a rather subtle way and effects only the rate at which neutrons leak from the assembly.

Having defined the initial condition and the removal cross section, we Laplace transform equation IV-5 to obtain

$$[s + v\Sigma_R(v)]\tilde{n}(v, s) = \beta v\Sigma_i(v)M(v)\int_0^\infty dv' v'\Sigma_i(v')\tilde{n}(v', s) + N(v), \qquad \text{(IV-16)}$$

where s is the transform variable. Defining the transformed inelastic scattering integral,

$$\tilde{\Theta}(s) \equiv \int_0^\infty dv' v' \Sigma_i(v')\tilde{n}(v', s) \quad , \qquad \text{(IV-17)}$$

we have for the transformed neutron distribution function

$$\tilde{n}(v, s) = \frac{\beta\tilde{\Theta}(s)\, v\Sigma_i(v)M(v)}{[\, s + v\Sigma_R(v)\,]} + \frac{N(v)}{[s + v\Sigma_R(v)]} \quad . \qquad \text{(IV-18)}$$

We can solve for $\tilde{\Theta}(s)$ by multiplying equation IV-18 by $v\Sigma_i(v)$ and integrating over v. After the algebra, this yields

$$\tilde{\Theta}(s) = \frac{\rho(s)}{1 - \beta\gamma(s)} \quad , \qquad \text{(IV-19)}$$

where the quantities $\rho(s)$ and $\gamma(s)$ are defined by the integrals

$$\rho(s) \equiv \int_o^\infty dv \ \frac{v\Sigma_i(v)N(v)}{v\Sigma_R(v) + s} \ . \qquad \text{(IV-20)}$$

$$\gamma(s) = \int_o^\infty dv \ \frac{[v\Sigma_i(v)]^2 M(v)}{v\Sigma_R(v) + s} \ . \qquad \text{(IV-21)}$$

Besides the time dependent energy distribution, we are also interested in the detector response, $D_r(t)$.

$$D_r(t) = \int_o^\infty dv \ v\Sigma_d(v) \ n(v, t) \qquad \text{(IV-22)}$$

If we assume the detector cross section $\Sigma_d(v)$ is proportional to $1/v$, the transformed detector response $\tilde{D}_r(s)$ is

$$\tilde{D}_r(s) = \beta\tilde{\odot}(s) \int_o^\infty dv \left[\frac{v\Sigma_i(v) M(v)}{s + v\Sigma_R(v)} \right] + \int_o^\infty dv \ \frac{N(v)}{s + v\Sigma_R(v)} \ . \qquad \text{(IV-23)}$$

Defining

$$\Psi(s) \equiv \int_o^\infty dv \left[\frac{v\Sigma_i(v) M(v)}{s + v\Sigma_R(v)} \right] \ , \quad \text{and} \qquad \text{(IV-24)}$$

$$\eta(s) \equiv \int_o^\infty dv \ \frac{N(v)}{s + v\Sigma_R(v)} \ , \qquad \text{(IV-25)}$$

we have

$$\tilde{D}_r(s) = \beta\tilde{\odot}(s) \cdot \Psi(s) + \eta(s) \ . \qquad \text{(IV-26)}$$

Although we can find the inverse transform of the product by using

the convolution theorm, we define

$$\chi(s) \equiv \tilde{\Omega}(s) \cdot \Psi(s) \qquad \text{(IV-27)}$$

in order to get the final expression for $D_r(t)$ in the desired form.

The transformed functions $\tilde{\Omega}(s)$ and $\chi(s)$ are analytic in the cut plane ($s < \lambda_*$) except for a discrete pole defined by

$$1 - \beta\gamma(s) = 0 \quad . \qquad \text{(IV-28)}$$

For sufficiently large B^2 the pole term is not present. Proof that only one pole exists and that it is real was given by Corngold and Durgun[16] in their analysis. The transform plane is shown in Figure IV-2. The inversion of transforms of this type have been studied in detail.[64] The contribution from the pole is straightforward and is given by

$$\frac{\rho(-\lambda_o)\,\Psi(-\lambda_o)}{\left[\frac{-d\gamma(s)}{ds}\right]_{-\lambda_o}} e^{-\lambda_o t} \quad . \qquad \text{(IV.29)}$$

The contribution from $\eta(s)$, $N(v)e^{-v\Sigma_R(v)t}$, represents the removal of the initial distribution neutrons which have not suffered inelastic collisions.

We pick up the contribution from the branch cut by deforming the inversion contour around it. Formally, we have

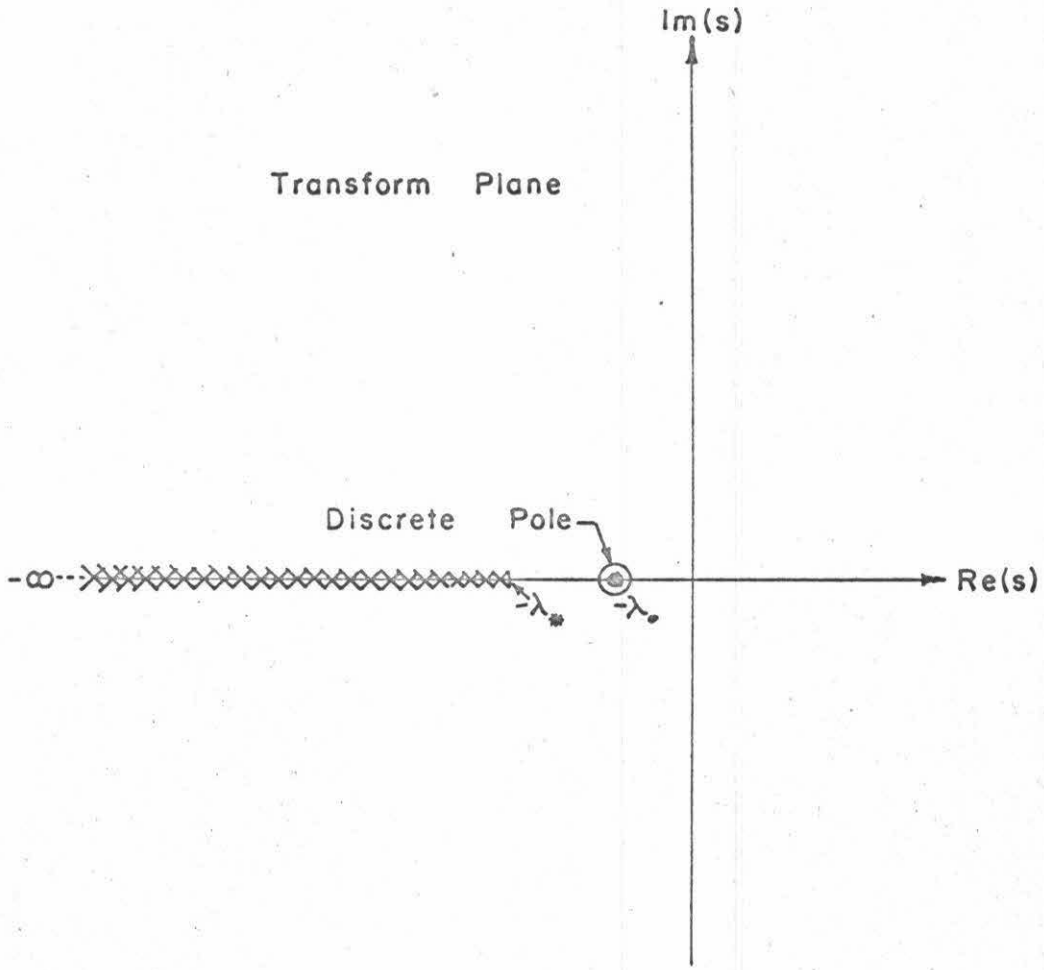

Figure IV-1 The Transform Plane

$$\frac{1}{2\pi i} \lim_{\epsilon \to o} \left\{ \int_{-\lambda_*}^{-\infty} ds\, e^{st}\, \chi(s+i\epsilon) + \int_{-\infty}^{-\lambda_*} ds\, e^{st}\, \chi(s-i\epsilon) \right\} . \qquad \text{(IV-30)}$$

Inverting the limits of integration and combining the integrands, we obtain

$$\frac{1}{\pi} \int_{-\lambda_*}^{\infty} ds \left\{ e^{st} \lim_{\epsilon \to o} \operatorname{Im} \left[\chi(s+i\epsilon) \right] \right\} . \qquad \text{(IV-31)}$$

The integrals $\rho(s)$, $\Psi(s)$, and $\gamma(s)$ have singularities when

$$v\Sigma_R(v) = -s \qquad \text{(IV-32)}$$

We can handle the integrals by making use of the Plemel j relations,[65] that is, the proper combination of the principal value and the residue. If we have the integral

$$F(s) \equiv \frac{1}{2\pi i} \int dx \frac{f(x)}{x-s} , \qquad \text{(IV-33)}$$

the Plemel j relations are defined as

$$F_+(s) \equiv F_p(s) + \tfrac{1}{2} \int dx\, f(x)\, \delta(x-s)$$

$$F_-(s) \equiv F_p(s) - \tfrac{1}{2} \int dx\, f(x)\, \delta(x-s) , \qquad \text{(IV-34)}$$

where $F_p(s)$ is the principal value of the integral. For our case, the singular point approaches the path of integration as positive ϵ decreases to zero. We therefore use the form $F_-(s)$[65] and define

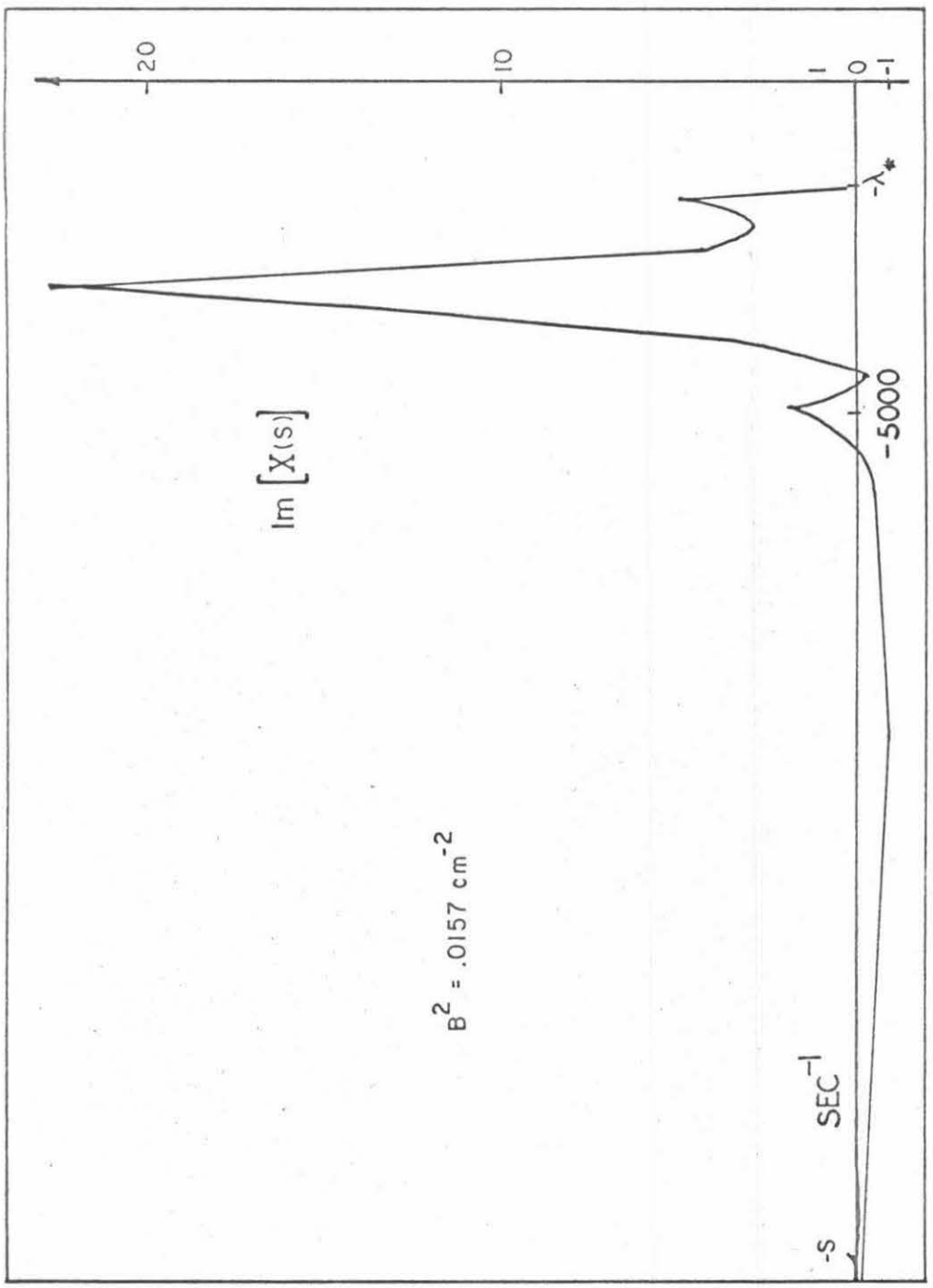

Figure IV-3

the quantities

$$\rho_-(s) \equiv \rho_p - \pi i \rho_o \ , \tag{IV-35}$$

$$\Psi_-(s) \equiv \Psi_p - \pi i \Psi_o \ , \tag{IV-36}$$

and

$$\gamma_-(s) \equiv \gamma_p - \pi i \gamma_o \ . \tag{IV-37}$$

ρ_p, Ψ_p, and γ_p are the principle values of the integrals.

The quantities ρ_o, Ψ_o, and γ_o are defined by

$$\rho_o \equiv \int_o^\infty dv \ v\Sigma_i(v) \ N(v) \ \delta(v\Sigma_R(v)+s) \ , \tag{IV-38}$$

$$\Psi_o \equiv \int_o^\infty dv \ v\Sigma_i(v) \ M(v) \ \delta(v\Sigma_R(v)+s) \ , \quad \text{and} \tag{IV-39}$$

$$\gamma_o \equiv \int_o^\infty dv \ [v\Sigma_i(v)]^2 \ M(v) \ \delta(v\Sigma_R(v)+s) \ . \tag{IV-40}$$

Hence,

$$\frac{1}{\pi} \text{Im}\,[\chi(s)] = -\left\{ \frac{[\rho_p \Psi_o + \rho_o \Psi_p][1-\beta\gamma_p] + \beta\gamma_o[\rho_p\Psi_p - \pi^2\rho_o\Psi_o]}{[1-\beta\gamma_p]^2 + \pi^2\beta^2\gamma_o^2} \right. \tag{IV-40}$$

(see figure IV-3)

and the solution for the detector response is

$$D_r(t) = \frac{\rho(-\lambda_o)\,\Psi(-\lambda_o)}{\left[\frac{d\gamma(s)}{ds}\right]_{-\lambda_o}} e^{-\lambda_o t} + \frac{\beta}{\pi} \int_{-\lambda_*}^{-\infty} ds \ e^{st} \text{Im}[\chi(s)] + N(v) e^{-v\Sigma_R(v)t} \tag{IV-41}$$

If we define A_o as the coefficient of $e^{-\lambda_o t}$, change the variable of integration from s to $-\lambda$, and define $A(\lambda)$ as

$\frac{\beta}{\pi} I_m[\chi(\lambda)]$, equation IV-41 reduces to the form of the detector response mentioned in the first chapter:

$$D_r(t) = A_o e^{-\lambda_o t} + \int_{\lambda_*}^{\infty} A(\lambda) e^{-\lambda t} d\lambda \quad . \tag{IV-42}$$

We have neglected the contribution from the initial distribution which damps out quickly relative to the other terms.

When no discrete pole exists, the effective decay constant is defined as the derivative of logarithm of the detector response.

$$-\lambda_{eff}(t) \equiv \frac{d}{dt} [\log D_r(t)] \quad . \tag{IV-43}$$

The contribution from $N(v)e^{-\Sigma_R(v)t}$ was retained for this part of the computation. A comparison of the experimental results with the effective decay constant computed via this simple model is shown in figures IV-4 through IV-8. The sensitivity of the effective decay constant to the initial source energy, which effects the terms ρ_o and $N(v)$, was found to be negligible after three milliseconds. Increasing the mean energy by a factor of seven increased the effective decay constant by eight percent at two milliseconds.

The formalism for obtaining the inverse transformation for $n(v, s)$ is identical to that for the detector response. The asymptotic energy distribution for a case with B^2 less than B_c^2 is shown in

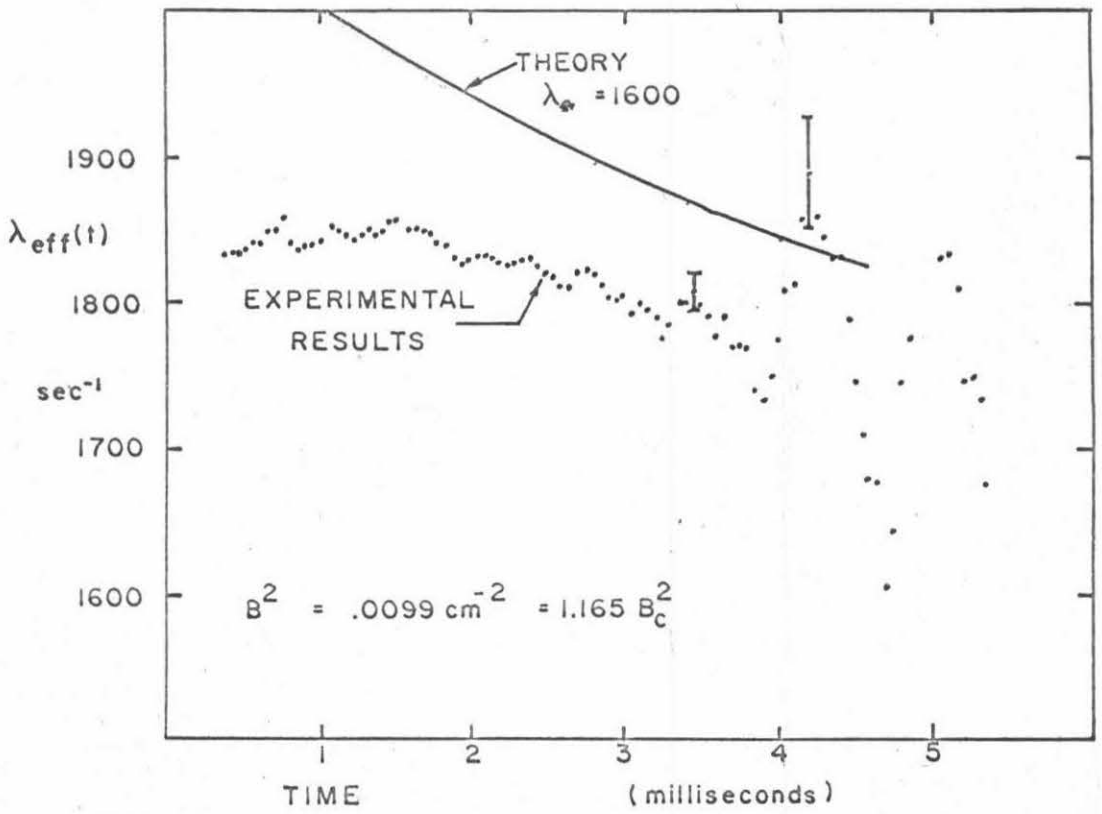

Figure IV-4. Comparison of the Theoretical and the Experimental Effective Decay Constants

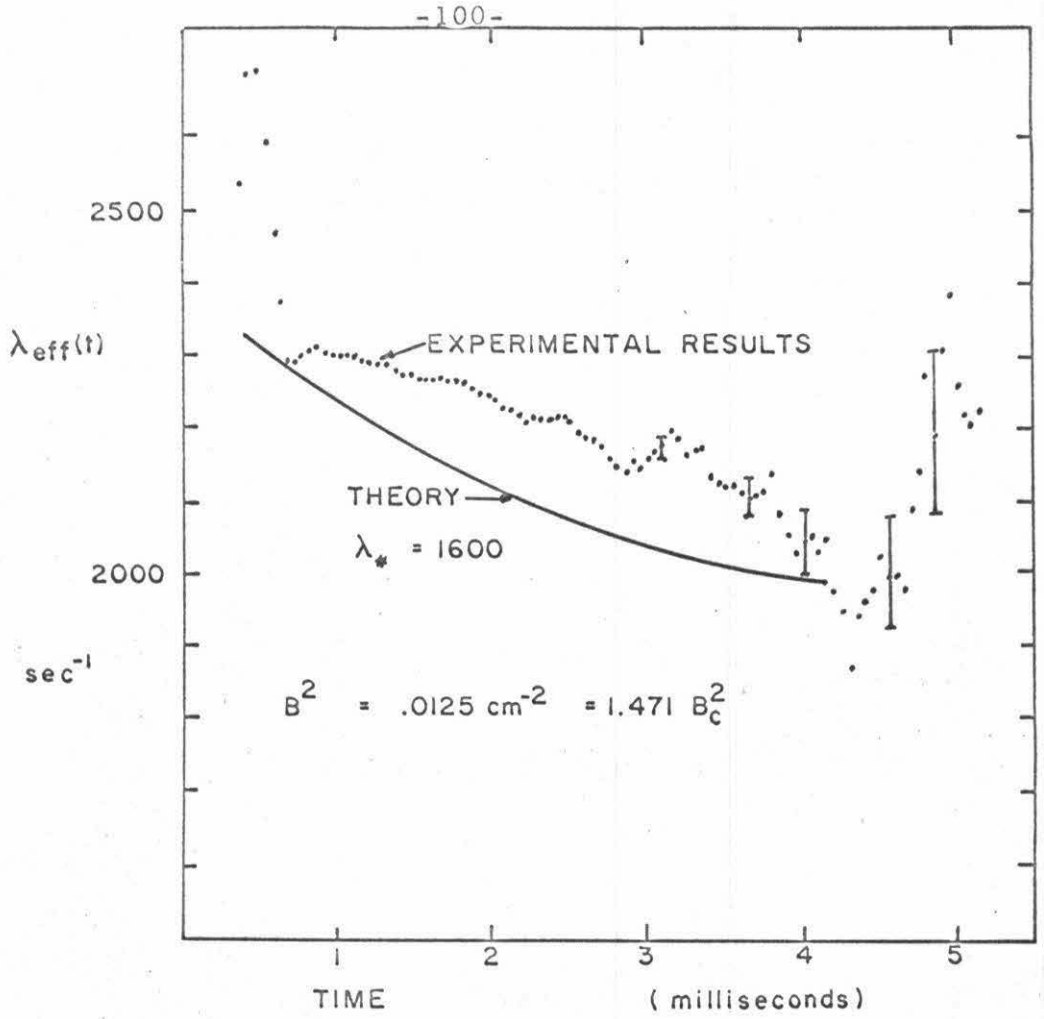

Figure IV-5 Comparison of the Theoretical and the Experimental Effective Decay Constants.

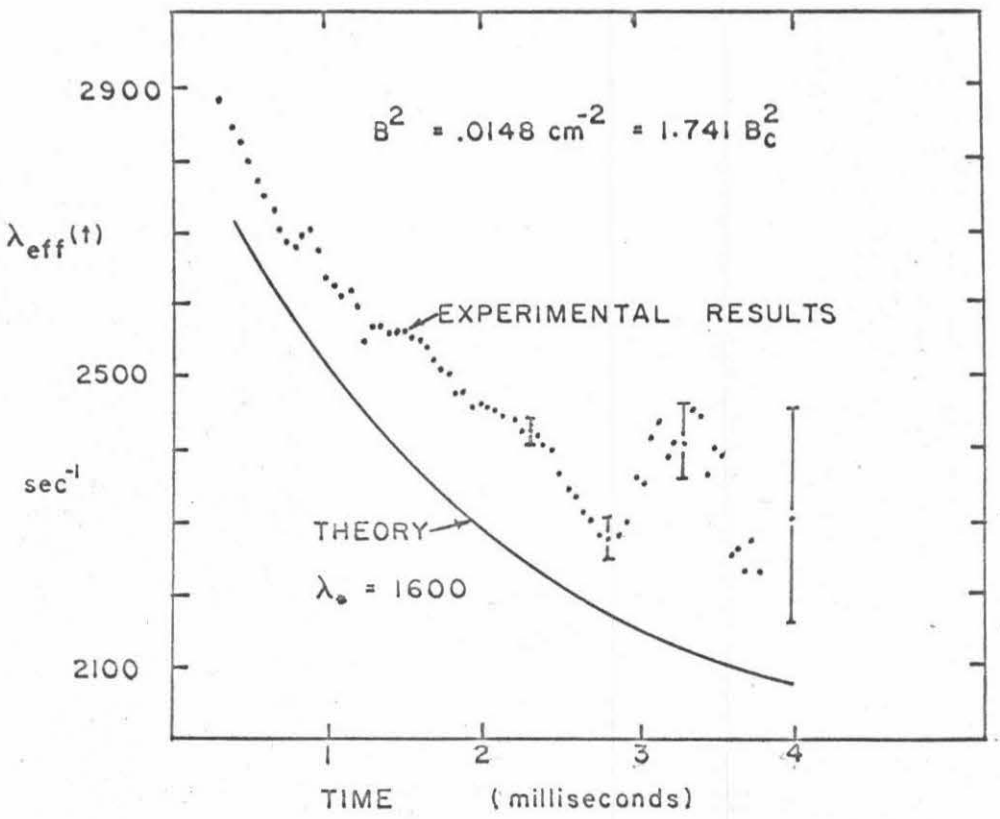

Figure IV-6 Comparison of the Theoretical and the Experimental Effective Decay Constants.

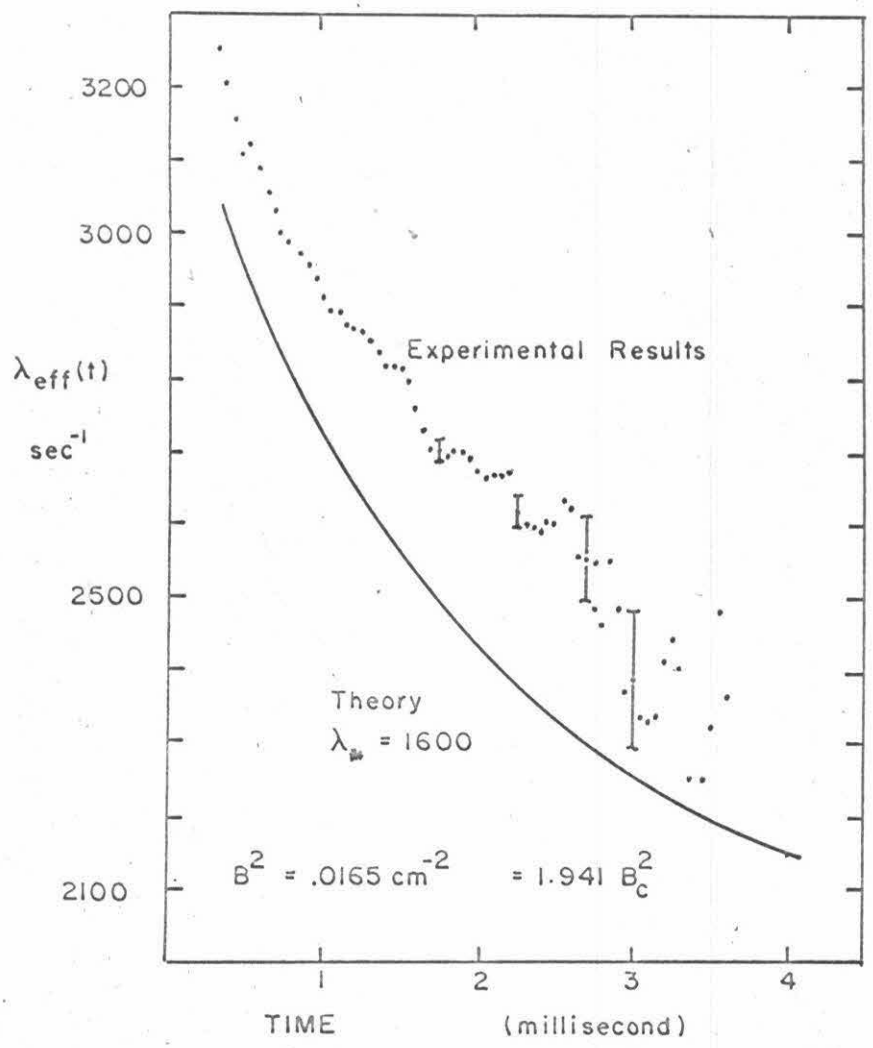

Figure IV-7 Comparison of the theoretical and the Experimental Effective Decay Constants.

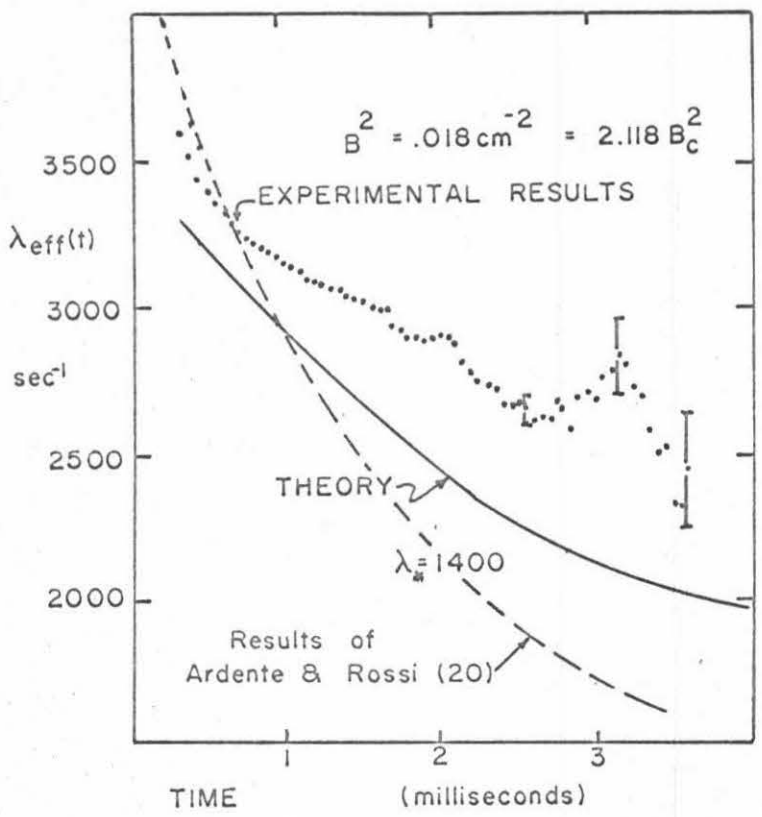

Figure IV-8 Comparison of the Theoretical and the Experimental Effective Decay Constants.

Figure IV-9. The time dependent energy distribution n(v, t) for a case with B^2 exceeding B_c^2 may be seen in Figure IV-10. Since the mechanics of the computations are unchanged for beryllium, and beryllium cross sections were modeled and n(v, t) computed for two beryllium assemblies to compare with the experimental data of Gaerttner et al.[43] The results are shown in figures IV-11 and IV-12. Effective decay constants were also computed for the beryllium assemblies, but since we have no experimental data for time dependent decay constants, these results are not presented.

Asymptotic decay constants computed for the graphite and the beryllium assemblies with B^2 less than B_c^2 agreed with the experimental results to within five percent. The uncertainty in the experimental decay constants is less than one percent in this range. Agreement with the effective decay constants for the graphite assemblies was less than spectacular with both the amplitude and the slope of the theoretical $\lambda_{eff}(t)$ curve deviating significantly from the experimental results. The success of the theory to predict the energy distribution in beryllium (Figures IV-11 and IV-12) indicates that in these leakage dominated assemblies the spectrum at the center is principally sensitive to how well the total neutron cross section is modeled. In summary, the qualitative agreement was satisfactory, but the theoretical model is inadequate for quantitative computations.

TABLE IV-1

Material	B^2 Cm^{-2}	Exp. λ_o (sec^{-1})	Theoretical λ_o (inclining λ_a) (sec^{-1})
B_e	0.026	3238 $\pm$40[62]	3312
Graphite	0.0051	1030 $\pm$1	1083
Graphite	0.0	$\approx$ 75	75
Graphite	0.0077	1470 $\pm$2	1539

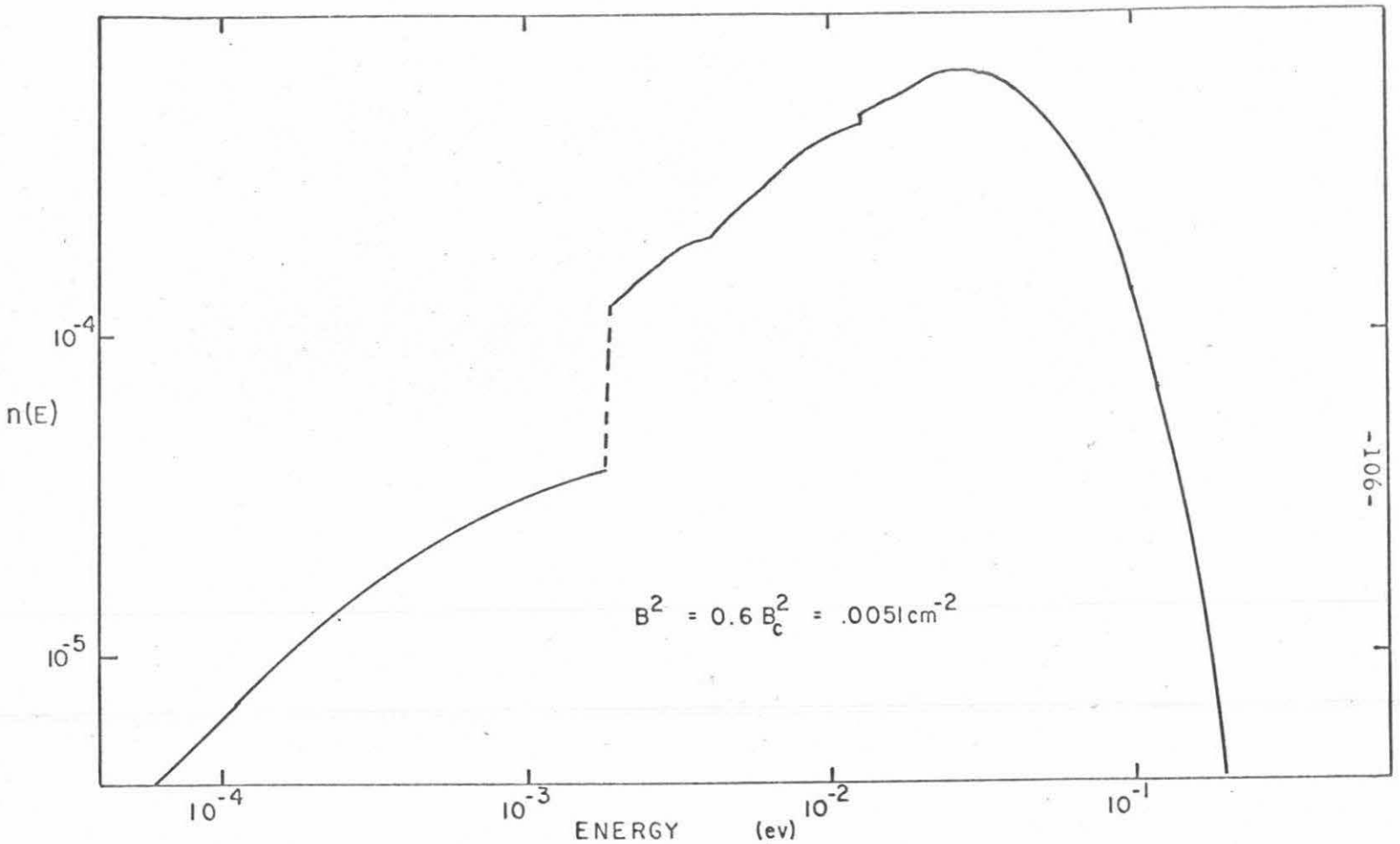

Figure IV-9. The Theoretical Asymptotic Energy Distribution for a Large Graphite Stack.

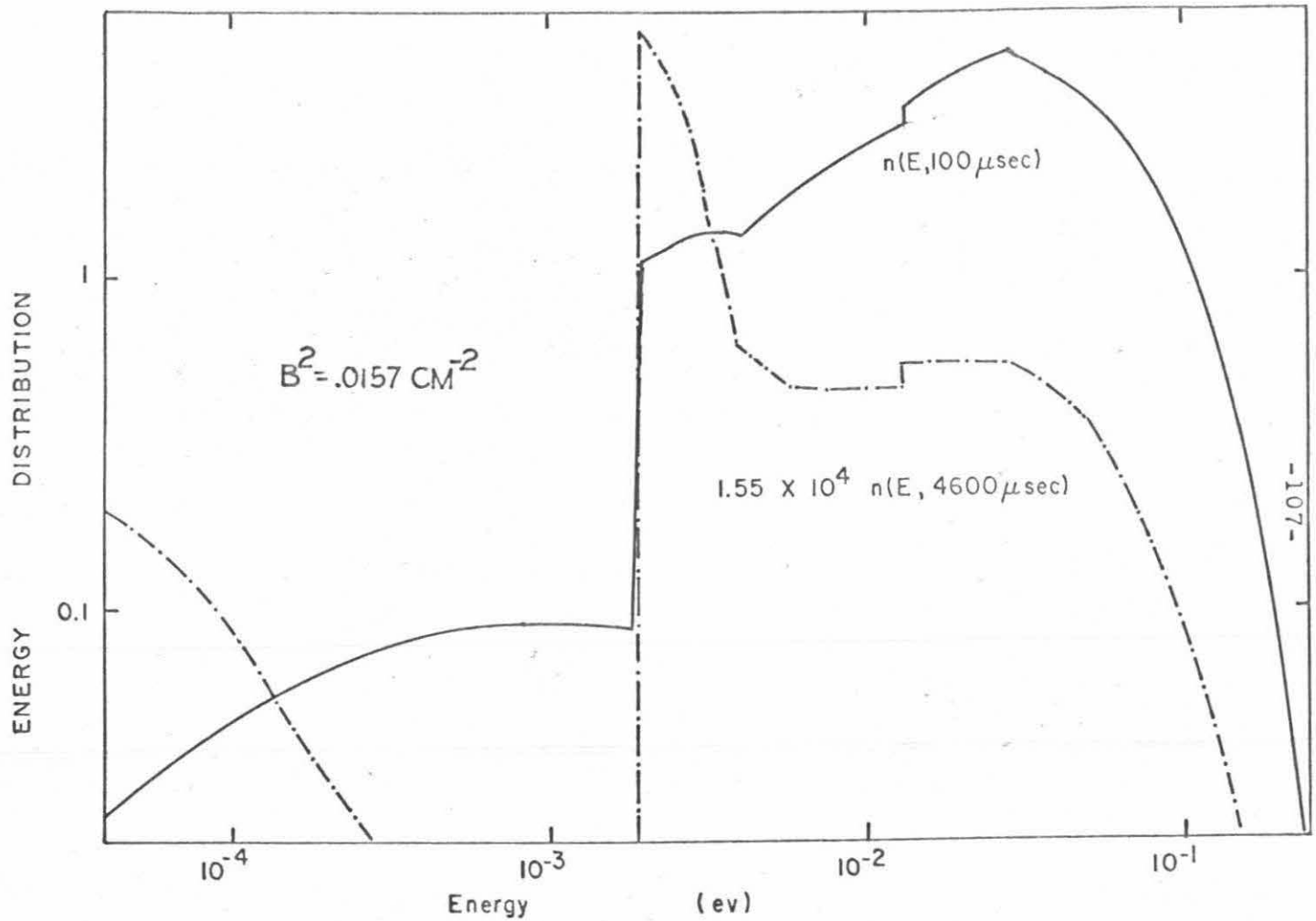

Figure IV-10. The Theoretical Time Dependent Energy Distribution for a Small Graphite Stack.

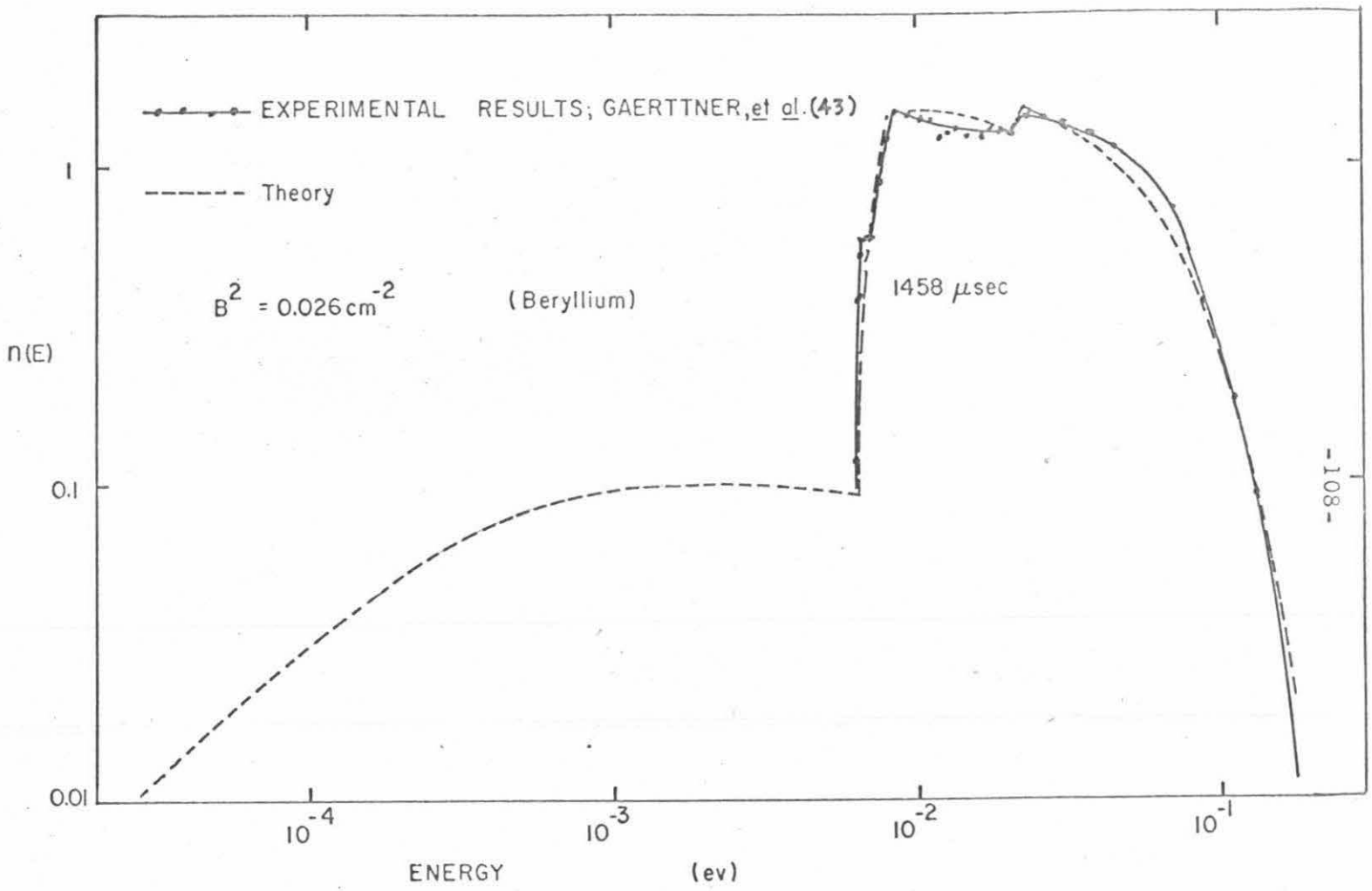

Figure IV-11. The Theoretical and Experimental Energy Distributions for a B_e Assembly.

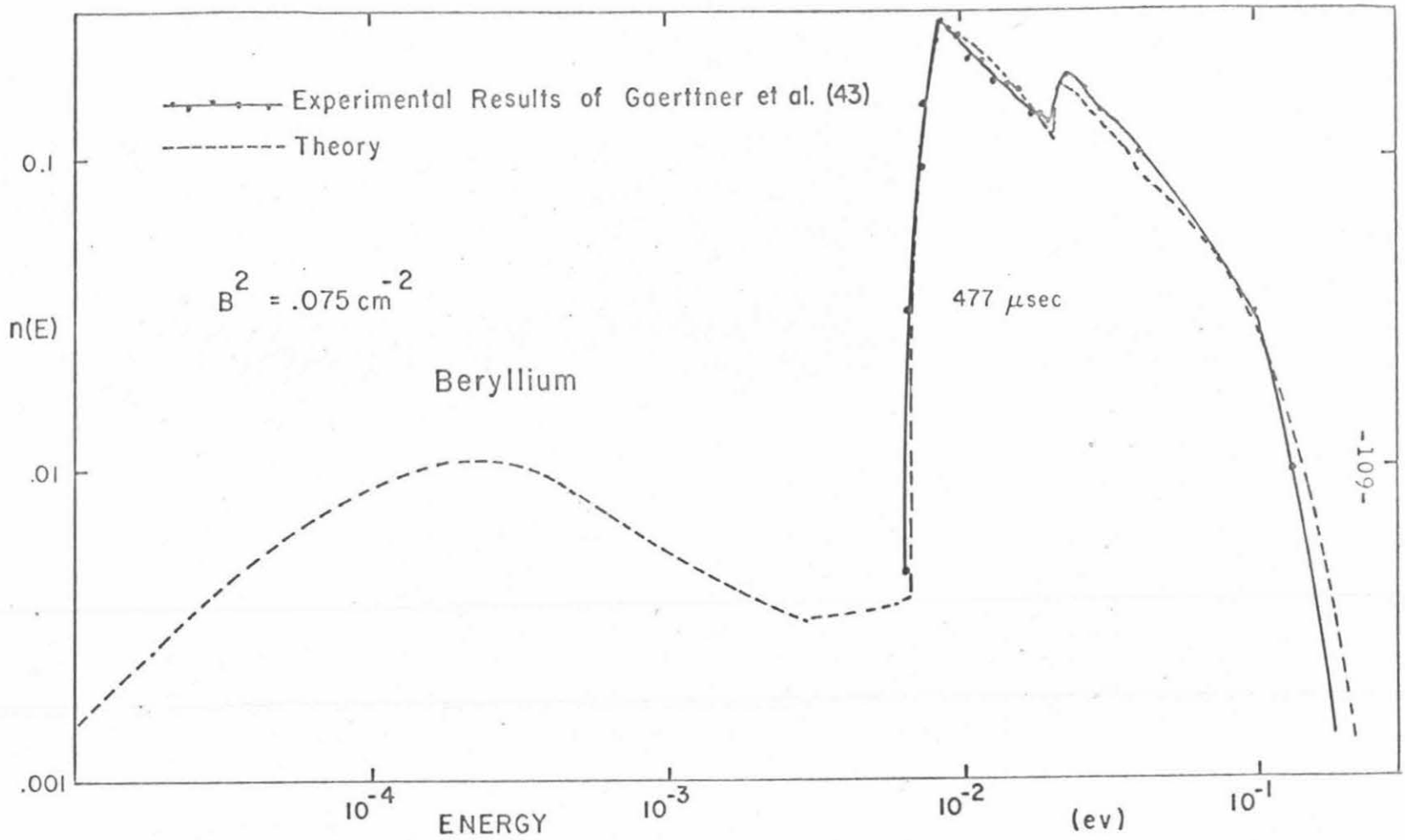

Figure IV-12. Transient Energy Distribution for a Small B_e Assembly.

V. CONCLUSIONS AND DISCUSSION

We have presented direct evidence of non-exponential decay in six graphite assemblies for significant measuring times after the source pulse. Additionally, for three larger assemblies, we found that the decay of the neutron population was well described by a single exponential during a significant interval (3 - 5 milliseconds), but that the decay near the beginning and the end of the total measurement interval could not be described as purely exponential. For the largest graphite stack, the decay appeared to be exponential over the entire ten millisecond measuring interval. Further experiments have shown that when the decay is clearly non-exponential the spatial distribution is also not adequately described by a simple diffusion theory representation. Attempts to describe these complicated experimental results by a simple modeled computation have been qualitatively interesting, but quantitavely unsuccessful. Hence, the experimental results present a real challenge to the theorist.

A. Interpretation of non-exponential decay

In Chapter II we defined the value of λ_* to be 1600 sec^{-1} based on the criterion that the effective decay constants exceeding this value failed to establish a "plateau" for any two millisecond interval during the measuring time after the source burst. Hüls[53] categorized the decay as non-exponential if the effective decay constant exhibited any "drift" after 2.5 milliseconds following the

source burst. Based on this criterion, he found non-exponential decay for λ_{eff} greater than 1250 sec^{-1}. Using his criterion, our value of λ_{*} would also be around 1250 sec^{-1}. However, below 1600 sec^{-1} our effective decay constants exhibit a tendency to increase for long times after the source burst, while above that value they monotonically decrease. This behavior is in qualitative agreement with Conn's[17] analysis for effective decay constants just above and below λ_{*}, but the amplitude of the effect is greater than one would expect from his work. Hüls also has results for an assembly, comparable to our 1.165 B_c^2 graphite stack, in which he shows that the decay is very non-exponential in the time interval 5.0 to 7.5 milliseconds after the source burst. Although the results are somewhat obscured by the high background of 14990 counts/channel (more than ten percent of the total counts/channel), the effective decay constant apparently decreases by approximately 11 percent/millisecond in this interval.

The experiments of Hüls and those presented in this work confirm that there exists a minimum size of graphite assembly in which the neutron population decays in a discrete asymptotic mode. Since the theories we discussed in Chapter I which predict this behavior are so complex that thus far they have yielded only qualitative results, more specific comparison to the theories is not possible at this time. One useful theoretical result would be more specific information about what we can expect when we measure the effective decay constants for assemblies in the immediate range of

λ_*. Given this information, the experimental value of λ_* can be more firmly established. This would be a very important result since the existing low energy cross section data are not sufficiently accurate for direct computation of λ_*. Because of their long wave length, the low energy neutrons are sensitive to the "graininess" of the graphite sample.[68] Hence, the effective slow neutron scattering cross sections reflect the average crystal size and the presence of voids in the sample. The experimental and determination of λ_* provides information about the magnitude of these effects. In addition, the time dependent effective decay constants that we have presented should be especially useful in checking theoretical models for the scattering kernel.

B. Implications of the Time Dependent Spatial Measurements

The time dependent spatial measurements also present some interesting theoretical challenges. One of the significant features of these measurements was the failure of the decay constants associated with the higher spatial modes to fall on the dispersion curve $\lambda(B^2)$ of the fundamental spatial mode. This effect is apparently not unique to graphite. Ritchie[30] noticed this effect over the whole range of his measurements on BeO assemblies. Even the water systems measured by Lopez and Beyster,[44] where the fundamental decay constants were discrete and well-defined, exhibited a trend for the higher order spatial decay constants to fall consistently above the fundamental dispersion curve. For our case,

the decay constants $\lambda(B_2^2)$ (associated with the second spatial mode) fall on a reasonably straight line when plotted against B^2. This apparent lack of "diffusion cooling" suggests that the energy distribution of the B_2^2 mode is considerably different from that of a fundamental mode corresponding to $B_1^2 = B_2^2$.

Although this phenomenon is not peculiar to polycrystalline media, we should point out that the difference $\Delta\lambda$ ($\Delta\lambda = \lambda(B_n^2) - \lambda(B_1^2)$, $B_n^2 = B_1^2$, $n \geq 2$) in the results of Lopez and Beyster is an order of magnitude larger than one obtains from the zero diffusion cooling argument. Furthermore, the BeO results for $\lambda(B_2^2)$ in excess of λ_* are lower than the fundamental dispersion curve. The nature of this phenomenon is apparently very complex.

Unfortunately, the decay constants of the higher spatial harmonics are difficult to measure in the smaller blocks because the ratio of initial amplitudes A_2/A_1 decreases as we decrease the size of the stack. Reducing the pulse width to a few microseconds increases the ratio, but at the expense of the total amplitude. Either the small ratio or the small total amplitude will severely restrict the length of the time interval available for the measurement of $\lambda(B_2^2)$. Hence, the experiments in the most interesting regime are also the most difficult to perform.

The other interesting result of the time dependent spatial distribution measurements was the tendency of the extrapolation length (or wave number) of the smallest assembly to increase with time after the pulse. The value of Z_o for the larger three stacks

also exhibited this trend to a lesser extent, but the increase was significant for the smallest assembly and was independent of whether graphite plugs filled the probe hole.

In transport theory the extrapolation length is defined in terms of the asymptotic part of the spatial distribution. Our measurements sampled the total distribution, and we were faced with the problem of extracting just the asymptotic part. Although we were careful to measure no closer than nine centimeters to the edge of the assembly, there was no way to guarantee that we were measuring the distribution in a region totally dominated by the asymptotic shape. Dropping the end points from the fitting procedure effected the results only trivially while increasing the uncertainty in Z_o.

These results raise the question of the validity of the buckling concept for small graphite systems. This problem has been attacked theoretically by Wood and Williams[66] in a numerical calculation for the pulsed slab problem. They considered graphite, beryllium, and water slabs. Their results for a 28 centimeter ($B^2 = 1.3\, B_c^2$) graphite slab indicate that the transient spatial solution is significant as deep as one-quarter of the width from the edge to the center. The mean energy and the angular distribution vary markedly as a function of position in the slab. Our results for Z_o are not really surprising when considered within this theoretical framework.

The experimental results of Gaerttner et al.[43] for the time dependent spectrum in beryllium are also consistent with this analysis. They found that the surface spectrum was radically different from the spectrum measured at the center of the $B^2 = 0.026\ cm^{-2}$ assembly. The surface spectrum exhibits a peak just below the Bragg energy, while the center spectrum dips to a minimum value.

The steady state measurements of DeJuren and Swanson[67] are also consistent with the concept of the variation of the energy distribution with position in the moderator. They measured the spatial distribution in a graphite stack as a function of distance from a plane source on one face of the assembly. Their interpretation of the measurements was that no asymptotic spectrum was established in the assemblies when the transverse buckling was less than $0.0035\ cm^{-2}$. For a cubical assembly, this corresponds to a total buckling of $0.00525\ cm^{-2}$. We measured no $\lambda_{eff}(B^2, t)$, which were constant over the entire measuring interval, for systems with B^2 in excess of $0.00545\ cm^{-2}$.

Hence, we see that there exists a substantial body of evidence that the disappearance of the discrete decay constants as one reduces the size of the graphite system is inseparably coupled to the space and energy distribution of the neutron population. The whole question of separability ($n(\underline{r}, v, t) = R(r)\phi(v)\, e^{-\lambda t}$) has been examined by Williams.[69] He finds that when the velocity and time variables are coupled, corresponding to $\lambda_* < \lambda$, the space

and time variables are also coupled. For these systems the buckling concept breaks down, and the measured effective decay constant is a function of detector position.

C. The Origin of the Oscillations in the Effective Decay Constants

One outstanding feature of the $\lambda_{eff}(t)$ curves is the presence of oscillations which appear to increase in amplitude near the end of the measured interval. Figure V-1 shows some of the experimental results of Hüls[53] which also exhibit the oscillations. We mentioned in Chapter II that oscillations of frequency $v_B B$ come directly from the analysis of the Laplace transform of the neutron distribution function,[58] but that the physical interpretation is quite difficult. For the latter reason, one is led to suspect that the oscillations are related to some parameter in the data collection and analysis. In table V-1, we have listed the buckling of the assemblies, the approximate oscillation frequency, the Bragg frequency ($v_B B$), and $2\pi/\Delta T$, where ΔT is the length of the fitting interval.

While the data appear to be correlated to the length of the fitting interval ΔT, the experimentally observed frequencies are too approximate to draw any definite conclusions. The question of whether the oscillations are related to the pollycrystalline structure of the graphite can be experimentally resolved. Data from a water system with an equivalent λ_{eff} can be analyzed by the same fitting procedure. If no regular oscillations appear in the results, we

TABLE V-1

Experiment	$B^2(cm^{-2})$	Experimental ω (sec^{-1})	$V_B B$ (sec^{-1})	$2\pi/\Delta T$ (sec^{-1})
Hüls[53]	0.0062	6280	4564	11,017
"	0.0070	8602	4854	11,017
"	0.0078	8971	5133	11,017
This work	0.0064	3600	4640	2512
"	0.0099	8970	5800	8373
"	0.0099	6280	5800	2500
"	0.0125	8263	6148	8373

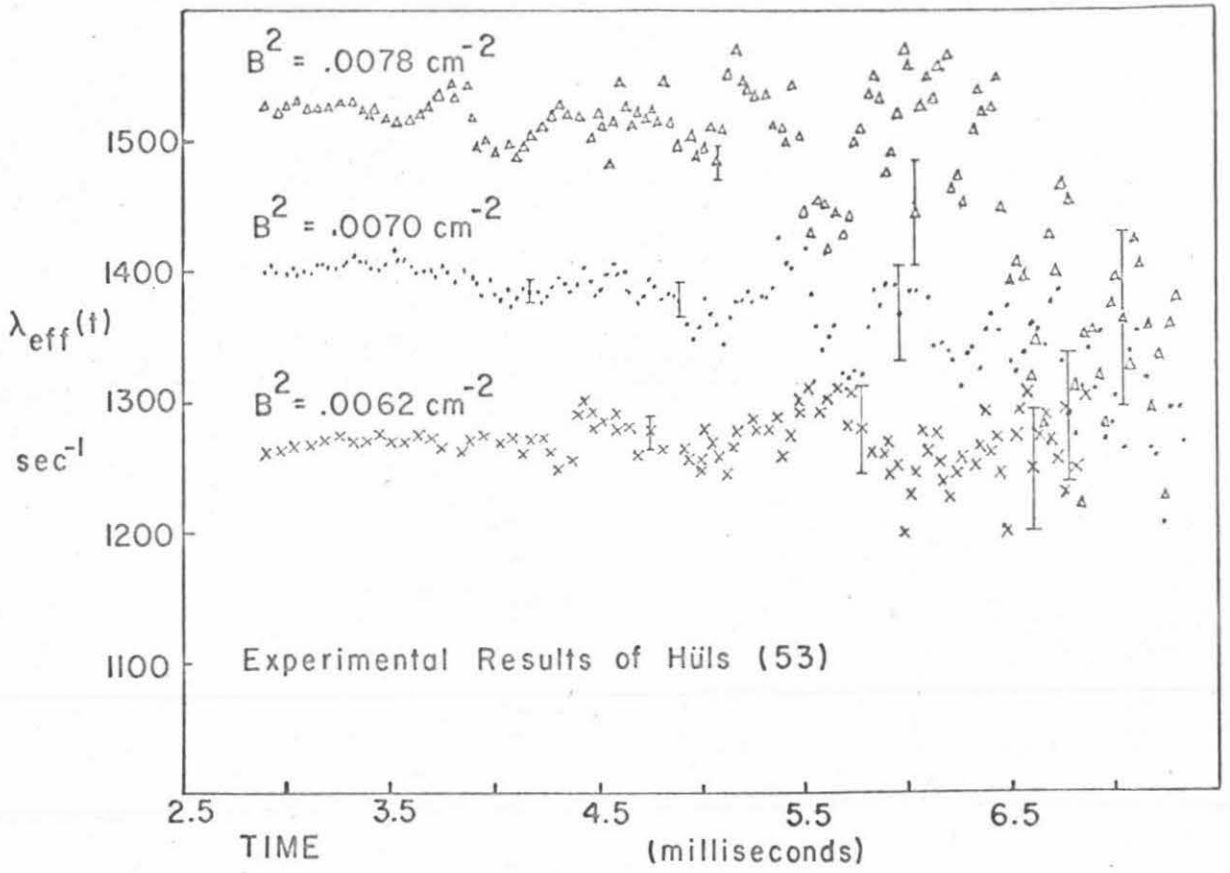

Figure V-1. Effective Decay Constants Exhibiting Oscillations.

can conclude that the oscillations in the graphite data are physical in origin. However, if regular oscillations appear, further experiments will be required to test the sensitivity of the results to such parameters as the width of data collection channels and the length of the fitting interval.

D. Suggestions for Further Research

While we have presented convincing evidence for non-exponential decay of transient neutron populations in small graphite assemblies, several experiments are still needed to supply data necessary for the complete interpretation of neutron die-away experiments in graphite. The most powerful of these experiments would be the measurement of time dependent spectra for small graphite assemblies such as Gaerttner et al.[43] have done for beryllium assemblies. Such detailed data are a more direct check on the theory than the integral experiments we have reported.

A simpler experiment, which may prove to be even more important than the energy distribution measurements, is a direct comparison of die-away experiments performed on two graphite systems which differ in the average size of the individual crystallites. The size of the crystallites effects the elastic scattering cross sections.[30] The dispersion in the experimental results for neutron die-away experiments in graphite may be in part due to variations in the average size and in the volume occupied by tiny voids between the individual crystallites. Variation in the void

fraction is reflected in density variation between samples.

Finally, a comparison of non-exponential decay measured with detectors of different energy sensitivity may be necessary to serve as a reference for any detailed theoretical computations. The existing data should provide sufficient impetus for such calculations.

REFERENCES

1. G. von Dardel, "The Interaction of Neutrons with Matter Studied with a Pulsed Neutron Source," Transactions of the Royal Institute of Technology, 75, (1954).

2. G. von Dardel, "A Study of the Interaction of Neutrons with Moderating Materials," Phys. Rev. 94, No. 5, 1272 (1954).

3. G. von Dardel and N. Sjostrand, "Diffusion Parameters of Thermal Neutrons in Water," Phys. Rev. 96, No. 5, 1245 (1954).

4. M. M. R. Williams, Slowing Down and Thermalization of Neutrons, (North Holland Publishing Company, Amsterdam, 1966).

5. D. E. Parks, M. S. Nelkin, J. R. Beyster, and N. F. Wikner, Slow Neutron Scattering and Thermalization, (W. A. Benjamin, Inc., New York, 1970).

6. B. Davison, Neutron Transport Theory, (Oxford University Press, Oxford, 1958).

7. R. C. Erdmann and J. L. Shapiro, "The Extrapolation Distance for Monoenergetic Neutrons, An Exact Calculation," Nukleonik 9, 302 (1967).

8. J. J. Dorning, Time-Dependent Nuetron Thermalization in Finite Media, BNL 11680 (1967).

9. K. H. Beckurts and W. Wirtz, Neutron Physics, (Springer-Verlag, New York, 1964).

References (Cont'd)

10. I. Kuscer, "Advances in Neutron Thermalization Theory: A Review," I. A. E. A. Sym. on Neutron Thermalization and Reactor Spectra, Vol. I, 3 (I. A. E. A., Vienna, 1968).

11. S. Albertoni and B. Montagnini, "Some Spectral Properties of the Transport Equation and Their Relevance to the Theory of Pulsed Neutron Experiments," I. A. E. A. Sym. on Pulsed Neutron Research, Vol. I, 239 (I. A. E. A., Vienna, 1965).

12. M. Borysiewicz and J. Mika, "Time Dependent Thermalization with Elastic Scattering," I. A. E. A. Sym. on Neutron Thermalization and Reactor Spectra, Vol. I, 45 (I. A. E. A., Vienna, 1968).

13. A. Weinberg and E. Wigner, The Physical Theory of Neutron Chain Reactors, (The University of Chicago Press, Chicago, 1958).

14. C. S. Shapiro and N. Corngold, "Time Eigenvalues and Degenerate Kernels in Neutron Thermalization," Phys. Rev. 137A, A1686 (1965).

15. R. Conn and N. Corngold, "A Theory of Pulsed Neutron Experiments in Moderators via a Simple Model," Nucl. Sci. & Eng. 29, 354 (1967).

17. R. Conn, The Theory of Pulsed Neutron Experiments in Polycrystalline Moderators, Thesis, Calif. Inst. Tech. (1968).

18. J. Wood, "An Interpretation of the Numerical Solution of the Neutron Pulsed Source Problem," J. Nucl. Energy 22, 525 (1968).

References (Cont'd)

19. J. Wood, "Pseudo-Exponential Decay of a Neutron Pulse in Small Beryllium Systems," J. Nuc. Energy, Parts A/B, 20, 649 (1966).

20. V. Ardente and G. Rossi, "Decay of a Thermal Neutron Pulse in a Finite Coherent Moderator," Neutron Thermalization and Reactor Spectra, Vol. I, I.A.E.A., Vienna, 169 (1968).

21. A. I. M. Ritchie, K. J. Maher, and G. D. Trimble, "Calculation of Decay Constants in BeO in the Region of ($v\Sigma$ inel) min," J. Nuc. Energy 24, 151 (1970).

22. A. V. Antonov, et al., "A Study of Neutron Diffusion in Beryllium, Graphite, and Water by the Impulse Method," Int. Conf. on Peaceful Uses of Atomic Energy, Vol. V, 3 (Geneva, 1955).

23. K. H. Beckurts, "Measurements with a Pulsed Neutron Source," Nucl. Sci. & Eng. 2, 516 (1957).

24. H. Klose, M. Küchle, and W. Riechardt, "Pulsed Neutron Measurements on Graphite," Proceedings of the Brookhaven Conference on Neutron Thermalization, Vol. III, 935 (1962).

25. E. Starr and G. A. Price, "Measurement of the Diffusion Parameters of Graphite and Graphite-Bismuth by Pulsed Neutron Methods," Proceedings of the Brookhaven Conference on Neutron Thermalization, Vol. III, 1034 (1962).

26. S. K. Davis, J. A. DeJuren, and M. Reier, "Pulsed Decay and Extrapolation Length Measurements in Graphite," Nuc. Sci. & Eng. 23, 74 (1965).

References (Cont'd)

27. N. Yamamuro, et al., "Pulsed Neutron Research [I]," Bulletin of the Tokyo Institute of Technology, 77, 27 (1966).

28. N. N. Hanna and M. J. Harris, "Decay of a Thermalized Neutron Pulse in Graphite," J. Nucl. Energy 22, 587 (1968).

29. S. R. Bull, K. D. Dana, and T. J. Connolly, "Pulsed Source Investigations on Graphite Systems," J. Nucl. Energy, 24, 473 (1970).

30. A. I. M. Ritchie, The Variation with Space and Time of the Neutron Energy Distribution in Pulsed BeO Assemblies, Thesis, University of New South Wales, (1970).

31. R. R. Fullwood, et al., "The Effects of Coherent Scattering on the Thermalization of Neutrons in Beryllium," Nucl. Sci. & Eng. 18, 138 (1964).

32. I. F. Zherzherun, "Pulsed Beam Method of Investigating Neutron Diffusion in Beryllium," J. of Nucl. Energy Parts A/B 19, 284 (1965).

33. K. H. Beckurts, "A Review of Pulsed Neutron Experiments on Non-multiplying Media," I. A. E. A. Sym. on Pulsed Neutron Research, Vol. I, 3 (I. A. E. A., Vienna, 1965).

34. E. Starr, H. Honeck, and J. DeVilliers, "Determination of Diffusion Cooling in Graphite by Measurement of the Average Neutron Velocity," Nucl. Sci. & Eng. 18, 230 (1964).

35. N. N. Hanna and M. J. Harris, "Neutron Thermalization Measurements in Graphite," J. Nucl. Energy 23, 29, (1969).

36. M. V. Polley and J. Walker, "Neutron Thermalization Measurements in Graphite by the Reaction Rates Method, Using a Ge (Li) Gamma Ray Detector," J. Nucl. Energy 24, 279, (1970).

37. E. Starr and J. W. L. DeVilliers, "Determination of Diffusion Cooling in Graphite by Measurement of the Average Neutron Velocity," Proceedings of the Brookhaven Conference on Neutron Thermalization, Vol. III, 997 (1962).

38. K. Serdula and J. Young, "Neutron Thermalization in Graphite," Nucl. Sci. & Eng. 22, 40 (1965).

39. Y. Kaneko and K. Sumita, "Neutron Slowing Down Time and Thermalization Time Constant in Graphite," I. A. E. A. Sym. on Pulsed Neutron Research, Vol. I, 139, (I. A. E. A., Vienna, 1965).

40. I. Purica, et al., "Determination of the Thermalization Time in Graphite by the Frequency Characteristic Method," I. A. E. A. Sym. on Neutron Thermalization and Reactor Spectra, Vol. II, 479 (I. A. E. A., Vienna, 1968).

41. E. Barnard, et al., "Thermalization of Neutrons in Graphite," Proceedings of the Brookhaven Conference on Neutron Thermalization, Vol. III, 805 (1962).

42. M. J. Poole, "Review of the Application of Pulsed Sources to the Measurement of Neutron Spectra in Moderators and Reactor Lattices," I. A. E. A. Sym. on Pulsed Neutron Research, Vol. I, 425 (I. A. E. A., Vienna, 1965).

References (Cont'd)

43. E. R. Gaerttner, et al., "The Effects of Coherent Scattering on the Thermalization of Neutrons in Beryllium," I. A. E. A. Sym. on Pulsed Neutron Research, Vol. I, 483, (I. A. E. A., Vienna, 1965).

44. W. M. Lopez and J. M. Beyster, "Measurement of Neutron Diffusion Parameters in Water by the Pulsed Neutron Method," Nucl. Sci. & Eng. 12, 190 (1965).

45. S. Chwaszczewski and A. T. Mikulski, "Determination of Neutron Slowing Down Parameters by the Pulsed Source Method," Nukleonik 12, 218 (1969).

46. W. M. Andrews, "Measurement of the Temperature Dependence of Neutron Diffusion Properties in Beryllium Using a Pulsed Neutron Technique," UCRL-6083, (1960).

47. J. S. Hewitt and J. Walker, "Pulsed Source Measurements on Neutron Thermalization in Graphite by the Reaction Rate Technique," I. A. E. A. Sym. on Neutron Thermalization and Reactor Spectra, Vol. II, 347 (I. A. E. A., Vienna, 1968).

48. J. R. Beyster, J. M. Neill, and J. C. Young, "Recent Developments in Integral Neutron Thermalization," Reactor Physics in the Resonance and Thermal Regions, Vol. I, 151 (The M. I. T. Press, Cambridge, Mass., 1966).

49. A. K. Ghatak and H. C. Honeck, "On the Feasibility of Measuring Higher Time Decay Constants," Nucl. Sci. & Eng. 21, 227 (1965).

References (Cont'd)

50. R. Conn, "Approximate Dispersion Relations and the Total Coherent Inelastic Neutron Scattering Cross Section for Graphite," Nucl. Sci. & Eng. 40, 17 (1970).

51. N. Corngold and P. Michael, "Some Transient Phenomena in Thermalization II," Nucl. Sci. & Eng. 19, 91 1964).

52. H. Takahashi, "Space and Time Dependent Eigenvalue Problem in Neutron Thermalization," Proceedings of the Brookhaven Conference on Neutron Thermalization, Vol. IV, 1299 (1962).

53. M. Hüls, "Ein Beitrag zur Problematik von Neutronenpuls-Experimenten an Kompaktgrafit sowie zur Frage der Heterogenitätseinflüsse von Hohlräumen auf das Diffusionsverhalten thermisher Neutronen in Systemen, die kugelförmige Grafitelemente enthalten," Berichte der Kernforschungsonlage Jülich 690, (1970).

54. J. T. Prud'homme, "Texas Nuclear Corporation Neutron Generators," T. N. C. 424 (1962).

55. P. C. Rogers, "Frantic Program for Analysis of Exponential Growth and Decay Curves," M. I. T. Lab. Nucl. Sci. 76 (1962).

56. W. J. Price, Nuclear Radiation Detection, (McGraw-Hill Book Company, New York, 1964).

57. G. P. Giraudbit, Pulsed Neutron Measurements in Two Adjacent Finite Media, Thesis, Cal. Inst. Tech., (1966).

58. N. Corngold, private communication.

59. See reference 48.

References (Cont'd)

60. G. Blumentritt and K. Fährmann, "Bestimmung der Diffusionparameter von Graphit nach der Impulsmethode," Kernonergii 11/12, 281 (1968).

61. G. Cuny, et al., "Etude du graphite et de l'oxide de Beryllium par la méthode de la source pulsée de neutrons," I.A.E.A. Sym. on Pulsed Neutron Research, Vol. I, 89, (I.A.E.A., Vienna, 1965).

62. K. H. Beckurts, "A Review of Pulsed Neutron Experiments on Non-Multiplying Media," I.A.E.A. Sym. on Pulsed Neutron Research, Vol. I, 3 (I.A.E.A., Vienna, 1965).

63. R. V. Meghreblian and D. K. Holmes, Reactor Analysis, (McGraw-Hill Book Company, Inc., New York, 1960).

64. N. Corngold, P. Michael, and W. Wollman, "The Time Decay Constants in Neutron Thermalization," Proceedings of the Brookhaven Conference on Neutron Thermalization, Vol. IV, 1103 (1962).

65. G. F. Carrier, M. Krook, and G. E. Pearson, "Functions of a Complex Variable," (McGraw-Hill, Inc., New York, 1966).

66. J. Wood and M. M. R. Williams, "The Validity of the Buckling Concept and the Importance of Spatial Transients in the Pulsed Neutron Experiment," J. Nucl. Energy 21, 113 (1967).

67. J. A. De Juren and V. A. Swanson, "Cold Neutron Diffusion in Graphite Diffusion Length Measurements," J. Nucl. Energy Parts A/B, 20, 905 (1966).

References (Cont'd)

68. G. E. Bacon, Neutron Diffraction, (Clarendon Press, Oxford, 1962).

69. M. M. R. Williams, "Space, Time, and Energy Separability in the Pulsed Neutron Experiment," Nukleonik 10, 252 (1967).

70. J. L. Shapiro, "Pulsed Neutron Measurements in Graphite," American Nuclear Society Transactions 11, 584 (1968).